NASA/CR—2004-213199/VOL3

Numerical, Analytical, Experimental Study of Fluid Dynamic Forces in Seals

Volume 3—Description of Spiral-Groove Codes SPIRALG and SPIRALI

Jed Walowit and Wilbur Shapiro
Mechanical Technology, Inc., Latham, New York

October 2004

The NASA STI Program Office . . . in Profile

Since its founding, NASA has been dedicated to the advancement of aeronautics and space science. The NASA Scientific and Technical Information (STI) Program Office plays a key part in helping NASA maintain this important role.

The NASA STI Program Office is operated by Langley Research Center, the Lead Center for NASA's scientific and technical information. The NASA STI Program Office provides access to the NASA STI Database, the largest collection of aeronautical and space science STI in the world. The Program Office is also NASA's institutional mechanism for disseminating the results of its research and development activities. These results are published by NASA in the NASA STI Report Series, which includes the following report types:

- TECHNICAL PUBLICATION. Reports of completed research or a major significant phase of research that present the results of NASA programs and include extensive data or theoretical analysis. Includes compilations of significant scientific and technical data and information deemed to be of continuing reference value. NASA's counterpart of peer-reviewed formal professional papers but has less stringent limitations on manuscript length and extent of graphic presentations.

- TECHNICAL MEMORANDUM. Scientific and technical findings that are preliminary or of specialized interest, e.g., quick release reports, working papers, and bibliographies that contain minimal annotation. Does not contain extensive analysis.

- CONTRACTOR REPORT. Scientific and technical findings by NASA-sponsored contractors and grantees.

- CONFERENCE PUBLICATION. Collected papers from scientific and technical conferences, symposia, seminars, or other meetings sponsored or cosponsored by NASA.

- SPECIAL PUBLICATION. Scientific, technical, or historical information from NASA programs, projects, and missions, often concerned with subjects having substantial public interest.

- TECHNICAL TRANSLATION. English-language translations of foreign scientific and technical material pertinent to NASA's mission.

Specialized services that complement the STI Program Office's diverse offerings include creating custom thesauri, building customized databases, organizing and publishing research results . . . even providing videos.

For more information about the NASA STI Program Office, see the following:

- Access the NASA STI Program Home Page at ***http://www.sti.nasa.gov***

- E-mail your question via the Internet to help@sti.nasa.gov

- Fax your question to the NASA Access Help Desk at 301–621–0134

- Telephone the NASA Access Help Desk at 301–621–0390

- Write to:
  NASA Access Help Desk
  NASA Center for AeroSpace Information
  7121 Standard Drive
  Hanover, MD 21076

NASA/CR—2004-213199/VOL3

Numerical, Analytical, Experimental Study of Fluid Dynamic Forces in Seals

Volume 3—Description of Spiral-Groove Codes SPIRALG and SPIRALI

Jed Walowit and Wilbur Shapiro
Mechanical Technology, Inc., Latham, New York

Prepared under Contract NAS3–25644

National Aeronautics and
Space Administration

Glenn Research Center

October 2004

Available from

NASA Center for Aerospace Information
7121 Standard Drive
Hanover, MD 21076

National Technical Information Service
5285 Port Royal Road
Springfield, VA 22100

Available electronically at http://gltrs.grc.nasa.gov

FOREWORD

The Computational Fluid Dynamics (CFD) computer codes and Knowledge-Based System (KBS) were generated under NASA contract NAS3-25644 originating from the Office of Advanced Concepts and Technology and administered through NASA-Lewis Research Center. The support of the Program Manager, Anita Liang, and the advice and direction of the Technical Monitor, Robert Hendricks, are gratefully appreciated. Major contributors to code development were:

- Dr. Bharat Aggarwal: KBS and OS/2 PC conversion of labyrinth seal code KTK
- Dr. Antonio Artiles: cylindrical and face seal codes ICYL and IFACE
- Dr. Mahesh Athavale and Dr. Andrzej Przekwas: CFD code SCISEAL
- Mr. Wilbur Shapiro: gas cylindrical and face seal codes GCYLT, GFACE, and seal dynamics code DYSEAL
- Dr. Jed Walowit: spiral groove gas and liquid cylindrical and face seal codes SPIRALG and SPIRALI.

The labyrinth seal code, KTK, was developed by Allison Gas Turbine Division of General Motors Corporation for the Aero Propulsion Laboratory, Air Force Wright Aeronautical Laboratories, Wright-Patterson Air Force Base, Ohio. It is included as part of the CFD industrial codes package by the permission of the Air Force.

TABLE OF CONTENTS

SECTION	PAGE
FOREWORD	iii
LIST OF FIGURES	vii
NOMENCLATURE FOR CODE SPIRALG	ix
NOMENCLATURE FOR CODE SPIRALI	xix
1.0 INTRODUCTION	1
2.0 INDUSTRIAL CODE SPIRALG – GAS-LUBRICATED, SPIRAL GROOVE, CYLINDRICAL AND FACE SEALS	3
2.1 Theoretical Development	4
2.1.1 Formulation of Equations Governing Gas-Lubricated Spiral Groove Seals	4
2.1.2 Discretization of Pressure Equations	14
2.1.3 Newton-Raphson Linearization Procedure	17
2.1.4 Determination of Loads, Moments, Torque, and Leakage	19
2.1.5 Determination of Stiffness and Damping Coefficients	20
2.1.6 Optimization of Groove Parameters for Maximum Stagnation Pressure in a Concentric Cylindrical Seal	24
2.2 Overview of Computer Code SPIRALG	25
2.3 Verification	27
3.0 INDUSTRIAL CODE SPIRALI - INCOMPRESSIBLE, TURBULENT SPIRAL-GROOVED CYLINDRICAL FACE SEALS	37
3.1 Formulation and Method of Solution	38
3.2 Overview of Computer Code SPIRALI	63
3.3 Verification	64

LIST OF FIGURES

NUMBER		PAGE
1	Coordinate System for Spiral Groove Analysis	5
2	Schematic of Spiral Groove Parameters, Global and Local Pressures	7
3	Schematic of Grid Network and Flow Control Area for Discretization Process	16
4	The Variation of the Stagnation Pressure Gradient about the Optimum Point	26
5	Flow Diagram for Logic Used in SUBROUTINE SPIRAL	28
6	Coordinate System for Spiral Groove Analysis	39
7	Velocities and Forces on a Differential Element in the θ Direction	41
8	Jump in Film Thickness	43
9	Examples of Degrees of Film Formation in Groove	46
10	Schematic of Spiral Groove Parameters, Global and Local Pressures, Case a	47
11	Schematic of Spiral Groove Parameters, Global and Local Pressures, Case b	49
12	Parameters for Characterizing Quadratic Film Variation	65
13	Flow Diagram for Overall Logic Used in Computations	66
14	Parallel-Groove Pressure Breakdown Seal	69
15	Parallel-Groove Seal Flow Coefficient	69
16	Tangential Force Coefficients	70
17	Normal Force Coefficients	71
18	Parallel-Groove Seal Effective Stiffness	72
19	Comparison Between C-k/ω and C_{ef} at Various Rotating Speeds	73
20	Effect of Local Pressure Discontinuities on Predicted Axial Flow Rates	74
21	Flow Coefficient: SPIRALI Compared to Reference 27	75
22	Effective Damping: SPIRALI Compared to Reference 27	76
23	Direct Stiffness: SPIRALI Compared to Reference 27	77

NOMENCLATURE FOR CODE SPIRALG

$\bar{A}$ = dimensionless flow control area, (area/R_0^2)

A_i = coefficients of second-order linear operator defined by Eq. (2-44), 1=1,...,6

{a} = column vector of eccentricity coefficients defined by Eq. (2-41)

$a_{i,j}^k$ = kth component of {a} evaluated at grid point (i,j)

B_{xy} = damping coefficient relating force in x direction to velocity in y direction, B_{xx}, B_{yx}, B_{yy} and B_{zz} are similarly defined

$B_{\phi\psi}$ = damping coefficient relating moment about x axis to angular velocity about y axis, $B_{\phi\phi}$, $B_{\psi\phi}$ and $B_{\psi\psi}$ are similarly defined

$B_{x\phi}$ = damping coefficient relating force in x direction to angular velocity about x axis, $B_{x\psi}$, $B_{y\phi}$, $B_{y\psi}$, $B_{z\phi}$ and $B_{z\psi}$ are similarly defined

$B_{\phi x}$ = damping coefficient relating moment about x axis to velocity in x direction, $B_{\psi x}$, $B_{\phi y}$, $B_{\psi y}$, $B_{\phi z}$ and $B_{\psi z}$ are similarly defined

$\tilde{B}B_{xy}$ = dimensionless damping coefficient B_{xy}/B_0, same definitions apply to $\tilde{B}_{xx}$, $\tilde{B}_{yx}$, $\tilde{B}_{yy}$, $\tilde{B}_{zz}$

$\tilde{B}_{\phi\psi}$ = dimensionless damping coefficient $B_{\phi\psi}/(B_0R_0^2)$, same definitions apply to $\tilde{B}_{\phi\phi}$, $\tilde{B}_{\psi\phi}$, $\tilde{B}_{\psi\psi}$

$\tilde{B}_{x\phi}$ = dimensionless damping coefficient $B_{x\phi}/(B_0R_0)$, same definitions apply to $\tilde{B}_{x\psi}$, $\tilde{B}_{y\phi}$, $\tilde{B}_{y\psi}$, $\tilde{B}_{z\phi}$, $\tilde{B}_{z\psi}$

$\tilde{B}B_{\phi x}$ = dimensionless damping coefficient $B_{\phi x}/(B_0R_0)$, same definitions apply to $\tilde{B}_{\psi x}$, $\tilde{B}_{\phi y}$, $\tilde{B}_{\psi y}$, $\tilde{B}_{\phi z}$, $\tilde{B}_{\psi z}$

B_0 = characteristic damping constant, $12\mu R_0^4/C^3$

$[\tilde{B}]$ = dimensionless damping coefficients in matrix form

{b} = column vector of coefficients of ε', arising from linearization of Eq. (2-39)

C = clearance (cylindrical seal) or reference film thickness (face seal)

$[C^j]$ = coefficient matrix used in Newton-Raphson linearization procedure, see Eq. (2-34)

$[\hat{C}^j]$ = coefficient matrix obtained from steady state solution

$[\hat{C}^{j,k}]$ = derivative of $[\hat{C}^j]$ with respect to ε_k

$[\bar{C}^j]$ = diagonal coefficient matrix whose components are given by Eq. (2-51)

$[C^{*j}]$ = complex coefficient matrix used in complex stiffness solution, $[\hat{C}^j] + \Im\sigma[\bar{C}^j]$

$[D^j]$ = coefficient matrix used in Newton-Raphson linearization procedure, see Eq. (2-34)

$[\hat{D}^j]$ = coefficient matrix obtained from steady state solution

$[\hat{D}^{j,k}]$ = derivative of $[\hat{D}^j]$ with respect to ε_k

$[E^j]$ = coefficient matrix used in Newton-Raphson linearization procedure, see Eq. (2-34)

$[\hat{E}^j]$ = coefficient matrix obtained from steady state solution

$[\hat{E}^{j,k}]$ = derivative of $[\hat{E}^j]$ with respect to ε_k

e_x, e_y = eccentricity in x,y direction (cylindrical seal)

e_z = axial displacement, (face seal)

$F_{i,j}$ = residual outflow function from flow balance at grid point (i,j)

G = second-order nonlinear operator defined by Eq. (2-39)

$\hat{H}$ = steady state, unperturbed, value of H_r

H_r = dimensionless film thickness, h_r/C

h_g = film thickness over grooves, see Fig. 2

h_r = film thickness over ridges, see Fig. 2

i,j,k = subscripts used generically as indices

$\vec{i}, \vec{j}$ = unit vectors in θ,s directions

$\Im$ = unit imaginary number, $\sqrt{-1}$

K_{xy} = stiffness coefficient relating force in x direction to displacement in y direction, K_{xx}, K_{yx}, K_{yy} and K_{zz} are similarly defined

$K_{\phi\psi}$ = stiffness coefficient relating moment about x axis to rotation about y axis, $K_{\phi\phi}$, $K_{\psi\phi}$ and $K_{\psi\psi}$ are similarly defined

$K_{x\phi}$ = stiffness coefficient relating force in x direction to rotation about x axis, $K_{x\psi}$, $K_{y\phi}$, $K_{y\psi}$, $K_{z\phi}$ and $K_{z\psi}$ are similarly defined

$K_{\phi x}$ = stiffness coefficient relating moment about x axis to displacement in x direction, $K_{\psi x}$, $K_{\phi y}$, $K_{\psi y}$, $K_{\phi z}$ and $K_{\psi z}$ are similarly defined

$\tilde{K}_{xy}$ = dimensionless stiffness coefficient K_{xy}/K_0, same definitions apply to $\tilde{K}_{xx}$, $\tilde{K}_{yx}$, $\tilde{K}_{yy}$, $\tilde{K}_{zz}$

$\tilde{K}_{\phi\psi}$ = dimensionless stiffness coefficient $K_{\phi\psi}/(K_0R_0^2)$, same definitions apply to $\tilde{K}_{\phi\phi}$, $\tilde{K}_{\psi\phi}$, $\tilde{K}_{\psi\psi}$

$\tilde{K}_{x\phi}$ = dimensionless stiffness coefficient $K_{x\phi}/(K_0R_0)$, same definitions apply to $\tilde{K}_{x\psi}$, $\tilde{K}_{y\phi}$, $\tilde{K}_{y\psi}$, $\tilde{K}_{z\phi}$, $\tilde{K}_{z\psi}$

$\tilde{K}_{\phi x}$ = dimensionless stiffness coefficient $K_{\phi x}/(K_0R_0)$, same definitions apply to $\tilde{K}_{\psi x}$, $\tilde{K}_{\phi y}$, $\tilde{K}_{\psi y}$, $\tilde{K}_{\phi z}$, $\tilde{K}_{\psi z}$

K_0 = characteristic stiffness constant, $p_0R_0^2/C$

$[\tilde{K}]$ = dimensionless stiffnesses in matrix form

k_i = spiral groove coefficient defined by Eq. (2-25), i=1,2,...,8

L = seal length, see Fig. 1

$\tilde{L}$ = dimensionless length, $L/(2R_0)$

l_g = groove width, $r\Delta\theta_g$

l_r = ridge width, $r\Delta\theta_r$

$\mathcal{L}$ = second-order linear operator defined by Eq. (2-44)

M = number of grid points in s direction

M_x, M_y = applied moment about x,y axis

$\tilde{M}_x, \tilde{M}_y$ = dimensionless moment, $(M_x, M_y)/(R_0^3 p_0)$

N = number of grid points in θ direction

N_g = number of spiral grooves

$\vec{n}$ = unit vector normal to $\bar{S}$

$\vec{n}_\beta$ = unit vector normal to groove

P = dimensionless pressure, $(p-p_0)/p_0$

$\hat{P}$ = steady state unperturbed value of P

$P_{i,j}$ = dimensionless pressure, P, at grid point (i,j)

P_i = dimensionless pressure, P, at point i shown in Fig. 3, i=1,...,9

P_l, P_r = dimensionless boundary pressures $(p_l-p_0)/p_0$, $(p_r-p_0)/p_0$

$\{P'\}$ = column vector of dimensionless pressure disturbances due to perturbation in $\{\varepsilon\}$

$\{P'^k_j\}$ = column vector of disturbance pressures associated with ε_k

$\{P^*\}$ = complex amplitude of $\{P'\}$, $\{P'\} = \{P^*\}e^{\Im\sigma\tilde{t}}$

$\{P^{*k}_j\}$ = column vector of complex stiffness pressures associated with ε_k

$\{P_\Re\}$ = real part of $\{P^*\}$

$\{P_\Im\}$ = imaginary part of $\{P^*\}$

p = global pressure in absolute units

p′ = local pressure in absolute units

p_0 = reference pressure in absolute units, normally taken to be the minimum of the boundary pressures

p_l, p_r = boundary pressures in absolute units at s_l, s_r

$\vec{Q}$ = dimensionless flow vector, $12\mu R_0\vec{q}/(p_0C^3)$

Q_s, Q_θ = components of dimensionless flow vector in s,θ directions

Q^+_{ij}, Q^-_{ij} = dimensionless flow components shown in Fig. 3

Q_{in} = dimensionless flow rate, $12\mu q_{in}/(p_0C^3)$

$\vec{q}$ = global flow vector, mass flow rate per unit transverse length divided by density at pressure p_0

q_s, q_θ = components of $\vec{q}$ in s,θ directions

q_A = global mass flow rate per unit area displaced by rate of decrease of film, divided by density at p_0

q_{in} = volumetric flow rate measured at pressure p_0

$\vec{q}'$ = local flow vector, mass flow rate per unit transverse length divided by density at pressure p_0

q_s', q_θ' = components of $\vec{q}'$ in s,θ directions

q_A' = local mass flow rate per unit area displaced by rate of decrease of film, divided by density at p_0

R = dimensionless coordinate, r/R_0, taken as 1 for cylindrical seal

R_0 = reference radius, taken as outside radius for face seal and shaft radius for cylindrical seal

R_i = inside radius of face seal

$\{R^j\}$ = column vector used in Newton-Raphson linearization procedure, see Eq. (2-34)

$\{\hat{R}^j\}$ = column vector obtained from steady state solution

$\{\hat{R}^{j,k}\}$ = derivative of $\{\hat{R}^j\}$ with respect to ε_k

$\{\bar{R}_i^{j,k}\}$ = column vectors whose components are given by Eq. (2-52)

$\{R^{j,k}\}$ = complex column vectors used complex stiffness solution $\{\hat{R}^{j,k}\} - \Im\sigma\{\bar{R}^{j,k}\}$

r = radial coordinate, taken as R_0 for cylindrical seal

S = dimensionless coordinate, s/R_0

S_l, S_r = dimensionless boundary coordinates s_l/R_0, s_r/R_0

$\bar{S}$ = dimensionless length of line surrounding flow control area (length/R_0)

s = transverse coordinate, s = r for a face seal and s = z for a cylindrical seal

s_g = transverse coordinate at start of groove

s_l = left boundary coordinate, $s_l = R_i$ for face seal and s_l = -L/2 for cylindrical seal

s_r = right boundary coordinate, $s_r = R_0$ for face seal and s_r = L/2 for cylindrical seal

T = torque

$\tilde{T}$ = dimensionless torque, $T/(p_0 R_0^2 C)$

$\tilde{T}_c$ = $\tilde{T}$ obtained with course grid in Romberg extrapolation example

$\tilde{T}_f$ = $\tilde{T}$ obtained with fine grid in Romberg extrapolation example

$\tilde{T}_r$ = $\tilde{T}$ obtained by Romberg extrapolation

t = time

$\tilde{t}$ = dimensionless time, $\omega t/(2\Lambda)$

$\vec{t}_\beta$ = unit vector tangential to groove

$\vec{u}_1$ = velocity of grooved surface

$\vec{u}_2$ = velocity of smooth surface

W_x, W_y = applied loads in x,y direction (cylindrical seal)

$\tilde{W}_x, \tilde{W}_y$ = dimensionless loads $(W_x, W_y)/(p_0 R_0^2)$

W_z = applied load in z direction (face seal)

$\tilde{W}_z$ = dimensionless load, $W_z/(p_0 R_0^2)$

$\{\tilde{W}\}$ = column vector containing dimensionless loads and moments $\{\tilde{W}_x, \tilde{W}_y, \tilde{M}_x, \tilde{M}_y\}$ for cylindrical seal, $\{\tilde{W}_z, \tilde{M}_x, \tilde{M}_y\}$ for face seal

$\{\tilde{W}\}_{old}$ = $\{\tilde{W}\}$ at previous iteration in eccentricity homing process

x,y = coordinate variables, see Fig. 1

Z = dimensionless axial coordinate for cylindrical seal, z/R_0

z = axial coordinate, measured from axial center for cyl. seal or from reference film, C, for face seal

α = groove to pitch ratio, $l_g/(l_g+l_r)$

α_{opt} = value of α for maximum stagnation pressure gradient in concentric cylindrical seal

β = spiral groove angle, angle between grooves and surface velocity

β_{opt} = value of β for maximum stagnation pressure gradient in concentric cylindrical seal

$\tilde{\beta}$ = numerical damping factor used in eccentricity homing process

Γ = film thickness ratio, h_g/h_r

$\Delta\bar{A}$ = dimensionless flow control area about single grid point, shaded area in Fig. 3

$\Delta\bar{A}_i$ = portion of $\Delta\bar{A}$ in quadrant containing point i, see Fig. 3

Δp = global pressure difference, see Fig. 2

$\Delta p'_g$ = pressure difference across groove, see Fig. 2

$\Delta p'_r$ = pressure difference across ridge, see Fig. 2

$\Delta\bar{S}^+_{ij}$ = line or arc length associated with Q^+_{ij}

$\Delta\bar{S}^-_{ij}$ = line or arc length associated with Q^-_{ij}

Δs = transverse length of groove-ridge pair

$\Delta\theta$ = circumferential extent of groove-ridge pair, see Fig. 2; (also used generally for change in θ)

$\Delta\theta_g$ = circumferential extent of groove, see Fig. 2

$\Delta\theta_r$ = circumferential extent of ridge, see Fig. 2

$\tilde{\delta}$ = dimensionless groove depth, $(h_g-h_r)/C$

$\tilde{\delta}_{opt}$ = value of $\tilde{\delta}$ for maximum stagnation pressure gradient in concentric cylindrical seal

$\varepsilon_x,\varepsilon_y$ = eccentricity ratio, $(e_x,e_y)/C$ (cylindrical seal)

ε_z = axial displacement ratio e_z/C, (face seal)

ε_k = kth component of eccentricity matrix

$[\varepsilon]$ = row matrix of eccentricity components, $[\varepsilon_z,\phi,\psi]$ (face seal) and $[\varepsilon_x,\varepsilon_y,\phi,\psi]$ (cylindrical seal)

$\{\varepsilon\}$ = column vector, transpose of $[\varepsilon]$

$\{\varepsilon\}_{old}$ = $\{\varepsilon\}$ at previous iteration in homing process

ε' = eccentricity disturbance function (scaler)

η = small increment used in perturbations and in evaluating derivatives

θ = angular coordinate, see Fig. 1

θ = angular coordinate at start of groove

Λ = compressibility number, $6\mu\omega R_0^2/(p_0C^2)$

Λ_δ = groove compressibility number, $\Lambda\tilde{\delta}\tilde{\omega}\alpha(1-\alpha)\sin\beta$

μ = viscosity

σ = squeeze number, $2\Lambda\tilde{\Omega}$

τ = global shear stress

$\tilde{\tau}$ = dimensionless shear stress, $\tau R_0/(p_0C)$

τ' = local shear stress

Φ = rotation about x axis

ϕ = reduced rotation, $\Phi R_0/C$

Ψ = rotation about y axis

ψ = reduced rotation $\Psi R_0/C$

Ω = angular velocity of disturbance

$\tilde{\Omega}$ - dimensionless disturbance frequency, Ω/ω

ω = total angular velocity, $\omega_1 + \omega_2$

$\tilde{\omega}$ = dimensionless angular velocity ratio, $(\omega_2-\omega_1)/\omega$

ω_1 = angular velocity of grooved surface

ω_2 = angular velocity of smooth surface

$\vec{\nabla}$ = gradient operator, $(1/r)(\partial/\partial\theta)\vec{i} + (\partial/\partial s)\vec{j}$, on dimensional quantities and $(1/R)(\partial/\partial\theta)\vec{i} + (\partial/\partial S)\vec{j}$, on dimensionless quantities

NOMENCLATURE FOR CODE SPIRALI

[A]	=	apparent mass matrix, see Eq. (3-90)
[B]	=	damping matrix, see subscripts below for definitions of components
$[\tilde{B}]$	=	dimensionless stiffness matrix, see Eq. (3-89) for component scale factors
C	=	clearance (cylindrical seal) or reference film thickness (face seal)
e_x, e_z	=	displacements of center of seal in x,z directions, see Fig. 6
$\tilde{e}_x, \tilde{e}_z$	=	dimensionless displacements, e_x/C, e_z/C
$\tilde{e}_{x0}, \tilde{e}_{z0}$	=	dimensionless displacement amplitudes, see Eq. (3-60)
F	=	function defining derivatives, see Eqs. (3-56)-(3-58)
f	=	shear factor (¼ friction factor)
f_a	=	shear factor at surface (a), see Eq. (3-4)
f_b	=	shear factor at surface (b), see Eq. (3-5)
H	=	first-order film thickness
$\tilde{H}$	=	dimensionless film thickness, H/C
H_{BRL}	=	film change defining quadratic "barreling", see Fig. 12
H_r	=	first-order film thickness over ridges
H_{TAP}	=	film change defining linear taper, see Fig. 12
h	=	film thickness
$\tilde{h}$	=	dimensionless film thickness, h/C
h'	=	second-order film thickness
$\tilde{h}'$	=	dimensionless film thickness, h'/C
h_g	=	film thickness over grooves, see Fig. 10
$\tilde{h}_g$	=	dimensionless film thickness, h_g/C
h_r	=	film thickness over ridges, see Fig. 10
$\tilde{h}_r$	=	dimensionless film thickness, h_r/C
[I]	=	unit diagonal matrix of order N
I_c	=	cylindrical seal flag parameter, I_c=1 for cylindrical seal, I_c=0 for face seal
I_f	=	face seal flag parameter, I_f=1 for face seal, I_f=0 for cylindrical seal

I_ω = rotating groove flag parameter, I_ω=1 for grooves on rotor, I_ω=0 for grooves on stator

I = unit imaginary number, $\sqrt{-1}$

$\vec{i}, \vec{j}$ = unit vectors in θ,s directions

$\Im(Z)$ = imaginary part of complex number, Z

J_k = see Eq. (3-64)

$[K]$ = stiffness matrix, see subscripts below for definitions of components

$[\tilde{K}]$ = dimensionless stiffness matrix, see Eq. (3-88) for component definitions

$[K^0]$ = stiffness matrix, [K] at Ω=0

$[k]$ = derivative matrix used in numerical solution, see Eq. (3-58) for definitions of components

L = seal length, see Fig. 6

M_x, M_y = applied moments about x, y axes

$\tilde{M}_x, \tilde{M}_y$ = dimensionless moments, $M_x/(p_0 r_0^3)$, $M_y/(p_0 r_0^3)$

m_a = exponent in shear factor power law relationship for surface(a), $f_a = n_a R_a^{m_a}$

m_b = exponent in shear factor power law relationship for surface(a), $f_b = n_b R_b^{m_b}$

m_0 = exponent for shear factor power law based on Blasius relationship, see Eq. (3-7)

N = order of system of ordinary differential equations, see Eqs. (3-56)-(3-58)

N_g = number of grooves

n_a = coefficient in shear factor power law relationship for surface(a), $f_a = n_a R_a^{m_a}$

n_b = coefficient in shear factor power law relationship for surface(a), $f_b = n_b R_b^{m_b}$

n_0 = coefficient for shear factor power law based on Blasius relationship, see Eq. (3-7)

$\vec{n}_\beta$ = unit vector normal to grooves, see Fig. 10

P = first-order pressure

$\tilde{P}$ = dimensionless pressure, P/p_0

$\tilde{P}_{g,\theta}$ = dimensionless first-order local tangential pressure gradient over grooves see Eq. (3-94)

p = pressure

$\tilde{p}$ = dimensionless pressure, p/p_0

p' = second-order pressure

$\tilde{p}'$ = dimensionless pressure, p'/p_0

p_0 = reference pressure

$\tilde{p}^*$ = dimensionless parameter, $\mu V_0 r_0/(4C^2 p_0)$

p_J = pressure at upstream side of jump in film thickness

p_J' = second-order pressure at upstream side of jump in film thickness

$\hat{p}_k$ = component of second-order pressure, $\tilde{p}'$, associated with δ_k, see Eq. (3-65)

$\hat{p}_k^+, \hat{p}_k^-$ = complex, second-order, dimensionless component pressures, see Eqs. (3-66)-(3-67)

$\bar{p}_k^+, \bar{p}_k^-$ = complex S dependent factors of $\hat{p}_k^+$ and $\hat{p}_k^-$ respectively, see Eq. (3-67)

p_{ex} = pressure at exit side of seal

p_{in} = pressure at inlet side of seal

$\tilde{p}_{ex}, \tilde{p}_{in}$ = dimensionless pressures, p_{ex}/p_0, p_{in}/p_0

$p_{g,\theta}, p_{g,s}$ = local pressure gradients over grooves in tangential ($p_{g,\theta}$) and transverse ($p_{g,s}$) directions

$\tilde{p}_{g,\theta}, \tilde{p}_{g,s}$ = dimensionless local pressure gradients $r_0 p_{g,\theta}/p_0$, $r_0 p_{g,s}/p_0$, see Eqs. (3-24)-(3-25)

$p_{r,\theta}, p_{r,s}$ = local pressure gradients over ridges in tangential ($p_{r,\theta}$) and transverse ($p_{r,s}$) directions

$\tilde{p}_{r,\theta}, \tilde{p}_{r,s}$ = dimensionless local pressure gradients $r_0 p_{r,\theta}/p_0$, $r_0 p_{r,s}/p_0$, see Eqs. (3-26)-(3-27)

$\wp$ = power loss

$\tilde{\wp}$ = dimensionless power loss, $\wp/(Cp_0 r_0^2 \omega)$

Q = volumetric flow rate in transverse (s) direction

$\tilde{q}_{g\theta}, \tilde{q}_{gs}$ = dimensionless flow components over grooves, $\tilde{u}_g \tilde{h}_g$, $\tilde{v}_g \tilde{h}_g$

$\tilde{q}_{r\theta}, \tilde{q}_{rs}$ = dimensionless flow components over ridges, $\tilde{u}_r \tilde{h}_r$, $\tilde{v}_r \tilde{h}_r$

q_n = flow rate in $\vec{n}_\beta$ direction relative to spiral groove motion

$\tilde{q}_n$ = dimensionless flow rate normal to spiral grooves, $q_n/(h_0 V_0)$

R = Reynolds number, see Eq. (3-9)

R^* = characteristic inertia parameter, $2CR/r_0$

R_a = local Reynolds number associated with surface (a), see Eq. (3-6)

R_b = local Reynolds number associated with surface (b), see Eq. (3-6)

r = radial coordinate, taken as r_0 for cylindrical seal

$\tilde{r}$ = dimensionless coordinate, r/r_0, taken as 1 for cylindrical seal

r_0 = reference radius, taken as outside radius for face seal and shaft radius for cylindrical seal

$\Re(Z)$ = real part of complex number, Z

S = dimensionless coordinate, s/r_0

S_J = dimensionless coordinate s_J/r_0

S_L, S_R = dimensionless boundary coordinates s_L/r_0, s_R/r_0

S_{in}, S_{ex} = dimensionless coordinates s_{in}/r_0, s_{ex}/r_0

s = transverse coordinate, s = r for a face seal and s = z for a cylindrical seal

s_J = s coordinate at jump in film thickness

s_L = left boundary coordinate, inside radius for face seal and s_L = -L/2 for cylindrical seal

s_R = right boundary coordinate, $s_R = r_0$ for face seal and s_R = L/2 for cylindrical seal

s_{ex} = s coordinate at exit from seal

s_{in} = s coordinate at inlet to seal

t = time

$\tilde{t}$ = dimensionless time, $V_0 t/r_0$

$\vec{t}_\beta$ = unit vector tangent to grooves, see Fig.10

U = first order tangential (θ) velocity component

$\tilde{U}$ = dimensionless velocity, U/V_0

u = tangential (θ) velocity component

$\tilde{u}$ = dimensionless velocity, u/V_0

u' = second-order tangential (θ) velocity component

$\tilde{u}'$ = dimensionless velocity u'/V_0

$\vec{u}$ = fluid velocity vector

$\vec{u}_a$ = velocity of surface a, see Fig. 7

$\vec{u}_b$ = velocity of surface b, see Fig. 7

u_g, u_r = tangential velocity over grooves (u_g), ridges (u_r)

$\tilde{u}_g, \tilde{u}_r$ = dimensionless velocity components u_g/V_0, u_r/V_0

u_{in} = tangential velocity component at inlet side of seal

$\tilde{u}_{in}$ = dimensionless velocity, u_{in}/V_0

$\hat{u}_k$ = component of $\tilde{u}'$, associated with δ_k, see Eq. (3-65)

$\hat{u}_k^+, \hat{u}_k^-$ = complex, second-order, dimensionless component tangential velocities, see Eqs. (3-66)-(3-67)

$\bar{u}_k^+, \bar{u}_k^-$ = complex S dependent factors of $\hat{u}_k^+$ and $\hat{u}_k^-$ respectively, see Eq. (3-67)

V = first-order transverse (s) velocity component

$\tilde{V}$ = dimensionless velocity, V/V_0

V_0 = reference velocity

v = transverse (s) velocity component

$\tilde{v}$ = dimensionless velocity component, v/V_0

v' = second-order transverse (s) velocity component

$\tilde{v}'$ = dimensionless velocity v'/V_0

v_g, v_r = transverse velocity over grooves (v_g), ridges (v_r)

$\tilde{v}_g, \tilde{v}_r$ = dimensionless velocity components v_g/V_0, v_r/V_0

v_J = s velocity component at upstream side of jump in film thickness

$\tilde{v}_J$ = dimensionless velocity v_J/V_0

v_J' = second-order s velocity component at upstream side of jump in film thickness

$\tilde{v}_J'$ = dimensionless velocity v_J'/V_0

$\hat{v}_k$ = component of $\tilde{v}'$, associated with δ_k, see Eq. (3-65)

$\hat{v}_k^+, \hat{v}_k^-$ = complex, second-order, dimensionless component transverse velocities, see Eqs. (3-66)-(3-67)

$\bar{v}_k^+, \bar{v}_k^-$ = complex S dependent factors of $\hat{v}_k^+$ and $\hat{v}_k^-$ respectively, see Eq. (3-67)

W_z = first-order axial load applied to face seal

$\tilde{W}_z$ = dimensionless load, $W_z/(p_0 r_0^2)$

w_x, w_y, w_z = applied loads in x, y, z directions

$\tilde{w}_x, \tilde{w}_y, \tilde{w}_z$ = dimensionless loads, $w_x/(p_0 r_0^2)$, $w_y/(p_0 r_0^2)$, $w_z/(p_0 r_0^2)$

x, y, z = coordinate variables, see Fig. 6

$\{Y\}$ = column vector of independent variables at old grid point, see Eqs. (3-56)-(3-58)

$\{Y^{new}\}$ = column vector of independent variables at new grid point, see Eqs. (3-56)-(3-58)

α = groove to pitch ratio, $\Delta\theta_g/(\Delta\theta_g+\Delta\theta_r)$

β = spiral groove angle, angle between grooves and surface velocity

Δh = jump in film thickness (downstream - upstream)

$\tilde{\Delta h}$ = dimensionless jump in film thickness, $\Delta h/C$

Δp = jump in pressure at s_J, $p-p_J$

$\Delta\tilde{p}$ = dimensionless jump in pressure, $\Delta p/p_0$

$\Delta\tilde{p}'$ = dimensionless second-order jump in pressure at S_J, $(p'-p_J')/p_0$

$\Delta p_g, \Delta p_r$ = spiral groove downstream - upstream pressure jump at entrance to grooves, (Δp_g) or ridges, (Δp_r)

$\Delta\tilde{p}_g, \Delta\tilde{p}_r$ = dimensionless spiral groove pressure jumps, $\Delta p_g/p_0$, $\Delta p_r/p_0$

ΔS = variable increment between grid points used in numerical solutions, see Eqs. (3-57)-(3-58)

$\Delta\theta$ = circumferential extent of groove-ridge pair, see Fig. 10

$\Delta\theta_g$ = circumferential extent of groove, see Fig. 10

$\Delta\theta_r$ = circumferential extent of ridge, see Fig. 10

δ = groove depth, h_g-h_r

$\tilde{\delta}$ = dimensionless groove depth, δ/C

δ_k = dimensionless component film displacements, see Eqs. (3-59)-(3-61)

δ_k^+, δ_k^- = complex dimensionless component displacements associated with $+\tilde{\Omega}$ and $-\tilde{\Omega}$, respectively, see Eq. (3-63)

ε_k = set of amplitudes, see Eq. (3-64)

ζ = loss coefficient due to contraction

η_k = see Eq. (3-64)

θ = angular coordinate, see Fig. 6

λ = correction factor applied to $\tilde{\tau}_c$, see Eq. (3-94)

μ = viscosity

ξ = loss coefficient, see Eq. (3-18)

ρ = density

τ = tangential shear stress

$\tilde{\tau}$ = dimensionless shear stress, $r_0\tau/(Cp_0)$

τ_a = tangential shear stress, surface (a)

$\tilde{\tau}_a$ = dimensionless shear stress, $r_0\tau_a/(Cp_0)$

$\vec{\tau}_a$ = shear traction vector for surface (a), see Fig. 7

τ_b = tangential shear stress, surface (b)

$\tilde{\tau}_b$ = dimensionless shear stress, $r_0\tau_b/(Cp_0)$

$\vec{\tau}_b$ = shear traction vector for surface (b), see Fig. 7

$\tilde{\tau}_c$ = dimensionless tangential Couette shear stress, $(\tilde{\tau}_a + \tilde{\tau}_b)/2$

$\vec{\tau}_c$ = Couette shear traction vector, $(\vec{\tau}_a + \vec{\tau}_b)/2$

$\tilde{\tau}_p$ = dimensionless tangential Poiseuille shear stress, $(\tilde{\tau}_a - \tilde{\tau}_b)/2$

$\vec{\tau}_p$ = Poiseuille shear traction vector, $(\vec{\tau}_a - \vec{\tau}_b)/2$

$\tilde{\tau}^*$ = dimensionless effective shear stress, see Eq. (3-92)

$\tilde{\tau}_g^*, \tilde{\tau}_r^*$ = values of $\tilde{\tau}^*$ obtained from first-order solutions for grooves and ridges, respectively

Φ, Ψ = turbulent shear functions, see Eqs. (3-14)-(3-15)

Φ^*, Ψ^* = global functions defined by Eqs. (3-42)-(3-43)

Φ_g, Ψ_g = turbulent shear functions over grooves, see Eq. (3-22)

Φ_r, Ψ_r = turbulent shear functions over ridges, see Eq. (3-23)

χ = function for predicting pressure change at jump in film thickness, see Eq. (3-17)

ψ = rotation about y axis, see Fig. 6

$\tilde{\psi}_0$ = dimensionless amplitude, see Eq. (3-60)

Ω = angular velocity of oscillation

$\tilde{\Omega}$ = dimensionless angular velocity, $\Omega r_0/V_0$

$\tilde{\Omega}^+, \tilde{\Omega}^-$ = see Eq. (3-71)

ω = angular velocity of rotor

$\tilde{\omega}$ = dimensionless angular velocity, $\omega r_0/V_0$

Subscripts

a,b = relating to surface (a),(b) shown in Fig. 2, generally (a) is moving, (b) is stationary

ex = exit

g = grooves

$\tilde{H},\tilde{U},\tilde{V}$	=	partial derivatives with respect to $\tilde{H}$, $\tilde{U}$ and $\tilde{V}$, respectively
in	=	inlet
J	=	jump discontinuity in global film thickness
k	=	index associated with displacements, see Eq. (3-64)
L	=	left or lower value of s
R	=	right or upper value of s
r	=	ridges
x	=	pertains to force or displacement in the x direction
y	=	pertains to force or displacement in the y direction
ϕ	=	pertains to moment or rotation about x axis
ψ	=	pertains to moment or rotation about y axis

1.0 INTRODUCTION

NASA's advanced engine programs are aimed at progressively higher efficiencies, greater reliability, and longer life. Recent studies have indicated that significant engine performance advantages can be achieved by employing advanced seals [1]*, and dramatic life extensions can also be achieved. Advanced seals are not only required to control leakage, but are necessary to control lubricant and coolant flow, prevent entrance of contamination, inhibit the mixture of incompatible fluids, and assist in the control of rotor response.

Recognizing the importance and need of advanced seals, NASA, in 1990, embarked on a five-year program (Contract NAS3-25644) to provide the U.S. aerospace industry with computer codes that would facilitate configuration selection and the design and application of advanced seals.

The program included four principal activities:

1. Development of a scientific code called SCISEAL, which is a Computational Fluid Dynamics (CFD) code capable of producing full three-dimensional flow field information for a variety of cylindrical configurations. The code is used to enhance understanding of flow phenomena and mechanisms, to predict performance of complex situations, and to furnish accuracy standards for the industrial codes. The SCISEAL code also has the unique capability to produce stiffness and damping coefficients that are necessary for rotordynamic computations.
2. Generation of industrial codes for expeditious analysis, design, and optimization of turbomachinery seals. The industrial codes consist of a series of separate stand-alone codes that were integrated by a Knowledge-Based System (KBS).
3. Production of a KBS that couples the industrial codes with a user friendly Graphical User Interface (GUI) that can in the future be integrated with an expert system to assist in seal selection and data interpretation and provide design guidance.
4. Technology transfer via four multiday workshops at NASA facilities where the results of the program were presented and information exchanged among suppliers and users of advanced seals. A Peer Panel also met at the workshops to provide guidance and suggestions to the program.

This final report has been divided into separate volumes, as follows:

Volume 1: Executive Summary and Description of Knowledge-Based System
Volume 2: Description of Gas Seal Codes GCYLT and GFACE
Volume 3: Description of Spiral-Groove Codes SPIRALG and SPIRALI
Volume 4: Description of Incompressible Seal Codes ICYL and IFACE
Volume 5: Description of Seal Dynamics Code DYSEAL and Labyrinth Seal Code KTK
Volume 6: Description of Scientific CFD Code SCISEAL.

*Numbers in brackets indicate references located in Section 4.0.

This volume describes two industrial codes used to predict the behavior of both cylindrical and face seals with or without the inclusion of spiral grooves: SPIRALG and SPIRALI. This includes load capacity (for face seals), leakage flow, power requirements and dynamic characteristics in the form of stiffness, damping, and apparent mass coefficients in 4 degrees of freedom for cylindrical seals and 3 degrees of freedom for face seals. The code SPIRALG treats laminar flow in gas seals operating at finite eccentricities. The code SPIRALI deals with high-speed incompressible flow and includes turbulence and other inertia effects but is limited to small eccentricities. References 2 and 3 provide the details of code implementation.

Turbulence and inertia have been included in the incompressible code, SPRIALI, at the expense of the effects of large eccentricity. Cryogenic liquids have relatively low kinematic viscosities, and seals for such liquids are sometimes designed to run at relatively high clearances. In such cases, stiffness effects associated with inertia can provide far greater stabilization than eccentricity effects for laminar gas seals. In addition, SPIRALG can be run at high ambient pressure to simulate noncavitating incompressible seals at finite eccentricities.

2.0 INDUSTRIAL CODE SPIRALG – GAS-LUBRICATED, SPIRAL GROOVE, CYLINDRICAL AND FACE SEALS

The computer code SPIRALG predicts performance characteristics of gas-lubricated, spiral groove, cylindrical and face seals. Performance characteristics include load capacity, leakage flow, power requirements and dynamic characteristics in the form of stiffness and damping coefficients in four degrees of freedom for cylindrical seals and three degrees of freedom for face seals. These performance characteristics are computed as functions of seal and groove geometry, loads or film thicknesses, running speed, fluid viscosity, and boundary pressures.

The basic assumptions that have gone into the computer code are listed below:

1. The flow is assumed to be laminar and isothermal.
2. Inertial effects are neglected.
3. The gas is assumed to be ideal.
4. The film thickness is assumed to be small compared with seal lengths and diameters but large compared with surface roughness and the mean free path of the gas.
5. Narrow groove theory is used which characterizes the effects of grooves by a global pressure distribution without requiring computations on a groove by groove basis. This involves neglecting edge effects and local compressibility effects associated with groove to groove pressure variations. In general, narrow groove theory is valid when there are a sufficiently large number of grooves so that $2\pi/N_g << 1$, where β is the groove angle and N_g is the number of grooves.
6. Transient effects are treated with the use of small perturbations on a primary steady-state flow. These transient effects are characterized by stiffness and damping coefficients that are dependent on the disturbance frequencies.
7. Although displacements and misalignments are treated, machined surfaces for face seals are assumed to be flat and machined clearances for cylindrical seals are assumed to be constant.

The above assumptions still leave the code applicable to a broad range of applications. Seals generally have small clearances and gasses have low densities resulting in sufficiently low Reynolds numbers for laminar flow. Practical designs should contain a fairly large number of grooves to ensure smooth, isotropic operation. At high sealed pressure differences the flow could become sonic thereby invalidating the first two assumptions but this will usually not be the case and can readily be checked based on the predicted leakage flow. Elastic and thermal distortions as well as machining tolerances should also be estimated to validate the constant clearance assumption. The overall accuracy of the program will depend on the grid size used. Factors such as high compressibility or squeeze numbers, small values of the minimum film thickness to clearance ratio and large values of the length to diameter ratio could require either a large number of grid points or carefully selected variable grids.

2.1 Theoretical Development

The first formulation of the equations governing gas-lubricated spiral groove bearings is generally credited to Vohr and Pan [4]. A more concise formulation is given in a second report [5] by these authors that has been used by Smalley [6] as a starting point in his generalized numerical treatment of the performance of spiral groove gas bearings. The work performed by Smalley may be applied to both bearings and seals. A principal limitation in all of the above references relates to the fact that solutions have only been provided for one dimensional forms of the equations which have been obtained by linearizing them based on near concentric and aligned conditions. The work described here deals with the numerical solution of the nonlinear equations for gas-lubricated spiral groove seals at both eccentric and misaligned conditions.

2.1.1 Formulation of Equations Governing Gas-Lubricated Spiral Groove Seals

For completeness, a derivation of the narrow groove equations for spiral groove gas bearings and seals along the lines of that developed in Reference 5 will be provided here. Coordinate variables will be used to make the equations applicable to both cylindrical and face seals as can be seen with the aid of Figure 1. The circumferential coordinate, θ, is as shown in Figure 1. The transverse coordinate is described by the variable, s, which is taken to equal the radial coordinate, r, for a face seal and the axial coordinate, z, for a cylindrical seal. The quantity r, when it appears will denote radial position for a face seal and should be set equal to the shaft radius, R_0 for a cylindrical seal.

The isothermal, compressible form of the "Reynolds" equation may be written as a flow balance equating the divergence of the flow vector, $\vec{q}'$, to the flow per unit area squeezed out by the time rate of decrease of the film thickness, q_A'.

$$\vec{\nabla}\cdot\vec{q}' = \frac{1}{r}\frac{\partial}{\partial s}(rq_s') + \frac{1}{r}\frac{\partial q_\theta'}{\partial \theta} = q_A' \quad , \tag{2-1}$$

The local flow vector $\vec{q}' = q_\theta'\vec{i} + q_s'\vec{j}$ represents the mass flow rate per unit transverse length divided by the density at a reference pressure, p_0, which may be written in vector form as

$$\vec{q}' = -\frac{h^3}{12\mu}\frac{p'}{p_0}\vec{\nabla}p' + \frac{\vec{u}_1 + \vec{u}_2}{2}\frac{p'}{p_0}h \quad .$$

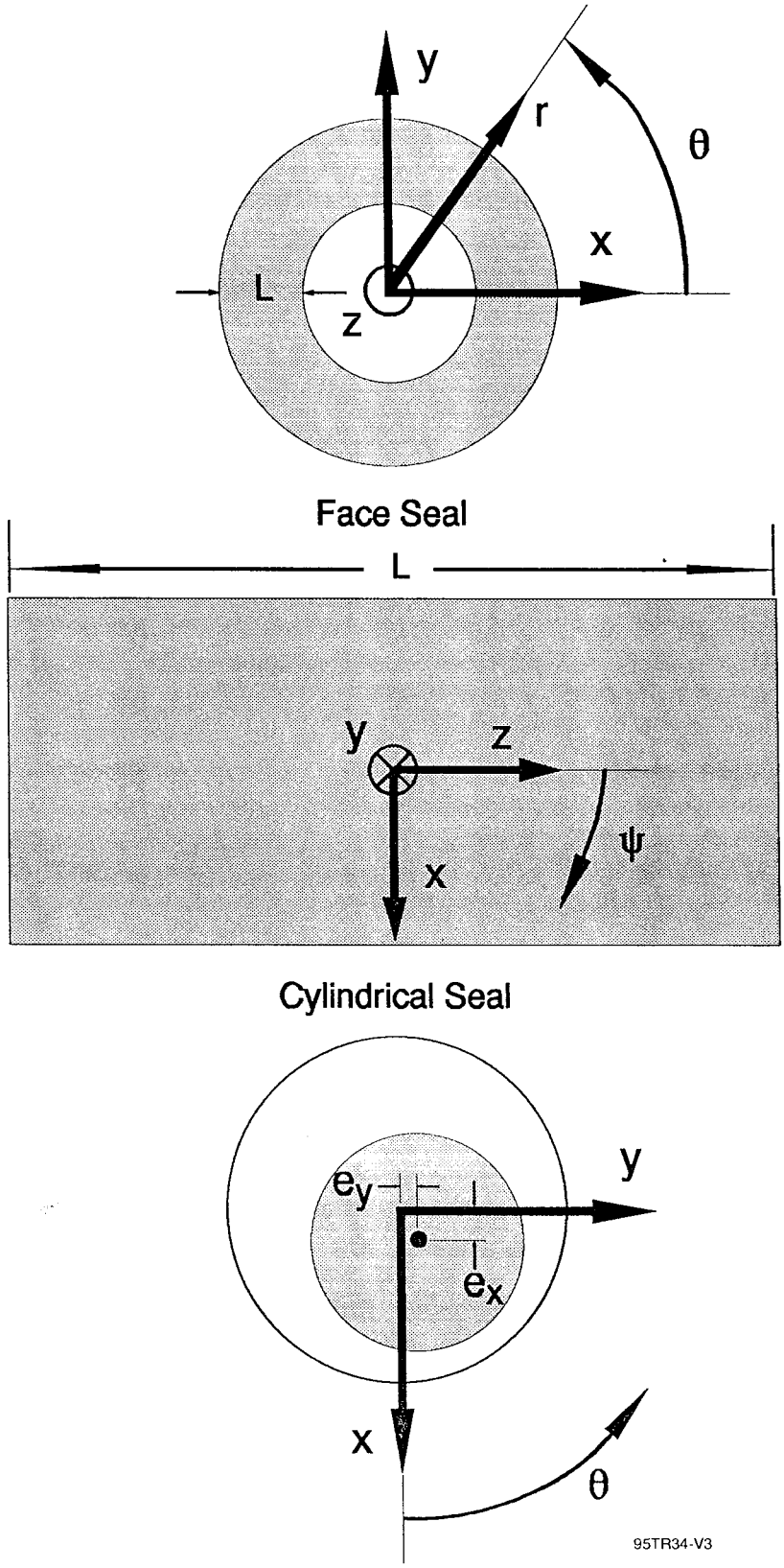

Figure 1. Coordinate System for Spiral Groove Analysis

Since surface motion will be in the circumferential direction, the surface velocity vectors may be written as $\vec{u}_1 = r\omega_1\vec{i}$ and $\vec{u}_2 = r\omega_2\vec{i}$ and the components of $\vec{q}'$ become

$$q_\theta' = -\frac{h^3}{12\mu}\frac{p'}{p_0}\frac{1}{r}\frac{\partial p'}{\partial \theta} + r\frac{\omega_1 + \omega_2}{2}\frac{p'}{p_0}h \quad , \tag{2-2}$$

$$q_s' = -\frac{h^3}{12\mu}\frac{p'}{p_0}\frac{\partial p'}{\partial s} \quad . \tag{2-3}$$

The "squeeze film" term or displaced mass flow per unit area due to film motion, divided by the density at p_0 is

$$q_A' = -\frac{1}{p_0}\frac{\partial (p'h)}{\partial t} \tag{2-4}$$

One could substitute Equations (2-2) - (2-4) for the corresponding flow quantities in Equation (2-1) to obtain the usual form of the compressible Reynolds Equation which could in principle be solved, for any film thickness profile, $h(s,\theta)$ and appropriate boundary conditions, for the pressures or flow components to obtain the pressure distribution. These could in turn be integrated to obtain the various forces and moments associated with the given bearing geometry. The torque opposing the motion of say the smooth surface may be determined, once the pressure distribution is known, by integrating the shear stress relationship that arises in the development of Reynolds equation

$$\tau' = \frac{h}{2r}\frac{\partial p'}{\partial \theta} + \mu r\frac{\omega_2 - \omega_1}{h} \quad . \tag{2-5}$$

The difficulty encountered in obtaining full numerical solutions to the above equations relates to the complexity of the grid network necessary to adequately describe the geometry of a surface containing the large number of spiral grooves usually required to provide sufficiently smooth pressure distributions to make the load characteristics independent of whether shaft displacement is over a ridge or over a groove. Narrow groove theory is generally used to circumvent this difficulty (References 4 - 6). It will be implemented here, as well and is described below.

Narrow groove theory provides the limiting form of the solution to Equations (2-1) - (2-5) as the number of grooves, N_g, becomes large, with the groove angle, β and the groove to pitch ratio, α, held constant. The discontinuities in film thickness associated with the grooves will give rise to discontinuities in the pressure gradients at the ridge-groove interfaces as illustrated schematically in Figure 2. The local pressure profile p' is shown by the sawtooth lines whose lower vertices, for purposes of illustration, are connected by the "global" pressure profile, p. The global pressure profile does not necessarily lie at the lower vertices of the local pressure profile but could lie anywhere between the lower and upper vertices. In the limit as the number of grooves becomes large the curve connecting the upper vertices will

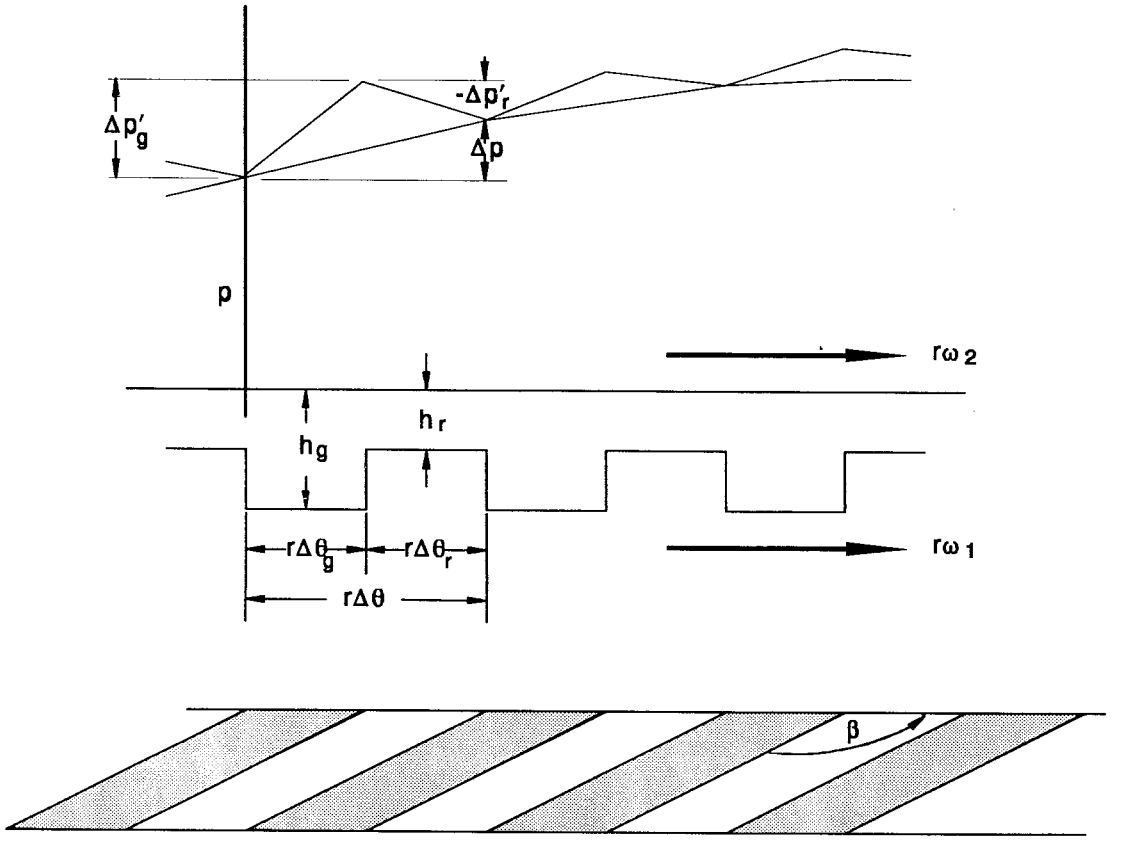

Figure 2. Schematic of Spiral Groove Parameters, Global and Local Pressures

approach the curve connecting the lower vertices. This limiting behavior is not true of $\partial p'/\partial\theta$, $\partial p'/\partial s$ or h, which will have different values over lands and grooves no matter how large the number of grooves. Narrow groove theory requires the development of expressions for the local (primed) quantities in terms of global quantities that approach single valued limits as the number of grooves becomes large. The local film thickness and pressure derivatives over the grooves will be denoted by h_g, $(\partial p'/\partial\theta)_g$ and $(\partial p'/\partial s)_g$ respectively and by h_r, $(\partial p'/\partial\theta)_r$ and $(\partial p'/\partial s)_r$ over the ridges. (The subscript r has been used here to denote ridges for consistency with References 4 - 6 and should not be confused when used in a different context later in the report to denote the right-hand boundary pressure or with the radial position variable, r, which is not used as a subscript.)

When the number of grooves becomes large, the sawtooth portion of the local pressure variation may be approximated with linear representations as shown in Figure 2. Thus, equating pressures over a groove-ridge pair in the circumferential direction

$$\frac{\Delta p}{\Delta\theta} = \frac{\Delta p_g'}{\Delta\theta} + \frac{\Delta p_r'}{\Delta\theta} = \left(\frac{\partial p'}{\partial\theta}\right)_g \frac{\Delta\theta_g}{\Delta\theta} + \left(\frac{\partial p'}{\partial\theta}\right)_r \frac{\Delta\theta_r}{\Delta\theta} \quad .$$

Noting that $\Delta\theta_g/\Delta\theta = \alpha$ and $\Delta\theta_r/\Delta\theta = 1 - \alpha$ and replacing $\Delta p/\Delta\theta$ with $\partial p/\partial\theta$ as $\Delta\theta \rightarrow 0$, the above equation becomes

$$\frac{\partial p}{\partial\theta} = \alpha\left(\frac{\partial p'}{\partial\theta}\right)_g + (1-\alpha)\left(\frac{\partial p'}{\partial\theta}\right)_r \quad . \qquad 2\text{-}6$$

The corresponding relationship in the transverse direction,

$$\frac{\partial p}{\partial s} = \alpha\left(\frac{\partial p'}{\partial s}\right)_g + (1-\alpha)\left(\frac{\partial p'}{\partial s}\right)_r \quad , \qquad 2\text{-}7$$

is obtained in a similar manner.

The remaining two equations required to solve for the four local pressure derivatives are obtained from continuity considerations. First, the pressure must be continuous at each groove-ridge interface, thus the derivative of the pressure in the direction of the interface, $\vec{\nabla}p' \bullet \vec{t}_\beta$, must also be continuous. The second requirement is for continuity of the flow normal to each groove-ridge interface as measured in a frame of reference moving with the grooves, $(\vec{q}' - r\omega_1 h p'/p_0\, \vec{i}) \bullet \vec{n}_\beta$. The unit tangent and normal vectors for a logarithmic spiral are given by

$$\vec{t}_\beta = \cos\beta\vec{i} + \sin\beta\vec{j} \ , \quad \vec{n}_\beta = \sin\beta\vec{i} - \cos\beta\vec{j} \quad .$$

The first of the above conditions requires continuity of

$$\frac{\cos\beta}{r}\frac{\partial p'}{\partial\theta} + \sin\beta\frac{\partial p'}{\partial s}$$

at each groove-ridge interface or

$$\frac{\cos\beta}{r}\left(\frac{\partial p'}{\partial\theta}\right)_g + \sin\beta\left(\frac{\partial p'}{\partial s}\right)_g = \frac{\cos\beta}{r}\left(\frac{\partial p'}{\partial\theta}\right)_r + \sin\beta\left(\frac{\partial p'}{\partial s}\right)_r \quad . \tag{2-8}$$

The second condition requires continuity of

$$(q_\theta' - r\omega h\frac{p'}{p_0})\sin\beta - q_r'\cos\beta \quad .$$

One may substitute Equations (2-2) and (2-3) for the circumferential and transverse components of the flow vector at each groove-ridge interface, respectively to obtain

$$-\frac{h_g^3}{12\mu}\left[\frac{\sin\beta}{r}\left(\frac{\partial p'}{\partial\theta}\right)_g - \cos\beta\left(\frac{\partial p'}{\partial s}\right)_g\right] + \frac{h_g}{2}r(\omega_2-\omega_1)\sin\beta =$$

$$-\frac{h_r^3}{12\mu}\left[\frac{\sin\beta}{r}\left(\frac{\partial p'}{\partial\theta}\right)_r - \cos\beta\left(\frac{\partial p'}{\partial s}\right)_r\right] + \frac{h_r}{2}r(\omega_2-\omega_1)\sin\beta \quad . \tag{2-9}$$

Density variation, p'/p_0, is continuous at each interface and cancels out of Equation (2-9).

Equations (2-6) - (2-9) represent the four linear equations needed to solve for the local pressure derivatives. We may obtain the solution by first solving Equations (2-8) and (2-9) for the components of the local pressure gradient over the grooves in terms of those over the ridges. The resulting equations may be written as

$$\frac{1}{r}\left(\frac{\partial p'}{\partial\theta}\right)_g = \frac{h_g^3\cos^2\beta + h_r^3\sin^2\beta}{h_g^3}\frac{1}{r}\left(\frac{\partial p'}{\partial\theta}\right)_r + \frac{h_g^3 - h_r^3}{h_g^3}\sin\beta\cos\beta\left(\frac{\partial p'}{\partial s}\right)_r$$

$$+ 6\mu r(\omega_2-\omega_1)\sin^2\beta\frac{h_g - h_r}{h_g^3} \quad , \tag{2-10}$$

$$\left(\frac{\partial p'}{\partial s}\right)_g = \frac{h_g^3 - h_r^3}{h_g^3}\sin\beta\cos\beta\frac{1}{r}\left(\frac{\partial p'}{\partial\theta}\right)_r + \frac{h_g^3\sin^2\beta + h_r^3\cos^2\beta}{h_g^3}\left(\frac{\partial p'}{\partial s}\right)_r$$

$$- 6\mu r(\omega_2-\omega_1)\sin\beta\cos\beta\frac{h_g - h_r}{h_g^3} \quad . \tag{2-11}$$

One may now substitute Equation (2-10) for $(\partial p'/\partial\theta)_g$ in Equation (2-6) and Equation (2-11) for $(\partial p'/\partial s)_g$ in Equation (2-7) to obtain two linear equations for the components of the ridge pressure gradient which may in turn be solved to yield the following expressions:

$$\frac{1}{r}\left(\frac{\partial p'}{\partial\theta}\right)_r = \frac{[h_g^3 - \alpha(h_g^3 - h_r^3\cos^2\beta)]\frac{1}{r}\frac{\partial p}{\partial\theta} - \alpha(h_g^3 - h_r^3)\sin\beta\cos\beta\frac{\partial p}{\partial s} - 6\mu r(\omega_2 - \omega_1)\alpha(h_g - h_r)\sin^2\beta}{(1-\alpha)h_g^3 + \alpha h_r^3}\ , \qquad 2\text{-}12$$

$$\frac{1}{r}\left(\frac{\partial p'}{\partial s}\right)_r = \frac{-\alpha(h_g^3 - h_r^3)\sin\beta\cos\beta\frac{1}{r}\frac{\partial p}{\partial\theta} + [h_g^3 - \alpha(h_g^3 - h_r^3\sin^2\beta)]\frac{\partial p}{\partial s} + 6\mu r(\omega_2 - \omega_1)\alpha(h_g - h_r)\sin\beta\cos\beta}{(1-\alpha)h_g^3 + \alpha h_r^3} \qquad 2\text{-}13$$

The components of the local groove pressure gradient may be expressed in terms of the above ridge components by simple rearrangement of Equations (2-6) and (2-7):

$$\frac{1}{r}\left(\frac{\partial p'}{\partial\theta}\right)_g = -\frac{1-\alpha}{\alpha}\frac{1}{r}\left(\frac{\partial p'}{\partial\theta}\right)_r + \frac{1}{\alpha}\frac{1}{r}\frac{\partial p}{\partial\theta}\ , \qquad 2\text{-}14$$

$$\left(\frac{\partial p'}{\partial s}\right)_g = -\frac{1-\alpha}{\alpha}\left(\frac{\partial p'}{\partial s}\right)_r + \frac{1}{\alpha}\frac{\partial p}{\partial s}\ . \qquad 2\text{-}15$$

Now that expressions have been developed for the components of the local pressure gradients in terms of global ones, it is necessary to determine the global flow components q_s and q_θ and a global squeeze film term q_A that may be substituted for the local ones in the flow balance given by Equation (2-1). These global flow components are determined by matching mass flow rates over a groove-ridge pair with the mass flows obtained by integration of the local flow components over the same interval.

If θ_g is taken as the circumferential coordinate at the start of a groove, the transverse flow crossing an arc at fixed s, subtending a groove-ridge pair in the interval $\theta_g < \theta < \theta_g + \Delta\theta$ is given by the left-hand term in the relationship

$$\int_{\theta_g}^{\theta_g+\Delta\theta} q_s' r\,d\theta \approx -\frac{h_g^3}{12\mu}\frac{p}{p_0}\left(\frac{\partial p'}{\partial s}\right)_g r\Delta\theta_g - \frac{h_r^3}{12\mu}\frac{p}{p_0}\left(\frac{\partial p'}{\partial s}\right)_r r\Delta\theta_r = q_s r\Delta\theta\ .$$

The approximation to the integral in the above expression was obtained by dividing the integration interval, $\Delta\theta$ into sub-intervals for the groove, $\Delta\theta_g$ and ridge, $\Delta\theta_r$ and approximating q'_s, noting that as the number of grooves becomes large $\partial p'/\partial s$, will approach a constant value within each sub-interval. Since the pressure at the groove-ridge interface is continuous, the local density variation term, p'/p_0 was replaced by its global value p/p_0. The far right-hand term in the above expression is based on the definition of the transverse component of the global flow rate described above. The right two equalities may be solved for q_s as

$$q_s = -\frac{h_g^3}{12\mu}\frac{p}{p_0}\alpha\left(\frac{\partial p'}{\partial s}\right)_g - \frac{h_r^3}{12\mu}\frac{p}{p_0}(1-\alpha)\left(\frac{\partial p'}{\partial s}\right)_r \quad . \qquad 2\text{-}16$$

One may obtain a relationship for the circumferential flow component q_θ in a similar manner by integrating q'_θ, given by Equation (2-3), at fixed θ, over a groove-ridge pair ($s_g < s < s_g+\Delta s$), approximating the integral over each sub-interval as above and equating the result to $q_\theta\Delta s$. The resulting expression may be written as

$$q_\theta = -\frac{h_g^3}{12\mu}\frac{p}{p_0}\alpha\frac{1}{r}\left(\frac{\partial p'}{\partial \theta}\right)_g - \frac{h_r^3}{12\mu}\frac{p}{p_0}(1-\alpha)\frac{1}{r}\left(\frac{\partial p'}{\partial \theta}\right)_r + r\frac{\omega_1+\omega_2}{2}\frac{p}{p_0}[\alpha h_g + (1-\alpha)h$$

2-17

By integrating the squeeze film term q_A', given by Equation (2-4), over an area $r\Delta\theta\Delta s$, equating it to $q_A r\Delta\theta\Delta s$ and noting that the groove area fraction will be α and the ridge area fraction will be $1 - \alpha$, the following expression is obtained:

$$q_A = -\frac{1}{p_0}\frac{\partial}{\partial t}(p[\alpha h_g + (1-\alpha)h_r]) \quad . \qquad 2\text{-}18$$

The global shear stress τ, may be determined by integrating the local shear stress τ', given by Equation (2-5), with respect to θ over the interval $\theta_g < \theta < \theta_g+\Delta\theta$, invoking the narrow groove approximations and equating the result to $\tau\Delta\theta$. The resulting expression may be written in the form

$$\tau = \frac{\alpha h_g}{2}\frac{1}{r}\left(\frac{\partial p'}{\partial \theta}\right)_g + \frac{(1-\alpha)h_r}{2}\frac{1}{r}\left(\frac{\partial p'}{\partial \theta}\right)_r + \mu r(\omega_2-\omega_1)\left(\frac{\alpha}{h_g}+\frac{1-\alpha}{h_r}\right) \quad . \qquad 2\text{-}19$$

Equation (2-1) may now be applied directly to the global flow vector $\vec{q} = q_\theta \vec{i} + q_s \vec{j}$, as $\vec{\nabla} \bullet \vec{q} = q_A$ and by substituting Equation (2-18) for q_A and putting the result in dimensionless form one obtains:

$$\vec{\nabla} \cdot \vec{Q} = \frac{1}{R}\frac{\partial}{\partial S}(RQ_s) + \frac{1}{R}\frac{\partial Q_\theta}{\partial \theta} = -\frac{\partial}{\partial \tilde{t}}[(\alpha\tilde{\delta} + H_r)(1+P)] \quad . \tag{2-20}$$

The components of the global flow vector, q_θ and q_s are given in terms of the local pressure derivatives by Equations (2-16) and (2-17), respectively. These local derivatives are, in turn, given in terms of the global ones by Equations (2-12) - (2-15). The global flow components may be expressed completely in terms of global pressure derivatives by first substituting Equations (2-14) and (2-15) for the local pressure derivatives over the grooves and then substituting Equations (2-12) and (2-13) for the local pressure derivatives over the ridges. One may then collect terms and put the resulting two equations in dimensionless form to obtain the following expressions for the components of the dimensionless flow vector $\vec{Q} = Q_\theta \vec{i} + Q_s \vec{j}$:

$$Q_\theta = -(1+P)\left[H_r^3\left(k_2\frac{\partial}{\partial S} + \frac{k_3}{R}\frac{\partial}{\partial \theta}\right)P + \Lambda_\delta k_4 R\sin\beta - \Lambda(\alpha\tilde{\delta} + H_r)R\right] \quad , \tag{2-21}$$

$$Q_s = -(1+P)\left[H_r^3\left(k_1\frac{\partial}{\partial S} + \frac{k_2}{R}\frac{\partial}{\partial \theta}\right)P - \Lambda_\delta k_4 R\cos\beta\right] \quad . \tag{2-22}$$

The dimensionless variables associated with the above equations are

$$P = \frac{p - p_0}{p_0} \; , \; \vec{Q} = \frac{12\mu R_0}{C^3 p_0}\vec{q} \; , \; H_r = \frac{h_r}{C} \; , \; S = \frac{s}{R_0} \; , \; R = \frac{r}{R_0} \; , \; \tilde{t} = \frac{\omega}{2\Lambda}t \; , \; \Gamma = \frac{h_g}{h_r} \quad . \tag{2-23}$$

The dimensionless gage pressure P in the above equations is taken relative to the absolute pressure p_o which will henceforth be taken as the minimum of the two boundary pressures in absolute units. The dimensionless parameters associated with the above equations are

$$\Lambda = \frac{6\mu\omega R_0^2}{p_0 C^2} \; , \; \Lambda_\delta = \Lambda\tilde{\delta}\tilde{\omega}\alpha(1-\alpha)\sin\beta \; , \; \tilde{\omega} = \frac{\omega_2 - \omega_1}{\omega} \; , \; \tilde{\delta} = \frac{(h_g - h_r)}{C} \; , \; \alpha = \frac{l_g}{l_r + l_g} \tag{2-24}$$

and the column matrix containing spiral groove coefficients, $k_i(\alpha,\beta,\Gamma)$, in the above equations is

$$k = \left\{ \begin{array}{c} \dfrac{\alpha(1-\alpha)(\Gamma^3-1)^2\sin^2\beta + \Gamma^3}{(1-\alpha)\Gamma^3+\alpha} \\ \dfrac{\alpha(1-\alpha)(\Gamma^3-1)^2\sin\beta\cos\beta}{(1-\alpha)\Gamma^3+\alpha} \\ \dfrac{\alpha(1-\alpha)(\Gamma^3-1)^2\cos^2\beta + \Gamma^3}{(1-\alpha)\Gamma^3+\alpha} \\ \dfrac{(\Gamma^3-1)}{(1-\alpha)\Gamma^3+\alpha} \\ \dfrac{(1-\alpha)\Gamma+\alpha}{\Gamma} \\ \dfrac{(\Gamma-1)\sin\beta}{(1-\alpha)\Gamma^3+\alpha} \\ \dfrac{\alpha(1-\alpha)(\Gamma^3-1)(\Gamma-1)\sin\beta\cos\beta}{(1-\alpha)\Gamma^3+\alpha} \\ \dfrac{\alpha(1-\alpha)(\Gamma^3-1)(\Gamma-1)\cos^2\beta + \alpha\Gamma + (1-\alpha)\Gamma^3}{(1-\alpha)\Gamma^3+\alpha} \end{array} \right\} . \qquad 2\text{-}25$$

Only the first four components of k are used in Equations (2-21) - (2-22). The remaining components are used in evaluating the shear stress. The relationships for k_i, i=1,2,3,4 derived here are consistent with Equation (3.27) of Reference 5.

The global shear stress is obtained by substituting Equation (2-14) for $(\partial p'/\partial\theta)_g/r$ in Equation (2-19) then substituting Equation (2-12) for $(\partial p'/\partial\theta)_f/r$ in the resulting expression. The latter result may be expressed in dimensionless form as

$$\tilde{\tau} = \frac{1}{2}\left[k_5\frac{\Lambda}{3}\frac{\tilde{\omega}R}{H_r} + k_6\Lambda_\delta\frac{R}{H_r^2} + k_7H_r\frac{\partial P}{\partial S} + k_8\frac{H_r}{R}\frac{\partial P}{\partial\theta}\right] , \qquad 2\text{-}26$$

which is consistent with Equation (3.88) of Reference 5.

The equations presented thus far are directly applicable to either a cylindrical seal or a face seal. As mentioned earlier, a face seal is represented in the above equations by setting the transverse coordinate s equal to the radial coordinate r. This is equivalent to setting S = R in dimensionless form. A cylindrical seal is represented in dimensionless form by setting S = Z and R = 1.

The quantities required to characterize the groove dimensions are shown in Figure 2. If by convention ω is taken to be positive (surface motion in the direction of increasing θ), then the groove angle, β, will be the angle measured from the groove to the direction of surface motion associated with ω. A positive acute value of β will tend to pump in the positive S direction if the grooves are on the stator and in the negative S direction for grooves on the rotor. By setting the groove depth parameter $\tilde{\delta} = 0$, Γ becomes 1 and Equations (2-20) - (2-26) reduce to those for ungrooved seals. By treating k and $\tilde{\delta}$ as sectionally continuous functions of S, these equations may be applied to composite smooth and grooved geometries with Q_s and P held continuous at all transition boundaries.

The film thickness relationship for H_r, which may be applied to either a cylindrical seal or a face seal is

$$H_r = 1 - \epsilon_z - (\epsilon_x + \psi S)\cos\theta - (\epsilon_y - \phi S)\sin\theta \qquad 2\text{-}27$$

with $\varepsilon_z = 0$ for a cylindrical seal and $\varepsilon_x = \varepsilon_y = 0$ for a face seal.

The boundary pressures will be taken to be p_l and p_r at the inside and outside radii respectively for a face seal or at the two ends (z = -L/2 and Z = L/2) for a cylindrical seal. This is expressed in dimensionless form

$$P = P_l \text{ at } S = S_l\,, \quad P = P_r \text{ at } S = S_r\,. \qquad 2\text{-}28$$

The remaining boundary condition relates to periodicity with respect to θ which requires P and Q_θ to have the same values at $\theta = 0$ as they do at $\theta = 2\pi$:

$$P|_{\theta=0} = P|_{\theta=2\pi} \quad \text{and} \quad Q_\theta|_{\theta=0} = Q_\theta|_{\theta=2\pi}\,. \qquad 2\text{-}29$$

The above treatment is intended to represent a complete statement of the mathematical problem for determining the pressures and surface shear stresses in plain or spiral groove face or cylindrical seals. The rest of this section will deal with the numerical determination of the pressure distribution and the computation of related quantities such as loads, leakage, power loss, stiffness and damping.

2.1.2 Discretization of Pressure Equations

Discretization will be carried out with the use of the cell method [7] which involves the performance of a flow balance about each interior grid point. One may integrate Equation (2-20) over an arbitrary control area within a seal

$$\int_{\bar{A}} \vec{\nabla}\cdot\vec{\tilde{Q}}\,d\bar{A} + \int_{\bar{A}} \frac{\partial}{\partial \tilde{t}}[(\alpha\tilde{\delta} + H_r)(1 + P)]\,d\bar{A} = 0$$

and apply the divergence theorem to the first integral on the left to obtain the relationship

$$\oint_{\bar{S}} \vec{Q}\cdot\vec{n}\,d\bar{S} + \int_{\bar{A}} \frac{\partial}{\partial \tilde{t}}[(\alpha\tilde{\delta} + H_r)(1+P)]\,d\bar{A} = 0 \quad , \tag{2-30}$$

which will be used as a starting point in the discretization process.

A grid network may be set up along with flow control areas about each grid point as shown in Figure 3. The grid will contain M lines in the S direction including boundaries and N lines in the θ direction from $\theta = 0$ to $\theta = 2\pi$, inclusive. The grid points at the intersections of these lines are noted by the solid circles. Flow control areas to be used in evaluation of the integrals in Equation (2-30) are set up about each grid point as shown by the shaded area in Figure 3. The corners of the flow control area denoted by the shaded points marked 1,2,3, and 4 are located at the geometric centers of the rectangles formed by the grid lines and will be referred to as half grid points. The flow components labeled Q^+_{12} etc., represent the components of the flow vector in the positive coordinate directions as indicated by the arrows. The subscripts (12 etc.) refer to the line connecting points 1 and 2, and the superscripts (+,-) refer to the positive or negative side of the point of intersection with the grid line.

We will adopt the convention that the subscripts i,j refer to grid points and subscripts such as i+½,j+½ refer to half grid points. The value of the radius R at half grid point 2 would thus be $R_{i+½}$. The differential control length, $d\bar{S}$, in Equation (2-30) will be approximated by the lengths of the various lines or arcs bounding the flow control area thus $\Delta\bar{S}^+_{12}$ refers to the length of the line associated with Q^+_{12} described above which for this example would be $\Delta S_i/2$. Similarly the arc length associated with Q^-_{14} would be $\Delta\bar{S}^-_{14} = R_{i+½}\Delta\theta_{j-1}/2$.

The area element $d\bar{A}$ will be made up of the parts of the flow control area in each of the four quadrants about the center point (i,j) and numbered based on the shaded half grid point that each contains. Thus $\Delta\bar{A}_1 = (R_i+R_{i+½})\Delta\theta_j\Delta S_i/8$, etc. and the discretized form of Equation (2-30) may be written as:The flow components on the left-hand side of Equation (2-31) are obtained

$$Q^-_{12}\Delta\bar{S}^-_{12} + Q^+_{12}\Delta\bar{S}^+_{12} + Q^+_{14}\Delta\bar{S}^+_{14} + Q^-_{14}\Delta\bar{S}^-_{14} - Q^+_{34}\Delta\bar{S}^+_{34} - Q^-_{34}\Delta\bar{S}^-_{34} - Q^-_{23}\Delta\bar{S}^-_{23} - Q^+_{23}\Delta\bar{S}^+_{23} =$$

$$-\frac{\partial}{\partial\tilde{t}}\left\{(1+P_{ij})\left[(\alpha\tilde{\delta}+H_r)_{i+\frac{1}{2},j+\frac{1}{2}}\Delta\bar{A}_1 + (\alpha\tilde{\delta}+H_r)_{i+\frac{1}{2},j-\frac{1}{2}}\Delta\bar{A}_4 + (\alpha\tilde{\delta}+H_r)_{i-\frac{1}{2},j-\frac{1}{2}}\Delta\bar{A}_3 + (\alpha\tilde{\delta}+H_r)_{i-\frac{1}{2},j+\frac{1}{2}}\Delta\bar{A}_2\right]\right\} \tag{2-3}$$

from discretization of Equations (2-21) and (2-22). A numbering system for the 9 pressures at the grid point (i,j) and the 8 surrounding points is shown in Figure 3, where $P_1 = P_{i+1,j-1}$, $P_5 = P_{i,j}$ etc. The determination of the flows out of the sub-area containing the half grid point labeled 1 is discussed here as an example. The flow component Q^+_{12}, is determined from Equation (2-21). The derivative of the pressure normal to the line connecting points 1 and 2 is evaluated at the

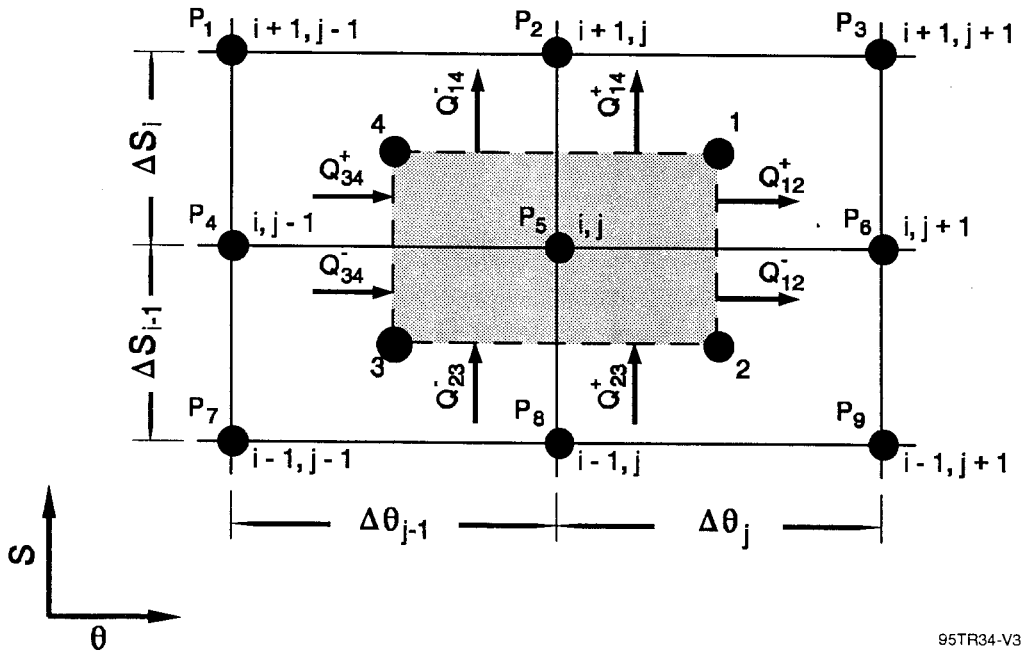

Figure 3. Schematic of Grid Network and Flow Control Area for Discretizaton Process

intersection of the line with the grid line. The tangential derivative is evaluated at the half grid point, 1 as the average of the difference between P_3 and P_6 with that between P_2 and P_5, divided by ΔS_i. Thus,

$$\frac{1}{R}\frac{\partial P}{\partial \theta} \approx \frac{P_6 - P_5}{R_i \Delta \theta_j}, \quad \frac{\partial P}{\partial S} \approx \frac{(P_3 - P_6) + (P_2 - P_5)}{2\Delta S_i} \quad (\text{for } Q_{12}^+) .$$

The flow component Q_{14}^+ is determined in a similar manner from Equation (2-22). The normal derivative is approximated as the difference between P_2 and P_5 divided by ΔS_i and the tangential derivative is approximated as the average of the differences between P_3 and P_2, and P_6 and P_5, divided by $R_{i+\frac{1}{2}}\Delta\theta_j$.

$$\frac{\partial P}{\partial S} \approx \frac{P_2 - P_5}{\Delta S_i}, \quad \frac{1}{R}\frac{\partial P}{\partial \theta} \approx \frac{(P_3 - P_2) + (P_6 - P_5)}{2R_{i+\frac{1}{2}}\Delta\theta_j} \quad (\text{for } Q_{14}^+) .$$

For both of the above flow components the pressure in the (1+P) term appearing in Equations (2-21) and (2-22) is evaluated at the half grid point by averaging the four surrounding pressures $(P_2+P_3+P_5+P_6)/4$. All of the remaining quantities (R, H_r, k_1, k_2, k_3, k_4, α, β and $\tilde{\delta}$) are evaluated directly at the half grid point.

The flow balances over the other quadrants are performed in a similar manner. For steady-state conditions, the right-hand side of Equation (2-31) will be 0 and the flow balance about any interior grid point (i,j) may be written in the form

$$F_{ij}(H_r, P_1, P_2, P_3, P_4, P_5, P_6, P_7, P_8, P_9) = 0 . \qquad 2\text{-}32$$

The definition of F_{ij} may be extended to make Equation (2-32) applicable to the ends of the seal as well as the interior points by applying Equation (2-28) at the endpoints as follows:

$$F_{1j} = P_5 - P_1 \quad (i = 1) \quad \text{and} \quad F_{Mj} = P_5 - P_r \quad (i = M) .$$

The solution to Equation (2-32) may be used to provide all of the steady-state quantities such as pressures, forces, moments, flow rate and power loss. The inclusion of the right-hand side of Equation (2-31) will be necessary for determination of frequency dependent stiffness and damping coefficients which will be discussed later.

2.1.3 Newton-Raphson Linearization Procedure

The Newton-Raphson [8] procedure is perhaps the most widely used method for obtaining solutions to nonlinear systems of algebraic equations and is described in many textbooks on numerical methods such as Reference 8. A procedure similar to that used here is described in a paper by Artiles, Walowit and Shapiro [9].

The procedure is started with an initial pressure distribution that satisfies the end conditions given by Equation (2-28). A new set of approximations to the pressures in Equation (2-32), P_k^{new} may be obtained by linearizing F_{ij} about a previously established set of approximations P_k as follows:

$$F_{ij} + \sum_{k=1}^{9} \frac{\partial F_{ij}}{\partial P_k} \left(P_k^{new} - P_k \right) = 0 \qquad 2\text{-}33$$

where a forward difference

$$\frac{\partial F_{ij}}{\partial P_k} = \frac{F_{ij}(H_r, P_1, \ldots, P_k + \eta, \ldots, P_9) - F_{ij}(H_r, P_1, \ldots, P_9)}{\eta}$$

may be used to numerically evaluate the partial derivatives.

Pressures without the superscript "new" relate to the previous or "old" approximation. It should be noted that the function F_{ij} will not be 0 unless the pressures comprising its arguments are exact. If we go back to using grid notation for P ($P_{i,j}$ in place of P_5 etc.) and introduce the column vector $\{P_j^{new}\}$ as the M new pressures at the jth column of grid points, Equation (2-33) may be written in the following form:

$$[C^j]\{P_j^{new}\} + [E^j]\{P_{j-1}^{new}\} + [D^j]\{P_{j+1}^{new}\} = \{R^j\} \quad , \qquad 2\text{-}34$$

where $[C^j]$, $[E^j]$ and $[D^j]$ are tri-diagonal matrices whose interior elements, from Equation (2-33), are

$$C_{i,i+k}^j = \frac{\partial F_{ij}}{\partial P_{i+k,j}} \quad , \quad E_{i,i+k}^j = \frac{\partial F_{ij}}{\partial P_{i+k,j-1}} \quad , \quad D_{i,i+k}^j = \frac{\partial F_{ij}}{\partial P_{i+k,j+1}} \quad , \quad k = -1, 0, 1 \; ; \quad i = 2, \ldots, M-1 \; .$$

The interior elements of the column vector $\{R^j\}$ are

$$R_i^j = \sum_{k=-1}^{1} \left(C_{i,i+k}^j P_{i+k,j} + E_{i,i+k}^j P_{i+k,j-1} + D_{i,i+k}^j P_{i+k,j+1} \right) - F_{ij} \quad .$$

The above equations may also be applied to the corner elements to produce the result

$$C_{1,1}^j = C_{M,M}^j = 1 \quad , \quad E_{1,1}^j = E_{M,M}^j = D_{1,1}^j = D_{M,M}^j = 0 \quad , \quad R_1^j = P_l \quad , \quad R_M^j = P_r \quad .$$

Equation (2-34) represents a linear system of simultaneous equations that may be solved by various matrix inversion procedures. The method used here is the column or transfer matrix method, which is described in References 7 and 10. It has been used extensively in solving

finite difference problems associated with various forms of the lubrication equations and produces accurate results in a fairly efficient manner. Convergence of the Newton-Raphson procedure is generally obtained within three to six iterations, depending on degree of nonlinearity and the accuracy required.

2.1.4 Determination of Loads, Moments, Torque, and Leakage

The dimensionless loads and moments may be obtained by integrating the pressure distribution over the seal area as shown below:

$$\tilde{W}_x = \int_0^{2\pi}\int_{S_i}^{S_r} P\cos\theta R\,dS\,d\theta\,,\quad \tilde{W}_y = \int_0^{2\pi}\int_{S_i}^{S_r} P\sin\theta R\,dS\,d\theta\,,\quad \tilde{W}_z = \int_0^{2\pi}\int_{S_i}^{S_r} PR\,dS\,d\theta\,,$$

$$\tilde{M}_x = -\int_0^{2\pi}\int_{S_i}^{S_r} P\sin\theta RS\,dS\,d\theta\,,\quad \tilde{M}_y = \int_0^{2\pi}\int_{S_i}^{S_r} P\cos\theta RS\,dS\,d\theta\,. \qquad 2\text{-}35$$

The dimensionless torque is obtained from integration of the shear stress given by Equation (2-26) over the seal area:

$$\tilde{T} = \text{sign}(\tilde{\omega})\int_0^{2\pi}\int_{S_i}^{S_r} \tilde{\tau} R\,dS\,d\theta\,. \qquad 2\text{-}36$$

The sign($\tilde{\omega}$) term has been added to make the torque positive when it opposes the net surface motion regardless of which surface (smooth or grooved) is moving.

Finally, the dimensionless leakage flow, Q_{in} going into the seal at $S = S_i$ may be obtained from integration of Q_θ, given by Equation (2-21), over the circumference of the seal:

$$Q_{in} = \int_0^{2\pi} Q_\theta R\,d\theta\,. \qquad 2\text{-}37$$

The integrand in the above expression is evaluated by summing the flow components to the right of the first θ grid line in the same manner as that used in developing Equation (2-31). It should be noted that any value of S can be used since Q_{in} is independent of S.

The physical quantities corresponding to the dimensionless ones given above are

$$W_{\{x,y,z\}} = R_0^2 p_0 \tilde{W}_{\{x,y,z\}} \ , \quad M_{\{x,y\}} = R_0^3 p_0 \tilde{M}_{\{x,y\}} \ , \quad q_{in} = \frac{C^3 p_0}{12\mu} Q_{in} \ , \quad T = R_0^2 p_0 C \tilde{T} \ . \qquad 2\text{-}38$$

In the above equations, the loads W_x and W_y apply only to a cylindrical seal and W_z applies only to a face seal. The leakage flow q_{in} is the volumetric flow rate going into the seal measured at pressure p_0.

2.1.5 Determination of Stiffness and Damping Coefficients

Equation (2-20) with flow components Q_θ and Q_s given by Equations (2-21) and (2-22) represents a second-order nonlinear partial differential equation that may be used to define a second-order nonlinear operator G, such that

$$G(P,H_r) = -\frac{\partial}{\partial \tilde{t}}[(\alpha\tilde{\delta} + H_r)(1+P)] \ . \qquad 2\text{-}39$$

The determination of P under steady-state conditions, where the right-hand side of Equation (2-39) is 0, was described earlier in this section. These steady-state pressures will now be referred to as $\hat{P}$. The various eccentricities and rotations used in determining H_r from Equation (2-27) may, for convenience, be put in the form of a row matrix as

$$[\epsilon] = \begin{cases} [\epsilon_z, \phi, \psi] \ , & \text{(face seal)} \\ [\epsilon_x, \epsilon_y, \phi, \psi] \ , & \text{(shaft seal)} \end{cases} \qquad 2\text{-}40$$

and Equation (2-27) may be written as

$$H_r = 1 + [\epsilon]\{a\} \ , \qquad 2\text{-}41$$

where the column vector {a} is given by

$$\{a\} = \begin{cases} \{-1, S\sin\theta, -S\cos\theta\} \ , & \text{(face seal)} \\ \{-\cos\theta, -\sin\theta, S\sin\theta, -S\cos\theta\} \ , & \text{(shaft seal)} \end{cases} \qquad 2\text{-}42$$

One could develop a perturbation analysis for prediction of stiffness and damping coefficients with the following procedure: (a) perturb say the ith component of the eccentricity matrix in Equation (2-40) by $\eta\varepsilon'$, where η is a small parameter and ε' is time dependent; (b) express H_r in the form $H_r = \hat{H} + \eta\varepsilon'\{a\}$ and the corresponding pressures as $P = \hat{P} + \eta\{P'\}$; (c) substitute the above expressions for P and H_r in Equation (2-39); (d) expand the resulting

expression neglecting terms of order η^2 and higher; (e) collect terms of order η. The resulting expression could be written in the form:

$$\mathcal{L}\{P'\} + \{b\}\epsilon' = -(\alpha\tilde{\delta} + \hat{H})\frac{\partial\{P'\}}{\partial\tilde{t}} - (1 + \hat{P})\{a\}\frac{\partial\epsilon'}{\partial\tilde{t}} \quad , \tag{2-43}$$

where $\mathcal{L}$ is a second-order linear operator given by

$$\mathcal{L} = A_1\frac{\partial^2}{\partial S^2} + A_2\frac{\partial^2}{\partial S\,\partial\theta} + A_3\frac{\partial^2}{\partial\theta^2} + A_4\frac{\partial}{\partial S} + A_5\frac{\partial}{\partial\theta} + A_6 \quad . \tag{2-44}$$

The coefficients in the above equations (A_1, A_2, {b} etc.) will depend on the coordinate variables as well as $\hat{P}$, $\hat{H}$ and their various derivatives. Only the form of the above equations is important to the numerical procedure under development and the significant amount of algebraic manipulation required to determine these coefficients will be shown to be unnecessary.

If the time dependence of the eccentricity is restricted to oscillatory disturbances one may set $\epsilon' = e^{3\sigma\tilde{\imath}}$ and look for solutions in the form $\{P'\} = \{P^*\}e^{3\sigma\tilde{\imath}}$, where $\{P^*\}$ is complex but independent of time. When this transformation is introduced into Equation (2-43), the result is

$$\mathcal{L}\{P^*\} + \{b\} = -\Im\sigma[(\alpha\tilde{\delta} + \hat{H})\{P^*\} + (1 + \hat{P})\{a\}] \quad . \tag{2-45}$$

The representation of $\{P^*\}$ and the eccentricity coefficients {a} as column vectors relates to the fact that each of the eccentricities must be perturbed to obtain the compete stiffness matrix but Equation (2-45) is solved independently for each perturbation. The periodic boundary conditions given by Equation (2-29) also apply to Equation (2-39) (continuity of $\{P^*\}$ and $\partial\{P^*\}/\partial\theta$ is sufficient when H_r and the spiral groove coefficients $k_1,...,k_4$ are continuous functions of θ as they are here). The end boundary conditions given by Equation (2-28) become $\{P^*\} = 0$ at $S = S_1$ and $S = S_r$.

If Equation (2-45) were solved for $\{P^*\}$ subject to the above boundary conditions, all of the dimensionless stiffness and damping coefficients could be obtained by substituting $\{P^*\}$ for P in Equation (2-35). The real parts of the computed forces and moments would be in phase with the eccentricity perturbations and constitute the dimensionless stiffness coefficients. Thus $\tilde{K}_{yx}$ would correspond to the real part of $\tilde{W}_y$ computed from the component of $\{P^*\}$ associated with the perturbation in ϵ_x and $\tilde{K}_{\phi y}$ would correspond to the real part of $\tilde{M}_x$ computed from the component of $\{P^*\}$ associated with the perturbation in ϵ_y etc. In a similar manner, the dimensionless damping coefficients which are 90° out of phase with the eccentricity perturbations would be obtained by dividing the imaginary parts of the forces and moments computed in the manner described above by σ.

The parameter σ, is a dimensionless disturbance frequency referred to as the "squeeze number" and is given by $\sigma = 2\Lambda\Omega/\omega$ where Ω is the angular velocity of the disturbance. The limiting form of the stiffness and damping coefficients as $\sigma \rightarrow 0$, is of interest as it applies to

incompressible flow, and the limiting stiffnesses are used in the homing procedure that has been implemented for determining eccentricities from given loads which will be described later. This limiting form may be obtained by expressing Equation (2-45) in terms of its real and imaginary parts as

$$\mathcal{L}\{P_{\mathcal{R}}\} + \{b\} = \sigma^2(\alpha\tilde{\delta} + \hat{H})\{P_{\mathcal{I}}\} \quad , \tag{2-46}$$

$$\mathcal{L}\{P_{\mathcal{I}}\} = -(\alpha\tilde{\delta} + \hat{H})\{P_{\mathcal{R}}\} - (1 + \hat{P})\{a\} \quad , \tag{2-47}$$

where

$$\{P^*\} = \{P_{\mathcal{R}}\} + \mathcal{I}\sigma\{P_{\mathcal{I}}\} \quad . \tag{2-48}$$

The column vectors $\{P_{\mathcal{R}}\}$ and $\{P_{\mathcal{I}}\}$ are the "stiffness" and "damping" pressures respectively. If one formally sets $\sigma = 0$ in Equation (2-46) it decouples from Equation (2-47) and may be solved directly. Since the right-hand side of Equation (2-46) becomes 0, the stiffness pressures are the same as those that would be obtained by computing the steady-state pressures at a perturbed eccentricity, subtracting the unperturbed pressures and dividing by the eccentricity perturbation. This latter method is frequently used for computing steady-state stiffnesses in incompressible flow and has been implemented here for the computation of "stiffnesses at 0 frequency" used in the above mentioned homing procedure. The 0 frequency damping pressures may be obtained by solving Equation (2-47) with $\{P_{\mathcal{R}}\}$ as determined from the solution to Equation (2-46).

The above discussion assumed that the perturbation coefficients in Equations (2-40) - (2-42) were determined prior to setting up the finite discretized equations for their solution. Identical results can be achieved by direct numerical perturbation of the difference equations. This approach, which has been implemented here and is described below, avoids algebraic error in determining the perturbation coefficients and may be used in complex situations where analytical determination of the perturbation coefficients is not feasible.

After desired convergence of the Newton-Raphson process has been achieved under steady (unperturbed) conditions one may denote the resulting steady-state pressure vectors as $\{\hat{P}_j\}$ and the coefficient matrices as $[\hat{C}^j]$, etc. and Equation (2-34) may be written as

$$[\hat{C}^j]\{\hat{P}_j\} + [\hat{E}^j]\{\hat{P}_{j-1}\} + [\hat{D}^j]\{\hat{P}_{j+1}\} = \{\hat{R}^j\} \quad . \tag{2-49}$$

One may now perturb the kth component of the eccentricity vector by an amount η, recalculate $[\hat{C}^j]$ at the new film thickness (but old pressure distribution, $\hat{P}$) then subtract $[\hat{C}^j]$ at the old film thickness and divide the difference by η to numerically obtain the derivative of $[\hat{C}^j]$ with respect to ε_k which will be denoted by $[\hat{C}^{j,k}]$. Thus

$$[\hat{C}^{j,k}] = \frac{[\hat{C}^{j}]|_{\epsilon_k+\eta} - [\hat{C}^{j}]|_{\epsilon_k}}{\eta} \quad .$$

The matrices $[\hat{E}^{j,k}]$, $[\hat{D}^{j,k}]$ and $\{\hat{R}^{j,k}\}$ are obtained in a similar manner from the other coefficient matrices. If we introduce a disturbance to ε_k of magnitude $\varepsilon'\eta$, as was done in deriving Equation (2-43), then the change in the coefficient matrix $[\hat{C}^j]$ would be $\varepsilon'\eta[\hat{C}^{j,k}]$ with corresponding changes in the other coefficient matrices. If we disturb Equation (2-49) by replacing $\{\hat{P}_j\}$ with $\{\hat{P}_j\} + \eta\{P'^k_j\}$, $[\hat{C}_j]$ with $[\hat{C}^j] + \varepsilon'\eta[\hat{C}^{j,k}]$, etc. and collect terms of order η, the following expression is obtained:If we set ε' to unity in Equation (2-50) then $\{P'^k_j\}$

$$[\hat{C}^j]\{P'^k_j\} + [\hat{E}^j]\{P'^k_{j-1}\} + [\hat{D}^j]\{P'^k_{j+1}\} = \left(\{\hat{R}^{j,k}\} - [\hat{C}^{j,k}]\{\hat{P}_j\} - [\hat{E}^{j,k}]\{\hat{P}_{j-1}\} - [\hat{D}^{j,k}]\{\hat{P}_{j+1}\}\right)\epsilon' \quad . \qquad 2\text{-}50$$

will become the 0 frequency stiffness pressure (the change in steady-state pressure per unit change in eccentricity). It should be noted that the coefficients of the 0 frequency stiffness pressures in Equation (2-50) are the same as those for the steady-state pressures in Equation (2-49); only the right-hand side has changed. Equation (2-50) thus represents the construction of the discretized form of Equation (2-43) when $\sigma = 0$. In order to complete the process for $\sigma \neq 0$, one may introduce the same disturbances to the right-hand side of Equation (2-31), with $H_r = \hat{H} + \varepsilon'\eta\{a\}$ and add the terms of order η to the right-hand side of Equation (2-50). The terms to be added are $-\partial([\bar{C}^j]\{P'^k_j\}+\{\bar{R}^{j,k}\}\varepsilon')/\partial\tilde{t}$, where $[\bar{C}^j]$ are diagonal matrices whose components are

$$\bar{C}^j_{ii} = (\alpha\tilde{\delta} + \hat{H})_{i+\frac{1}{2},j+\frac{1}{2}}\Delta\bar{A}_1 + (\alpha\tilde{\delta} + \hat{H})_{i+\frac{1}{2},j-\frac{1}{2}}\Delta\bar{A}_4 + (\alpha\tilde{\delta} + \hat{H})_{i-\frac{1}{2},j-\frac{1}{2}}\Delta\bar{A}_3 + (\alpha\tilde{\delta} + \hat{H})_{i-\frac{1}{2},j+\frac{1}{2}}\Delta\bar{A}_2 \qquad 2\text{-}51$$

and $\{\bar{R}^{j,k}\}$ are column vectors whose components are

$$\bar{R}^{j,k}_i = (1 + \hat{P}_{ij})(a^k_{i+\frac{1}{2},j+\frac{1}{2}}\Delta\bar{A}_1 + a^k_{i+\frac{1}{2},j-\frac{1}{2}}\Delta\bar{A}_4 + a^k_{i-\frac{1}{2},j-\frac{1}{2}}\Delta\bar{A}_3 + a^k_{i-\frac{1}{2},j+\frac{1}{2}}\Delta\bar{A}_2) \approx (1 + \hat{P}_{ij})a^k_{i,j}\Delta\bar{A} \quad . \qquad 2\text{-}52$$

The far right side of Equation (2-52) is a quadradically equivalent representation that was used in the computer program described in Section 3. One may now set $\varepsilon' = e^{\Im\sigma\tilde{t}}$ in Equation (2-50) and look for solutions in the form $\{P'^k_j\} = \{P^{*k}_j\}e^{\Im\sigma\tilde{t}}$, by introducing these substitutions into Equation (2-50) and combining terms to obtain the final set of linear difference equations for the complex stiffness pressures $\{P^{*k}_j\}$:

$$[C^{*j}]\{P^{*k}_j\} + [\hat{E}^j]\{P^{*k}_{j-1}\} + [\hat{D}^j]\{P^{*k}_{j+1}\} = \{R^{j,k}\} - [\hat{C}^{j,k}]\{\hat{P}_j\} - [\hat{E}^{j,k}]\{\hat{P}_{j-1}\} - [\hat{D}^{j,k}]\{\hat{P}_{j+1}\} \quad , \qquad 2\text{-}53$$

where $[C^{*j}] = [\hat{C}^j] + \Im\sigma[\bar{C}^j]$ and $\{R^{j,k}\} = \{\hat{R}^{j,k}\} - \Im\sigma\{\bar{R}^{j,k}\}$.

The system of equations given by Equation (2-53) has been solved by the column method in a directly analogous manner to that used in solving Equation (2-34). The principal difference lies in the fact that all of the matrix operations were performed using complex arithmetic. The dimensionless, frequency dependent stiffness and damping coefficients were computed from the complex stiffness pressures in the previously described manner. Relationships of the following type may be used to calculate the physical stiffness and damping coefficients from the dimensionless ones:

$$K_{xx} = K_0 \tilde{K}_{xx} \ , \quad K_{\phi\phi} = K_0 R_0^2 \tilde{K}_{\phi\phi} \ , \quad K_{x\phi} = K_0 R_0 \tilde{K}_{x\phi} \qquad 2\text{-}54$$

and

$$B_{xx} = B_0 \tilde{B}_{xx} \ , \quad B_{\phi\phi} = B_0 R_0^2 \tilde{B}_{\phi\phi} \ , \quad B_{x\phi} = B_0 R_0 \tilde{B}_{x\phi} \ , \qquad 2\text{-}55$$

where $K_0 = p_0 R_0^2/C$ and $B_0 = 12\mu R_0^4/C^3$.

2.1.6 Optimization of Groove Parameters for Maximum Stagnation Pressure in a Concentric Cylindrical Seal

Since spiral grooves are solely responsible for the axial stiffness of an aligned, gas-lubricated face seal with parallel surfaces under steady-state conditions, it is often desirable to optimize groove parameters for maximum axial stiffness. An optimization procedure for doing this has been implemented in the computer code SPIRALP described in Reference 11. The analogous situation is not as evident in a concentric gas-lubricated cylindrical seal which will have considerable, if not maximum stiffness without spiral grooves. A large portion of the stiffness in the absence of spiral grooves will be cross coupled, particularly at low values of Λ, thus giving rise to stability problems which may be alleviated with the use of spiral grooves. The criteria for optimizing groove geometry from a dynamic standpoint would thus depend on both the desired load capacity and the various other elements in the system affecting rotordynamic performance.

An alternate approach for developing a stand-alone criterion for optimizing groove geometry in a cylindrical seal is to maximize the pressure gradient that the grooves can generate at stagnation. If the grooves are being used to pump against a pressure gradient, the maximum stagnation pressure gradient would represent the maximum pressure gradient that the grooves could pump against without allowing any net flow to go through. It would also represent the maximum axial pressure gradient that the grooves could generate in an aligned, symmetric herringbone bearing in the absence of an imposed pressure gradient. In any event, the stagnation pressure gradient is a strong measure of spiral groove performance and even though optimizing it is not a precise criterion for optimizing dynamic performance, computations obtained with geometries optimized in this manner should provide a strong indication of the maximum benefits obtainable with the use of spiral grooves.

The stagnation pressure gradient for a cylindrical seal under concentric conditions may be obtained from Equation (2-22) by setting $Q_s = 0$ (stagnation), $\partial P/\partial\theta = 0$, $H_r = 1$ (concentric), $S = Z$ and $R = 1$ (cylindrical seal). The resulting equation may be solved for $\Delta P/\Delta Z$ making use of the definition of Λ_δ given by Equation (2-24) and the definitions of k_1 and k_4 given by Equation (2-25) to obtain the following relationship

$$\frac{\partial P}{\partial Z} = \Lambda\tilde{\omega}\frac{\tilde{\delta}\,\alpha(1-\alpha)\sin\beta\cos\beta(\Gamma^3-1)}{\alpha(1-\alpha)(\Gamma^3-1)^2\sin^2\beta+\Gamma^3}\,.$$

The right-hand side of the above equation may be treated as a function of α, β and $\tilde{\delta}(\Gamma = 1 + \tilde{\delta})$ and has a maximum value of $\partial P/\partial Z = 0.09118\,\Lambda\tilde{\omega}$ at $\alpha_{opt} = 0.5$, $\beta_{opt} = 0.2736$ (15.68°) and $\tilde{\delta} = 2.653$.

The variation of the pressure gradient near the optimum point is shown in Figure 4. The curve marked α was obtained by holding β and $\tilde{\delta}$ at their optimum values and varying α. The other curves were obtained in an analogous manner. The curves show the sensitivity of the optimum pressure gradient to the various parameters and verify the existence of a relative maximum at the optimum point.

Other approaches to the optimization problem are given in Reference 5 for spiral groove bearings and Reference 12 for spiral groove viscous pumps.

2.2 Overview of Computer Code SPIRALG

SPIRALG has been written to implement the analysis developed in the preceding section. Full input and output descriptions along with a number of sample runs are given in Reference 13. A brief discussion of a few items not covered in Section 2.1 is given below.

The analytical procedure contained in Section 2.1 has been oriented toward determining pressure distribution, load, flow, torque, stiffness and damping for a given film thickness distribution. In practice it is often desirable to determine the equilibrium film thickness or eccentricities from prescribed loads and possibly moments. SPIRALG provides a homing option for determining the eccentricities based on the steady-state bearing stiffnesses. This homing option is controlled by the input flag IHOME and is based on the procedure described below.

If one were to write the dimensionless load and eccentricity as column vectors $\{\tilde{W}\}$ and $\{\varepsilon\}$ (transpose row matrix $[\varepsilon]$) and take the previous estimate (or initial guess) of $\{\varepsilon\}$ as $\{\varepsilon\}_{old}$ and the load vector computed from $\{\varepsilon\}_{old}$ as $\{\tilde{W}\}_{old}$, the steady-state stiffness matrix $[\tilde{K}]$ could be used to arrive at a new approximation for $\{\varepsilon\}$. The method for doing this is shown by first writing the equation for the change in load as $\{\tilde{W}\} - \{\tilde{W}\}_{old} = [\tilde{K}](\{\varepsilon\} - \{\varepsilon\}_{old})$. The new approximation to $\{\varepsilon\}$ is obtained by inverting the stiffness matrix and solving for $\{\varepsilon\}$ as $\{\varepsilon\} = \{\varepsilon\}_{old} + [\tilde{K}]^{-1}(\{\tilde{W}\} - \{\tilde{W}\}_{old})$. This approach is in effect the application of the Newton-Raphson method for determining the eccentricities.

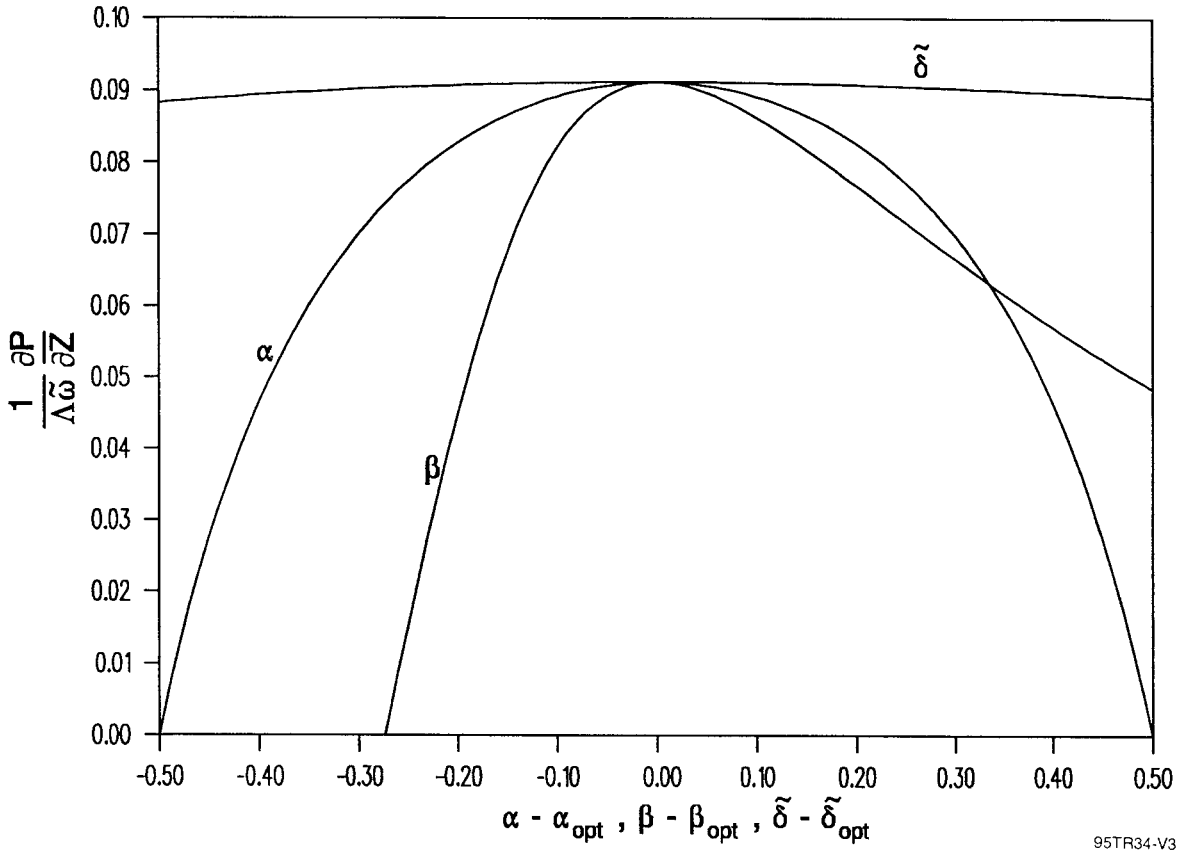

Figure 4. The Variation of the Stagnation Pressure Gradient about the Optimum Point

While the above approach can be very effective it can also diverge if the initial guesses are bad. This divergence is usually accompanied by the generation of negative film thicknesses in the course of the iteration process. In order to attempt to correct this problem, an optional numerical damping algorithm has been implemented which replaces $\{\varepsilon\}$ with $\{\varepsilon\} = \{\varepsilon\}_{old} + \tilde{\beta}[\tilde{K}]^{-1}(\{\tilde{W}\} - \{\tilde{W}\}_{old})$ when the originally calculated value of $\{\varepsilon\}$ would result in a negative film thickness. The numerical damping factor $\tilde{\beta}$ is determined by the program based on the value of the input parameter NUMDMP described in the input description.

The cell method of discretization is designed to obtain quadratic accuracy. Numerical testing indicates that this has apparently been achieved. One may make use of this property to obtain greater accuracy, (or the same degree of accuracy with coarser grids and ensuing reductions in computer time) with the use of Romberg extrapolation. Suppose for example we computed the dimensionless torque $\tilde{T}$ with a coarse grid and denoted it by $\tilde{T}_c$ then halved the grid spacing in both directions and recomputed $\tilde{T}$ denoting it as $\tilde{T}_f$ (subscript denotes fine grid). If the truncation error were to approach 0 as the square of the grid spacing and $\tilde{T}_r$ were the true solution then $(\tilde{T}_f - \tilde{T}_r) = (\tilde{T}_c - \tilde{T}_r)/4$, or $\tilde{T}_r = (4\tilde{T}_f - \tilde{T}_c)/3$. The above extrapolation can, in principal, increase the rate of convergence from quadratic to cubic. The subroutine SPIRAL, provides the option of implementing Romberg extrapolation for all of the outputs by setting the flag IACC as explained in the input description.

The logic used in SPIRALG for performing the pressure iterations, computing stiffness and damping coefficients, homing in on eccentricities and implementing Romberg extrapolation is shown in Figure 5. It can be seen there that when the homing process is implemented, it is completed for both coarse grid and fine grid solutions prior to performing the Romberg extrapolation. The extrapolation is thus performed with solutions obtained at two different displacements. When the displacements are specified (IHOME=0) extrapolations are performed with solutions obtained at the same displacement, which is believed to be a more accurate approach. If one were to compute displacements for a given loading and then recompute the loading from the displacements using Romberg extrapolation for both computations the computed loading would thus differ slightly from the input loading even though all tolerances were met. The degree of this difference will depend on the grid size and caution should be exercised in using Romberg extrapolation when homing in on the displacements with very coarse grids.

2.3 Verification

SPIRALG has been compared with the results of two computer codes. The first of these is MTI Computer Code PN471 which is fully described in Reference 6. The program is based on perturbation analyses and is only applicable to bearings and seals operating in the concentric, aligned position ($\varepsilon_x=\varepsilon_y=\phi=\psi=0$). The program does not predict loads and moments that would occur at finite displacements but it does predict stiffness and damping values as well as flow, torque, and power loss for spiral groove bearings as well as cylindrical and face seals. Since the program solves ordinary rather than partial differential equations it can be made to rapidly produce highly accurate results for evaluating the accuracy of SPIRALG. The second MTI computer code, named GASBEAR, is used to verify SPIRALG

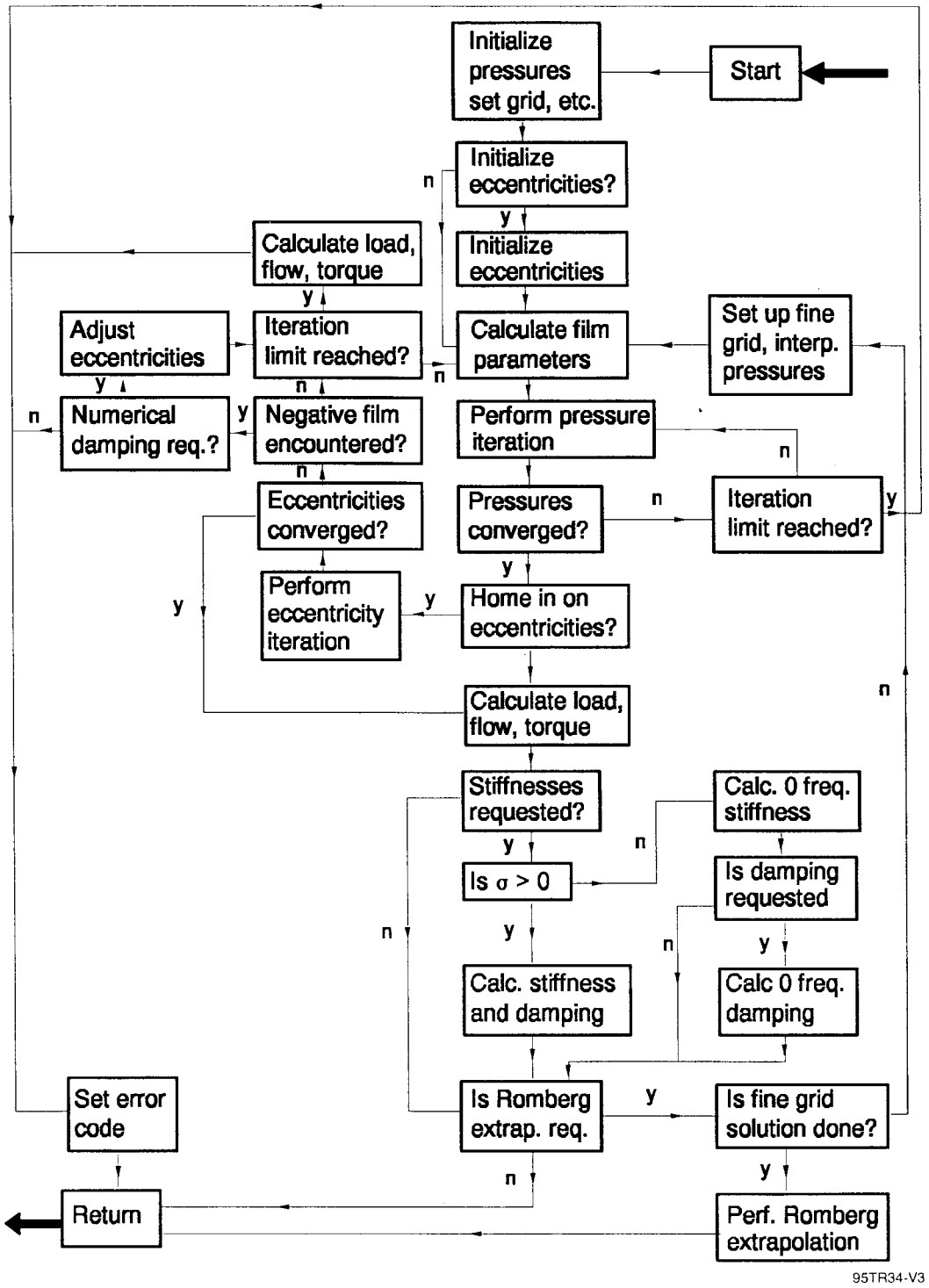

Figure 5. Flow Diagram for Logic Used in SUBROUTINE SPIRAL

under displaced and misaligned conditions. GASBEAR was written for use in conjunction with plane journal bearings and cylindrical seals. It does not treat spiral grooves or face seals. Since SPIRALG does not contain and special instructions for treating concentric behavior and has relatively few instructions for distinguishing between face and cylindrical seals, the above two programs should provide reasonable verification. Since the treatment of the effects of spiral grooves under eccentric and misaligned conditions is believed to be new, terms that become significant only under those conditions remain unverified.

The results of 7 verification tests are reported on the following pages. A SPIRALG output listing followed by the relevant output from the verification code, converted to equivalent units and format, is given for each case. The somewhat strange looking input values (unit ambient pressure, high RPM but low viscosity etc.) were selected to simplify the conversion process between dimensional quantities and the dimensionless ones that were used throughout the development of the code. The compressibility number of Λ=10 used for all cases and the seal pressure ratio of 2 used for imposed pressure gradients should be typical of many practical applications under fairly compressible conditions.

Cases 1 - 6 show comparisons between SPIRALG and PN471. Romberg extrapolation was used for each of these cases, with 21 grid points in the circumferential direction and 5 sub-intervals in each of the two regions in the transverse direction for the coarse grid solution. The fine grid solutions thus use 41 circumferential points and 10 sub-intervals per region in the transverse direction.

The first case verifies stiffness and damping values for a synchronous disturbance acting on a cylindrical seal with a herringbone groove pattern and an imposed pressure gradient. Cases 2 and 3 verify the differences in stiffness and damping values predicted to occur for a cylindrical seal when grooves are placed on the rotor (with groove angles reversed) rather than on the stator. The static quantities (flow, torque and power loss) remain unchanged. Cases 4 - 6 show comparisons between SPIRALG and PN471 for a spiral groove face seal with an imposed pressure gradient at three different disturbance frequencies; zero (case 4), synchronous (case 5) and ten times synchronous (case 6).

Case 7 shows a comparison between SPIRALG and GASBEAR for an eccentric, tilted cylindrical seal with an imposed pressure gradient. The grid size was chosen to match the maximum size allowable for the available version of GASBEAR. A separate program was written to perform Romberg extrapolations with the results of GASBEAR. The agreement between the two programs is good. The apparent discrepancy between the moments about the y axis is a result of the fact that the component is very small. The relative error obtained by dividing the discrepancy by the absolute magnitude of the moment vector is 0.33%.

(CASE 1) Concentric cyl. seal with pres. grad. Λ=10, σ=20

SPIRAL GROOVE SHAFT SEAL, ROTATING SURFACE IS SMOOTH

LENGTH, DIAMETER, CLEARANCE = 2.0000E+00, 2.0000E+00, 1.0000E-03 (IN)

ROTATION SPEED, DISTURBANCE SPEED = 1.9099E+05, 1.9099E+05 (RPM)

PRESSURE AT START, END AXIAL BOUNDARIES = 2.0000E+00, 1.0000E+00 (PSI)

VISCOSITY = 8.3333E-11 (PSI-SEC), AMBIENT PRESSURE = 1.0000E+00 (PSI)

CALCULATED FORCES IN X,Y DIRECTIONS = -1.0902E-15, -8.1153E-16 (LB)
CALCULATED MOMENTS ABOUT X,Y AXES = -9.3565E-16, -2.4405E-16 (IN-LB)

MINIMUM FILM THICKNESS = 1.0000E-03 (IN)

FLOW = 1.2816E+01 (IN^3/SEC) MEASURED AT 1.0000E+00 (PSI)

TORQUE = 1.7015E-02 (IN-LB), FILM POWER LOSS = 5.1562E-02 (HP)

COMPRESSIBILITY NUMBER = 1.0000E+01, SQUEEZE NUMBER = 2.0000E+01

DYNAMIC COEFFICIENTS (FORCE UNIT / DISP. UNIT)

DISP.	x (IN)	y (IN)	ϕ (RAD)	ψ (RAD)	FORCE UNIT
Kx	5.4607E+03	9.0379E+01	-6.8886E+01	2.6847E+02	LB
Ky	-9.0379E+01	5.4607E+03	-2.6847E+02	-6.8886E+01	LB
Kϕ	-1.0824E+02	-1.7773E+01	7.0561E+02	1.9521E+02	IN-LB
Kψ	1.7773E+01	-1.0824E+02	-1.9521E+02	7.0561E+02	IN-LB
Bx	7.3200E-02	-5.5832E-02	-1.5172E-02	-2.9538E-02	LB-SEC
By	5.5832E-02	7.3200E-02	2.9538E-02	-1.5172E-02	LB-SEC
Bϕ	1.9442E-03	6.9321E-03	2.7091E-02	-1.1690E-02	IN-LB-SEC
Bψ	-6.9321E-03	1.9442E-03	1.1690E-02	2.7091E-02	IN-LB-SEC

COMPARISON OF CASE 1 WITH PN471

FLOW = 1.282E+01 (IN^3/SEC) MEASURED AT 1.0000E+00 (PSI)

TORQUE = 1.701E-02 (IN-LB), FILM POWER LOSS = 5.156E-02 (HP)

DYNAMIC COEFFICIENTS (FORCE UNIT / DISP. UNIT)

DISP.	x (IN)	y (IN)	ϕ (RAD)	ψ (RAD)	FORCE UNIT
Kx	5.4608E+03	9.0292E+01	-6.8846E+01	2.6823E+02	LB
Ky	-9.0292E+01	5.4608E+03	-2.6823E+02	-6.8846E+01	LB
Kϕ	-1.0809E+02	-1.7525E+01	7.0356E+02	1.9537E+02	IN-LB
Kψ	1.7525E+01	-1.0809E+02	-1.9537E+02	7.0356E+02	IN-LB
Bx	7.3215E-02	-5.5805E-02	-1.5192E-02	-2.9534E-02	LB-SEC
By	5.5805E-02	7.3215E-02	2.9534E-02	-1.5192E-02	LB-SEC
Bϕ	1.9403E-03	6.9195E-03	2.7097E-02	-1.1667E-02	IN-LB-SEC
Bψ	-6.9195E-03	1.9403E-03	1.1667E-02	2.7097E-02	IN-LB-SEC

(CASE 2) Concentric asymmetric cyl. seal, Λ=10, σ=0

SPIRAL GROOVE SHAFT SEAL, ROTATING SURFACE IS SMOOTH

LENGTH, DIAMETER, CLEARANCE = 2.0000E+00, 2.0000E+00, 1.0000E-03 (IN)

ROTATION SPEED, DISTURBANCE SPEED = 1.9099E+05, 0.0000E+00 (RPM)

PRESSURE AT START, END AXIAL BOUNDARIES = 1.0000E+00, 1.0000E+00 (PSI)

VISCOSITY = 8.3333E-11 (PSI-SEC), AMBIENT PRESSURE = 1.0000E+00 (PSI)

CALCULATED FORCES IN X,Y DIRECTIONS = -2.8151E-15, -1.6233E-15 (LB)
CALCULATED MOMENTS ABOUT X,Y AXES = 2.7524E-16, -5.2158E-17 (IN-LB)

MINIMUM FILM THICKNESS = 1.0000E-03 (IN)

FLOW = 3.5000E+00 (IN^3/SEC) MEASURED AT 1.0000E+00 (PSI)

TORQUE = 1.8850E-02 (IN-LB), FILM POWER LOSS = 5.7122E-02 (HP)

COMPRESSIBILITY NUMBER = 1.0000E+01, SQUEEZE NUMBER = 0.0000E+00

DYNAMIC COEFFICIENTS (FORCE UNIT / DISP. UNIT)

DISP.	x (IN)	y (IN)	ϕ (RAD)	ψ (RAD)	FORCE UNIT
Kx	4.9657E+03	1.5689E+03	-4.9960E+02	2.6673E+02	LB
Ky	-1.5689E+03	4.9657E+03	-2.6673E+02	-4.9960E+02	LB
Kϕ	5.3012E+01	-3.6877E+02	6.0778E+02	5.3984E+02	IN-LB
Kψ	3.6877E+02	5.3012E+01	-5.3984E+02	6.0778E+02	IN-LB
Bx	-6.9953E-02	-1.1123E-01	4.3933E-02	-1.2462E-02	LB-SEC
By	1.1123E-01	-6.9953E-02	1.2462E-02	4.3933E-02	LB-SEC
Bϕ	-8.3037E-03	-4.4522E-03	2.2471E-02	-4.3624E-02	IN-LB-SEC
Bψ	4.4522E-03	-8.3037E-03	4.3624E-02	2.2471E-02	IN-LB-SEC

COMPARISON OF CASE 2 WITH PN471

FLOW = 3.500E+00 (IN^3/SEC) MEASURED AT 1.0000E+00 (PSI)

TORQUE = 1.885E-02 (IN-LB), FILM POWER LOSS = 5.712E-02 (HP)

DYNAMIC COEFFICIENTS (FORCE UNIT / DISP. UNIT)

DISP.	x (IN)	y (IN)	ϕ (RAD)	ψ (RAD)	FORCE UNIT
Kx	4.9648E+03	1.5692E+03	-4.9982E+02	2.6552E+02	LB
Ky	-1.5692E+03	4.9648E+03	-2.6552E+02	-4.9982E+02	LB
Kϕ	5.3156E+01	-3.6793E+02	6.0602E+02	5.3900E+02	IN-LB
Kψ	3.6793E+02	5.3156E+01	-5.3900E+02	6.0602E+02	IN-LB
Bx	-6.9955E-02	-1.1143E-01	4.3975E-02	-1.2344E-02	LB-SEC
By	1.1143E-01	-6.9955E-02	1.2344E-02	4.3975E-02	LB-SEC
Bϕ	-8.3373E-03	-4.4940E-03	2.2617E-02	-4.3536E-02	IN-LB-SEC
Bψ	4.4940E-03	-8.3373E-03	4.3536E-02	2.2617E-02	IN-LB-SEC

(CASE 3) Same case with grooves on moving surf., groove angle rev.

SPIRAL GROOVE SHAFT SEAL, ROTATING SURFACE IS GROOVED

LENGTH, DIAMETER, CLEARANCE = 2.0000E+00, 2.0000E+00, 1.0000E-03 (IN)

ROTATION SPEED, DISTURBANCE SPEED = 1.9099E+05, 0.0000E+00 (RPM)

PRESSURE AT START, END AXIAL BOUNDARIES = 1.0000E+00, 1.0000E+00 (PSI)

VISCOSITY = 8.3333E-11 (PSI-SEC), AMBIENT PRESSURE = 1.0000E+00 (PSI)

CALCULATED FORCES IN X,Y DIRECTIONS = -3.4729E-16, -1.2658E-15 (LB)
CALCULATED MOMENTS ABOUT X,Y AXES = 1.6213E-16, 6.2386E-17 (IN-LB)

MINIMUM FILM THICKNESS = 1.0000E-03 (IN)

FLOW = 3.5000E+00 (IN^3/SEC) MEASURED AT 1.0000E+00 (PSI)

TORQUE = 1.8850E-02 (IN-LB), FILM POWER LOSS = 5.7122E-02 (HP)

COMPRESSIBILITY NUMBER = 1.0000E+01, SQUEEZE NUMBER = 0.0000E+00

DYNAMIC COEFFICIENTS (FORCE UNIT / DISP. UNIT)

DISP.	x (IN)	y (IN)	ϕ (RAD)	ψ (RAD)	FORCE UNIT
Kx	4.5241E+03	1.2933E+03	-3.6977E+02	2.1989E+02	LB
Ky	-1.2933E+03	4.5241E+03	-2.1989E+02	-3.6977E+02	LB
Kϕ	3.4694E+02	-4.7068E+02	5.9016E+02	5.1362E+02	IN-LB
Kψ	4.7068E+02	3.4694E+02	-5.1362E+02	5.9016E+02	IN-LB
Bx	-2.3432E-02	-1.2667E-01	3.4823E-02	-5.9373E-03	LB-SEC
By	1.2667E-01	-2.3432E-02	5.9373E-03	3.4823E-02	LB-SEC
Bϕ	-2.7769E-02	6.0874E-03	2.3559E-02	-4.4038E-02	IN-LB-SEC
Bψ	-6.0874E-03	-2.7769E-02	4.4038E-02	2.3559E-02	IN-LB-SEC

COMPARISON OF CASE 3 WITH PN471

FLOW = 3.500E+00 (IN^3/SEC) MEASURED AT 1.0000E+00 (PSI)

TORQUE = 1.885E-02 (IN-LB), FILM POWER LOSS = 5.712E-02 (HP)

DYNAMIC COEFFICIENTS (FORCE UNIT / DISP. UNIT)

DISP.	x (IN)	y (IN)	ϕ (RAD)	ψ (RAD)	FORCE UNIT
Kx	4.5236E+03	1.2934E+03	-3.6992E+02	2.1883E+02	LB
Ky	-1.2934E+03	4.5236E+03	-2.1883E+02	-3.6992E+02	LB
Kϕ	3.4697E+02	-4.6939E+02	5.8843E+02	5.1292E+02	IN-LB
Kψ	4.6939E+02	3.4697E+02	-5.1292E+02	5.8843E+02	IN-LB
Bx	-2.3471E-02	-1.2673E-01	3.4849E-02	-5.8520E-03	LB-SEC
By	1.2673E-01	-2.3471E-02	5.8520E-03	3.4849E-02	LB-SEC
Bϕ	-2.7798E-02	5.9155E-03	2.3693E-02	-4.3962E-02	IN-LB-SEC
Bψ	-5.9155E-03	-2.7798E-02	4.3962E-02	2.3693E-02	IN-LB-SEC

(CASE 4) Face seal, no tilt, with pres. grad., Λ=10, σ=0

SPIRAL GROOVE FACE SEAL, ROTATING SURFACE IS SMOOTH

ID, OD, REFERENCE FILM THICKNESS = 1.0000E+00, 2.0000E+00, 1.0000E-03 (IN)

ROTATION SPEED, DISTURBANCE SPEED = 1.9099E+05, 0.0000E+00 (RPM)

INSIDE, OUTSIDE PRESSURE = 2.0000E+00, 1.0000E+00 (PSI)

VISCOSITY = 8.3333E-11 (PSI-SEC), AMBIENT PRESSURE = 1.0000E+00 (PSI)

CALCULATED FORCE IN Z DIRECTION = 1.3612E+00 (LB)
CALCULATED MOMENTS ABOUT X,Y AXES = -3.0782E-16, 1.1794E-15 (IN-LB)

MINIMUM FILM THICKNESS = 1.0000E-03 (IN)

FLOW = 2.2763E+01 (IN^3/SEC) MEASURED AT 1.0000E+00 (PSI)

TORQUE = 2.2645E-03 (IN-LB), FILM POWER LOSS = 6.8621E-03 (HP)

COMPRESSIBILITY NUMBER = 1.0000E+01, SQUEEZE NUMBER = 0.0000E+00

DYNAMIC COEFFICIENTS (FORCE UNIT / DISP. UNIT)

DISP.	z (IN)	ϕ (RAD)	ψ (RAD)	FORCE UNIT
Kz	3.9524E+02	-4.8585E-04	-4.8576E-04	LB
Kϕ	-6.1349E-07	2.0998E+02	8.2256E+01	IN-LB
Kψ	-3.0546E-07	-8.2256E+01	2.0998E+02	IN-LB
Bz	2.9491E-02	-7.3530E-07	-7.3551E-07	LB-SEC
Bϕ	-1.1280E-09	7.0914E-03	-1.8082E-03	IN-LB-SEC
Bψ	-2.3148E-09	1.8082E-03	7.0914E-03	IN-LB-SEC

COMPARISON OF CASE 4 WITH PN471

CALCULATED FORCE IN Z DIRECTION = 1.3612E+00 (LB)

FLOW = 2.2763E+01 (IN^3/SEC) MEASURED AT 1.0000E+00 (PSI)

TORQUE = 2.2644E-03 (IN-LB), FILM POWER LOSS = 6.8620E-03 (HP)

DYNAMIC COEFFICIENTS (FORCE UNIT / DISP. UNIT)

DISP.	z (IN)	ϕ (RAD)	ψ (RAD)	FORCE UNIT
Kz	3.9524E+02			LB
Kϕ		2.0998E+02	8.2240E+01	IN-LB
Kψ		-8.2240E+01	2.0998E+02	IN-LB
Bz	2.9485E-02			LB-SEC
Bϕ		7.0901E-03	-1.8058E-03	IN-LB-SEC
Bψ		1.8058E-03	7.0901E-03	IN-LB-SEC

(CASE 5) Face seal, no tilt, with pres. grad., Λ=10, σ=20

SPIRAL GROOVE FACE SEAL, ROTATING SURFACE IS SMOOTH

ID, OD, REFERENCE FILM THICKNESS = 1.0000E+00, 2.0000E+00, 1.0000E-03 (IN)

ROTATION SPEED, DISTURBANCE SPEED = 1.9099E+05, 1.9099E+05 (RPM)

INSIDE, OUTSIDE PRESSURE = 2.0000E+00, 1.0000E+00 (PSI)

VISCOSITY = 8.3333E-11 (PSI-SEC), AMBIENT PRESSURE = 1.0000E+00 (PSI)

CALCULATED FORCE IN Z DIRECTION = 1.3612E+00 (LB)
CALCULATED MOMENTS ABOUT X,Y AXES = -3.0782E-16, 1.1794E-15 (IN-LB)

MINIMUM FILM THICKNESS = 1.0000E-03 (IN)

FLOW = 2.2763E+01 (IN^3/SEC) MEASURED AT 1.0000E+00 (PSI)

TORQUE = 2.2645E-03 (IN-LB), FILM POWER LOSS = 6.8621E-03 (HP)

COMPRESSIBILITY NUMBER = 1.0000E+01, SQUEEZE NUMBER = 2.0000E+01

DYNAMIC COEFFICIENTS (FORCE UNIT / DISP. UNIT)

DISP.	z (IN)	ϕ (RAD)	ψ (RAD)	FORCE UNIT
Kz	5.3566E+02	-2.9756E-04	-2.9746E-04	LB
Kϕ	-2.1294E-07	2.4013E+02	7.0968E+01	IN-LB
Kψ	2.5103E-07	-7.0968E+01	2.4013E+02	IN-LB
Bz	2.7697E-02	3.8068E-09	3.8070E-09	LB-SEC
Bϕ	2.2173E-12	6.7533E-03	-1.6346E-03	IN-LB-SEC
Bψ	-2.0783E-12	1.6346E-03	6.7533E-03	IN-LB-SEC

COMPARISON OF CASE 5 WITH PN471

CALCULATED FORCE IN Z DIRECTION = 1.3612E+00 (LB)

FLOW = 2.2763E+01 (IN^3/SEC) MEASURED AT 1.0000E+00 (PSI)

TORQUE = 2.2644E-03 (IN-LB), FILM POWER LOSS = 6.8620E-03 (HP)

DYNAMIC COEFFICIENTS (FORCE UNIT / DISP. UNIT)

DISP.	z (IN)	ϕ (RAD)	ψ (RAD)	FORCE UNIT
Kz	5.3557E+02			LB
Kϕ		2.4011E+02	7.0959E+01	IN-LB
Kψ		-7.0959E+01	2.4011E+02	IN-LB
Bz	2.7692E-02			LB-SEC
Bϕ		6.7528E-03	-1.6341E-03	IN-LB-SEC
Bψ		1.6341E-03	6.7528E-03	IN-LB-SEC

(CASE 6) Face seal, no tilt, with pres. grad., Λ=10, σ=200

SPIRAL GROOVE FACE SEAL, ROTATING SURFACE IS SMOOTH

ID, OD, REFERENCE FILM THICKNESS = 1.0000E+00, 2.0000E+00, 1.0000E-03 (IN)

ROTATION SPEED, DISTURBANCE SPEED = 1.9099E+05, 1.9099E+06 (RPM)

INSIDE, OUTSIDE PRESSURE = 2.0000E+00, 1.0000E+00 (PSI)

VISCOSITY = 8.3333E-11 (PSI-SEC), AMBIENT PRESSURE = 1.0000E+00 (PSI)

CALCULATED FORCE IN Z DIRECTION = 1.3612E+00 (LB)
CALCULATED MOMENTS ABOUT X,Y AXES = -3.0782E-16, 1.1794E-15 (IN-LB)

MINIMUM FILM THICKNESS = 1.0000E-03 (IN)

FLOW = 2.2763E+01 (IN^3/SEC) MEASURED AT 1.0000E+00 (PSI)

TORQUE = 2.2645E-03 (IN-LB), FILM POWER LOSS = 6.8621E-03 (HP)

COMPRESSIBILITY NUMBER = 1.0000E+01, SQUEEZE NUMBER = 2.0000E+02

DYNAMIC COEFFICIENTS (FORCE UNIT / DISP. UNIT)

DISP.	z (IN)	ϕ (RAD)	ψ (RAD)	FORCE UNIT
Kz	2.3872E+03	-4.1732E-05	-4.1685E-05	LB
Kϕ	-2.5267E-08	7.2912E+02	-7.4833E+00	IN-LB
Kψ	5.8389E-08	7.4833E+00	7.2912E+02	IN-LB
Bz	4.1358E-03	5.3850E-10	5.3818E-10	LB-SEC
Bϕ	4.2377E-13	1.2426E-03	-5.8922E-05	IN-LB-SEC
Bψ	-5.5928E-13	5.8922E-05	1.2426E-03	IN-LB-SEC

COMPARISON OF CASE 6 WITH PN471

CALCULATED FORCE IN Z DIRECTION = 1.3612E+00 (LB)

FLOW = 2.2763E+01 (IN^3/SEC) MEASURED AT 1.0000E+00 (PSI)

TORQUE = 2.2644E-03 (IN-LB), FILM POWER LOSS = 6.8620E-03 (HP)

DYNAMIC COEFFICIENTS (FORCE UNIT / DISP. UNIT)

DISP.	z (IN)	ϕ (RAD)	ψ (RAD)	FORCE UNIT
Kz	2.3870E+03			LB
Kϕ		7.2907E+02	-7.4987E+00	IN-LB
Kψ		7.4987E+00	7.2907E+02	IN-LB
Bz	4.1383E-03			LB-SEC
Bϕ		1.2438E-03	-5.8939E-05	IN-LB-SEC
Bψ		5.8939E-05	1.2438E-03	IN-LB-SEC

(CASE 7) Misaligned shaft seal with pres. grad. to comp. w/ GASBEAR

SPIRAL GROOVE SHAFT SEAL, ROTATING SURFACE IS SMOOTH

LENGTH, DIAMETER, CLEARANCE = 2.0000E+00, 2.0000E+00, 1.0000E-03 (IN)

ROTATION SPEED, DISTURBANCE SPEED = 1.9099E+05, 0.0000E+00 (RPM)

PRESSURE AT START, END AXIAL BOUNDARIES = 2.0000E+00, 1.0000E+00 (PSI)

VISCOSITY = 8.3333E-11 (PSI-SEC), AMBIENT PRESSURE = 1.0000E+00 (PSI)

CALCULATED FORCES IN X,Y DIRECTIONS = 3.1535E+00, 1.2350E+00 (LB)
CALCULATED MOMENTS ABOUT X,Y AXES = 3.7793E-01, -1.9883E-03 (IN-LB)

MINIMUM FILM THICKNESS = 5.0000E-04 (IN)

FLOW = 4.7315E+00 (IN^3/SEC) MEASURED AT 1.0000E+00 (PSI)

TORQUE = 2.3248E-02 (IN-LB), FILM POWER LOSS = 7.0448E-02 (HP)

COMPRESSIBILITY NUMBER = 1.0000E+01, SQUEEZE NUMBER = 0.0000E+00

DYNAMIC COEFFICIENTS (FORCE UNIT / DISP. UNIT)

DISP.	x (IN)	y (IN)	ϕ (RAD)	ψ (RAD)	FORCE UNIT
Kx	9.2287E+03	4.8183E+03	1.1084E+03	5.7870E+02	LB
Ky	-2.6167E+03	9.5964E+03	4.7033E+02	8.7124E+02	LB
Kϕ	-9.8594E+01	6.5068E+02	1.5189E+03	7.7760E+02	IN-LB
Kψ	7.1674E+02	-9.7210E+01	-1.0491E+03	1.2765E+03	IN-LB
Bx	-2.0553E-01	-4.5816E-01	-1.0900E-01	6.2037E-02	LB-SEC
By	2.5253E-01	-2.9852E-01	-6.7612E-02	-7.7454E-02	LB-SEC
Bϕ	2.3869E-02	1.4706E-02	3.7737E-02	-8.3553E-02	IN-LB-SEC
Bψ	-7.4893E-02	-5.8155E-02	5.7003E-02	6.7719E-02	IN-LB-SEC

COMPARISON OF CASE 7 WITH GASBEAR USING SAME GRID AND ROMBERG EXTRAPOLATION

CALCULATED FORCES IN X,Y DIRECTIONS = 3.1529E+00, 1.2362E+00 (LB)
CALCULATED MOMENTS ABOUT X,Y AXES = 3.7751E-01, -7.3904E-04 (IN-LB)

DYNAMIC COEFFICIENTS (FORCE UNIT / DISP. UNIT)

DISP.	x (IN)	y (IN)	ϕ (RAD)	ψ (RAD)	FORCE UNIT
Kx	9.2287E+03	4.8097E+03	1.1044E+03	5.7867E+02	LB
Ky	-2.6113E+03	9.5993E+03	4.7249E+02	8.7343E+02	LB
Kϕ	-1.0249E+02	6.5339E+02	1.5237E+03	7.7076E+02	IN-LB
Kψ	7.1455E+02	-9.4976E+01	-1.0403E+03	1.2793E+03	IN-LB
Bx	-2.0561E-01	-4.5802E-01	-1.0909E-01	6.1715E-02	LB-SEC
By	2.5292E-01	-2.9885E-01	-6.7494E-02	-7.7535E-02	LB-SEC
Bϕ	2.3875E-02	1.4639E-02	3.7502E-02	-8.3706E-02	IN-LB-SEC
Bψ	-7.4561E-02	-5.7965E-02	5.6982E-02	6.7347E-02	IN-LB-SEC

3.0 INDUSTRIAL CODE SPIRALI - INCOMPRESSIBLE, TURBULENT SPIRAL-GROOVED CYLINDRICAL FACE SEALS

Spiral groove bearings and seals are used to provide stability, load support and pumping for both cylindrical and face seal geometries. In the case of a cylindrical bearing, grooves are usually designed to pump against each other in a symmetric arrangement to provide enhanced stability. A lightly loaded cylindrical seal operating at a low axial flow rate will produce a force that is nearly 90 degrees out of phase with the displacement which will tend to destabilize the rotating shaft. The introduction of spiral grooves can significantly increase the component of force in phase with the displacement and decrease the out of phase component thereby improving stability.

In the case of a face seal or thrust bearing, spiral grooves are often introduced as the primary means of load support. Since a symmetric arrangement is not possible in a radial geometry, the grooves are usually designed to pump towards an ungrooved dam region. The resistance of the dam region increases as the film thickness decreases hence the pumping pressure rise increases thereby giving rise to a positive axial stiffness. The spiral grooves can also be used to pump against an applied pressure gradient thereby resulting in either reduced or reversed leakage.

The computer code SPIRALI predicts performance characteristics of incompressible cylindrical and face seals. Performance characteristics include load capacity (for face seals), leakage flow, power requirements and dynamic characteristics in the form of stiffness, damping and apparent mass coefficients in 4 degrees of freedom for cylindrical seals and 3 degrees of freedom for face seals. These performance characteristics are computed as functions of seal and groove geometry, load or film thickness, running and disturbance speeds, fluid viscosity, and boundary pressures.

The basic assumptions that have gone into the computer code are listed below:

1. The flow is assumed to be isothermal and incompressible.
2. Turbulence is treated with an extended form of the Hirs bulk flow model (Reference 14), generalized to include separate and arbitrary friction factor - Reynolds number relationships for each surface.
3. Inertia effects (which throughout this report will refer to additional effects to those inherent in turbulence) associated with film discontinuities will be treated with the use of loss coefficients.
4. Circumferential and transient effects are treated with the use of small perturbations to a steady state first-order solution for a concentric, aligned seal. These effects are characterized by either by stiffness and damping coefficients that are dependent on the disturbance frequencies or by stiffness, damping, and apparent mass coefficients.
5. The film thickness is assumed to be small compared with seal lengths and diameters but large compared with surface roughness.

6. Narrow groove theory is used to characterize the effects of grooves by a global pressure distribution without requiring computations on a groove by groove basis. This has previously involved neglecting edge effects and local inertia effects associated with groove to groove pressure variations. In general, narrow groove theory is valid when there are a sufficiently large number of grooves so that $2\pi/N_g << 1$, where N_g is the number of grooves. This theory has been extended to account for the pressure jumps arising from the effects of local inertia associated with the sudden changes in cross section at the inlet to each groove and ridge which can be of the order of N_g larger than the other local inertia effects which have been neglected.
7. Although transverse (axial for cylindrical seals or radial for face seals) variations in the film thickness profiles are permitted, machined surfaces for seals are assumed to be axisymmetric with the exception of effects of spiral grooves.

The above assumptions still leave the code applicable to a broad range of cylindrical and face seal applications. Practical designs should contain a fairly large number of grooves to ensure smooth, isotropic operation. Elastic and thermal distortions as well as machining tolerances should also be estimated to validate the axisymmetric clearance assumption and may be characterized in part by inclusion of film variations in the transverse direction. The overall accuracy of the program will depend on the grid size used. Factors such as large film thickness variations in the transverse direction, inclusion of very small transverse inertia effects and large values of the length to diameter ratio could require an increased number of grid points.

A derivation of the equations governing the performance of turbulent, incompressible, spiral groove cylindrical and face seals along with a description of their solution is given in the next section. This will be followed by a description of the computer codes including an input description, sample cases and comparisons with results of other codes.

3.1 Formulation and Method of Solution

Coordinate variables will be used to make the equations developed here applicable to both cylindrical and face seals and may be defined with the aid of Figure 6. The circumferential coordinate, θ, is as shown in Figure 6. The transverse coordinate is described by the variable, s, which is taken to equal the radial coordinate, r, for a face seal and the axial coordinate, z, for a cylindrical seal. The quantity r, when it appears will denote radial position for a face seal and should be set equal to the shaft radius, R_0 for a cylindrical seal. The symbols $\vec{i}$, $\vec{j}$ will be used to denote unit vectors in the θ and s directions respectively.

Formulation of Bulk Flow Equations for Turbulent Lubrication

The equations for turbulent bulk flow to be presented here will be based on a generalization of the Hirs model. Figure 7 shows the velocities and forces associated with a differential element in the θ direction. The bulk flow integrated momentum equations for the θ and s directions are

$$\rho h\left(\frac{\partial u}{\partial t}+v\frac{\partial u}{\partial s}+\frac{u}{r}\frac{\partial u}{\partial \theta}+\frac{uvl_f}{r}\right)=-\frac{h}{r}\frac{\partial p}{\partial \theta}+(\vec{\tau}_b-\vec{\tau}_a)\cdot\vec{i}\quad , \qquad 3\text{-}1$$

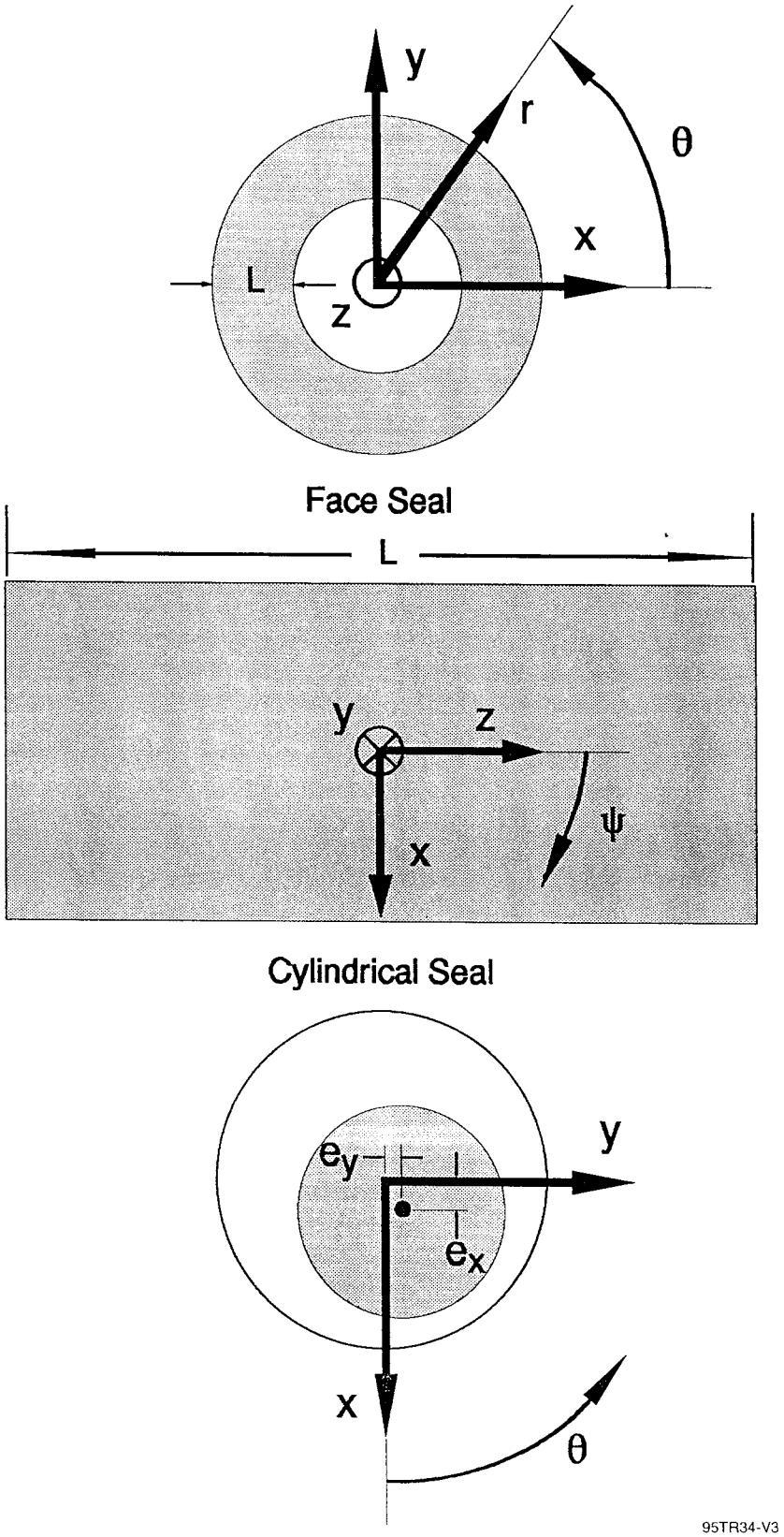

Figure 6. Coordinate System for Spiral Groove Analysis

$$\rho h\left(\frac{\partial v}{\partial t}+v\frac{\partial v}{\partial s}+\frac{u}{r}\frac{\partial v}{\partial \theta}-\frac{u^2 I_f}{r}\right)=-h\frac{\partial p}{\partial s}+(\vec{\tau}_b-\vec{\tau}_a)\cdot\vec{j} \quad . \tag{3-2}$$

The integrated continuity equation is

$$\frac{1}{r}\frac{\partial}{\partial s}(rvh)+\frac{1}{r}\frac{\partial}{\partial \theta}(uh)+\frac{\partial h}{\partial t}=0 \quad . \tag{3-3}$$

In the above equations u and v represent the components of the velocity vector, $\vec{u}=u\vec{i}+v\vec{j}$, p denotes the pressure, $\vec{\tau}_a$ and $\vec{\tau}_b$ are the shear stresses acting on the fluid at surfaces (a) and (b) respectively as shown in Figure 7 and I_f is a flag parameter set equal to 1 for a face seal and 0 for a cylindrical seal.

Each of these shear stresses is assumed to act in the direction of the fluid velocity relative to the respective surface and is related to that velocity by means of a coefficient of resistance or friction factor as follows:

$$\vec{\tau}_a=-\frac{1}{2}\rho|\vec{u}-\vec{u}_a|f_a\left(\frac{2h\rho|\vec{u}-\vec{u}_a|}{\mu}\right)(\vec{u}-\vec{u}_a)=-\frac{1}{4}\frac{\mu}{h}R_a f_a(R_a)(\vec{u}-\vec{u}_a) \quad , \tag{3-4}$$

for surface (a) and for surface (b)

$$\vec{\tau}_b=-\frac{1}{2}\rho|\vec{u}-\vec{u}_b|f_b\left(\frac{2h\rho|\vec{u}-\vec{u}_b|}{\mu}\right)(\vec{u}-\vec{u}_b)=-\frac{1}{4}\frac{\mu}{h}R_b f_b(R_b)(\vec{u}-\vec{u}_b) \quad , \tag{3-5}$$

where the shear factors f_a and f_b are one fourth of the resistance coefficients or friction factors for the respective surfaces (Reference 15) and are functions of the respective Reynolds numbers R_a and R_b which are in turn defined as

$$R_a=2h|\vec{u}-\vec{u}_a|\rho/\mu \quad , \quad R_b=2h|\vec{u}-\vec{u}_b|\rho/\mu \quad . \tag{3-6}$$

The use of various shear functions in the prediction of turbulent behavior of bearings and seals may be found in References 16 - 19. Power law relationships of the form $f=nR^m$ have been used in References 16 - 18 to characterize both smooth and rough surfaces. If both surfaces are smooth the relationship

$$f_a(R_a)=n_0 R_a^{m_0} \quad , \quad f_b(R_b)=n_0 R_b^{m_0} \tag{3-7}$$

may be used with n_0 and m_0 obtained from the Blasius Equation (Reference 14) as $n_0=0.0751$, $m_0=-.25$ for turbulent flow (Reynolds numbers ranging from 4,000 to 100,000). The corresponding values for laminar flow are $n_0=24$ and $m_0=-1$.

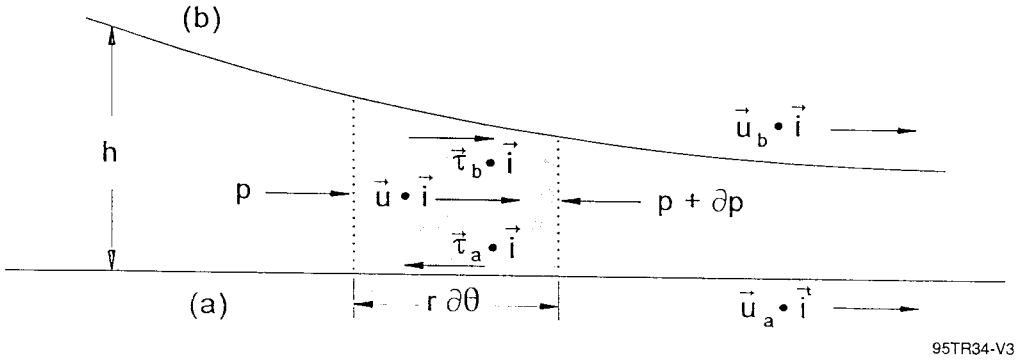

Figure 7. Velocities and Forces on a Differential Element in the θ Direction

Equations (3-1) - (3-3) may be expressed in dimensionless form with the use of the following dimensionless variables

$$\tilde{h} = \frac{h}{C} \quad , \quad \tilde{p} = \frac{p}{p_0} \quad , \quad \tilde{u} = \frac{u}{V_0} \quad , \quad \tilde{v} = \frac{v}{V_0} \quad , \quad \tilde{r} = \frac{r}{r_0}$$

$$S = \frac{s}{r_0} \quad , \quad \tilde{t} = \frac{V_0}{r_0} t \quad , \quad \tilde{T} = \frac{r_0}{C} \frac{T}{p_0} \qquad 3\text{-}8$$

and parameters

$$R = \frac{2CV_0\rho}{\mu} \quad , \quad R^* = \frac{2C}{r_0} R \quad , \quad \tilde{\omega} = \frac{\omega r_0}{V_0} \quad , \quad \tilde{p}^* = \frac{\mu V_0 r_0}{4C^2 p_0} \quad . \qquad 3\text{-}9$$

In the above equations V_0 represents a characteristic velocity, p_0 a characteristic pressure, r_0 and C represent the radius and clearance for a cylindrical seal and the outside radius and characteristic film thickness for a face seal.

Henceforth surface (b) will be taken to be stationary and surface (a) will be taken to move with a circumferential velocity $\mathbf{r\omega}$. The Reynolds numbers R_a and R_b given by Equation (3-6) then become

$$R_a = R\tilde{h}\sqrt{(\tilde{u} - \tilde{r}\tilde{\omega})^2 + \tilde{v}^2} \quad , \quad R_b = R\tilde{h}\sqrt{\tilde{u}^2 + \tilde{v}^2} \quad . \qquad 3\text{-}10$$

The integrated momentum and continuity equations may now be expressed in the dimensionless form

$$-\frac{1}{\tilde{r}} \frac{\partial \tilde{p}}{\partial \theta} = \tilde{p}^* \Phi(\tilde{u}, \tilde{v}, \tilde{h}) + \tilde{p}^* R^* \left(\frac{\partial \tilde{u}}{\partial \tilde{t}} + \tilde{v} \frac{\partial \tilde{u}}{\partial S} + \frac{\tilde{u}}{\tilde{r}} \frac{\partial \tilde{u}}{\partial \theta} + l_f \frac{\tilde{u}\tilde{v}}{\tilde{r}} \right) \quad , \qquad 3\text{-}11$$

$$-\frac{\partial \tilde{p}}{\partial S} = \tilde{p}^* \Psi(\tilde{u}, \tilde{v}, \tilde{h}) + \tilde{p}^* R^* \left(\frac{\partial \tilde{v}}{\partial \tilde{t}} + \tilde{v} \frac{\partial \tilde{v}}{\partial S} + \frac{\tilde{u}}{\tilde{r}} \frac{\partial \tilde{v}}{\partial \theta} - l_f \frac{\tilde{u}^2}{\tilde{r}} \right) \quad , \qquad 3\text{-}12$$

$$\frac{1}{\tilde{r}} \frac{\partial (\tilde{r}\tilde{v}\tilde{h})}{\partial S} + \frac{1}{\tilde{r}} \frac{\partial (\tilde{u}\tilde{h})}{\partial \theta} + \frac{\partial \tilde{h}}{\partial \tilde{t}} = 0 \qquad 3\text{-}13$$

where

$$\Phi(\tilde{u}, \tilde{v}, \tilde{h}) = \frac{(\tilde{u} - \tilde{r}\tilde{\omega}) R_a f_a(R_a) + \tilde{u} R_b f_b(R_b)}{\tilde{h}^2} \quad , \qquad 3\text{-}14$$

and

$$\Psi(\tilde{u}, \tilde{v}, \tilde{h}) = \frac{R_a f_a(R_a) + R_b f_b(R_b)}{\tilde{h}^2} \tilde{v} \quad . \qquad 3\text{-}15$$

Equations (3-11) - (3-13) together with the functions defined by Equations (3-10), (3-14) and (3-15) constitute the dimensionless differential equations for the generalized Hirs bulk flow model under consideration. These equations require a prescribed film thickness profile, $\tilde{h}(S,\theta,\tilde{t})$, definitions of f_a and f_b such as those given by Equation (3-7) and boundary conditions which will be treated below.

Boundary and Continuity Conditions

This analysis is limited to essentially axisymmetric surface shapes and constant boundary pressures. Although spiral grooves will be considered, the groove angle, depth and spacing will be independent of θ. Individual pads and partial films are not treated here. As such, all θ (and time) dependence will be associated with displacements of the sealing surfaces. The only conditions on θ are the requirement of periodicity. That is, pressure and flow rates at $\theta + 2\pi$ must equal those at θ for all θ.

Variations of surface shapes in the **s** direction, including discontinuities are considered. The upstream values of v and p at discontinuities in h are denoted by v_J and p_J as shown in Figure 8. The film thickness changes from the upstream value of h - Δh to the downstream value of h across the jump.

Since the flow rate normal to the jump must be continuous

$$(h - \Delta h)v_J = hv \quad @ \; s = s_J \quad ,$$

where s_J denotes the s coordinate at the jump.

The pressure change at s_J may be expressed in terms of a loss coefficient ξ, based on downstream conditions (Reference 20) as follows:

$$p_J + \tfrac{1}{2}\rho v_J^2 = p + \tfrac{1}{2}\rho v^2(1+\xi) \quad @ \; s = s_J \quad .$$

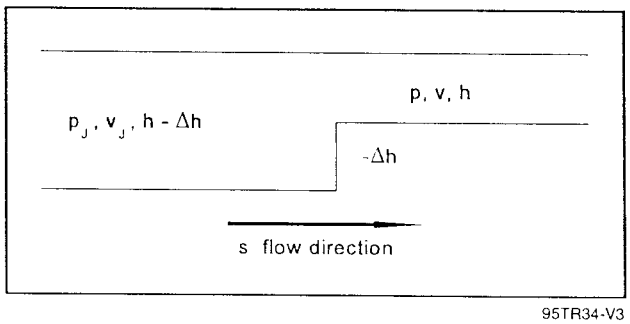

Figure 8. Jump in Film Thickness

The preceding two equations may be rearranged and expressed in dimensionless form as

$$\tilde{v} = (1 - \frac{\Delta\tilde{h}}{\tilde{h}})\tilde{v}_J \ , \quad \Delta\tilde{p} = \tilde{p} - \tilde{p}_J = \frac{1}{2}\tilde{\rho}\tilde{R}\chi(\tilde{v},\tilde{h},\Delta\tilde{h}) \quad @S = S_J \ , \tag{3-16}$$

where

$$\chi(\tilde{v},\tilde{h},\Delta\tilde{h}) = -\left[1 - \left(\frac{\tilde{h}}{\tilde{h} - \Delta\tilde{h}}\right)^2 + \xi\right]\tilde{v}^2 \ . \tag{3-17}$$

The loss coefficient ξ, due to a contraction will in general be a function of the axial Reynolds number and will be denoted by the function $\zeta(\tilde{R}\tilde{h}\tilde{v})$ but is frequently taken to be constant (References 16 - 18). The loss coefficient for an expansion may be found in Reference 20 and is given together with the corresponding relationship for a contraction below:

$$\xi = \begin{cases} \zeta(R,\tilde{h},\tilde{v}) & , \ \Delta\tilde{h} < 0 \ \text{(contraction)} \\ \left(1 - \dfrac{\tilde{h}}{\tilde{h} - \Delta\tilde{h}}\right)^2 & , \ \Delta\tilde{h} \geq 0 \ \text{(expansion)} \end{cases} \ . \tag{3-18}$$

The above considerations together with the requirement that the tangential component of velocity is continuous at jumps across constant s boundaries provides sufficient information to prescribe the boundary conditions at the inlet and exit to the seal as well as the continuity conditions at jumps.

The tangential component of the velocity, u_{in} and the pressure, p_{in} are prescribed at the inlet side of the seal. The relationship between p_{in} and v at the inlet is obtained by setting $\tilde{p}_J = \tilde{p}_{in}$ and evaluating χ as $\Delta\tilde{h} \to -\infty$ in Equations (3-16) - (3-18). These conditions may be written in dimensionless form as

$$\tilde{u} = \tilde{u}_{in} \ , \quad \tilde{p} = \tilde{p}_{in} + \frac{1}{2}\tilde{\rho}\tilde{R}\chi(\tilde{v},\tilde{h},-\infty) = \tilde{p}_{in} - \frac{1}{2}\tilde{\rho}\tilde{R}(1+\zeta)\tilde{v}^2 \quad @ \ S = S_{in} \ . \tag{3-19}$$

The pressure at the exit from the seal will be taken to be continuous and equal to the exit side pressure, p_{ex}.

$$\tilde{p} = \tilde{p}_{ex} \quad @ \ S = S_{ex} \ . \tag{3-20}$$

It should be noted that S_{in} may correspond to either the left or right hand sides of the seal (lower or upper values of S) depending on the direction of flow. S_{ex} will be the value of S at the opposite side of the seal from $S = S_{in}$.

Narrow Groove Theory for Spiral Groove Seals

The development of the narrow groove equations to be presented here will expand upon equations used in Reference 21 which, in turn, contains a reformulation of the lubrication equations for laminar, compressible spiral groove seals presented in Reference 22.

The purpose of narrow groove theory is to obtain equations and solutions for continuous, smooth global pressure and velocity distributions that approximate the limiting form of the solution to Equations (3-10) - (3-15) as the number of grooves becomes large, with the groove angle, β and the groove to pitch ratio, α, held constant. This process greatly reduces the complexity of the solution and eliminates the need for the large grid that would be required to adequately describe all of the grooves individually.

The discontinuities in film thickness associated with the grooves will give rise to discontinuities in the pressures, pressure gradients, and velocities at the ridge-groove interfaces. The relative discontinuities in the velocity components normal to the grooves will be of the same order as the relative film discontinuities. The predicted discontinuities in the local pressures at the interfaces would be of the order of the inertia ($\tilde{p}^*R^*$) terms on the right hand sides of Equations (3-11) and (3-12). It is important to note however, that as both the number of grooves and the inertia terms become large, flows will not be able to fully develop within or between grooves.

Figure 9 shows three conceptual states of flow development in the order of increasing significance of local fluid inertia and decreasing degree of flow development. These are Case a, where the local pressure changes at the inlet to each groove (or ridge) are negligible; Case b, where a wake forms at the inlet to a groove whose extent is small compared to the length of a groove and Case c, where a jet forms and prevails over most or all of the length of the groove. These three cases are discussed individually below:

a. **Negligible inlet pressure changes.** Spiral groove seals frequently operate at relatively small clearances (as opposed to labyrinth seals or even damping seals) and will pump at relatively low flow rates compared with those produced by imposed pressure gradients of sufficient magnitude to produce large inertia effects. Under these conditions, the flow can be treated as fully developed over the entire groove and inertia effects may be neglected in the analysis of the local pressures and velocities. All inertia effects in Equations (3-11) - (3-20) may, however, be included in the treatment of the global pressure and velocities. As such, pumping affected by turbulent shear in regions containing spiral grooves would be accounted for and global inertia effects due to circular steps and grooves and other axial clearance variations would still be included in all regions.

   A schematic showing a global and local pressure distribution for this case along with some of the spiral groove film variables under consideration is presented in Figure 10. The local pressure profile is shown by the sawtooth lines whose lower vertices, for purposes of illustration, are connected by the global pressure profile, p. The global pressure profile does not necessarily lie at the lower vertices of the local pressure profile but could lie anywhere between the lower and upper vertices. In the limit as the number of grooves becomes large, curves connecting the upper and lower vertices will approach each other (subject to the approximations discussed above). This limiting behavior is not true of u, v, h or the local pressure gradients which will have different values over lands and grooves no matter how large the number of grooves.

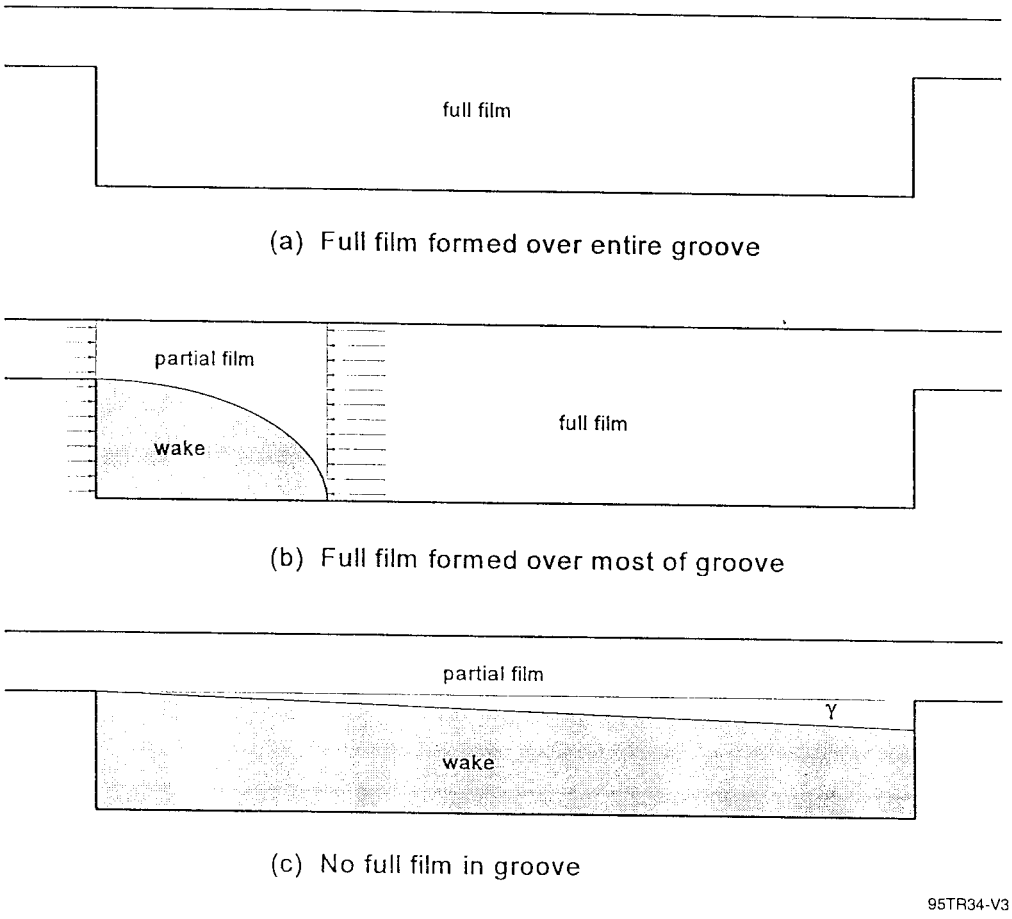

Figure 9. Examples of Degrees of Film Formation in Groove

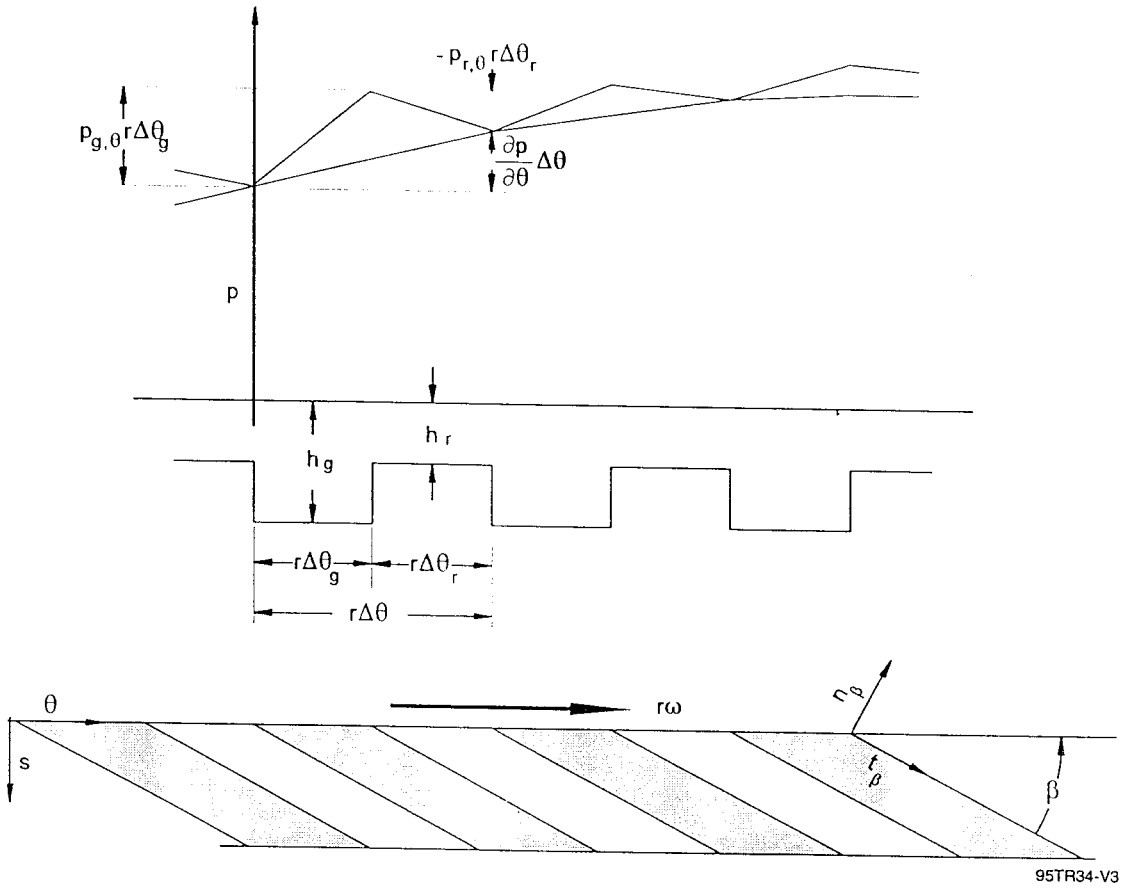

Figure 10. Schematic of Spiral Groove Parameters, Global and Local Pressures, Case a

b. **Fully developed films with significant inlet pressure changes.** This case extends Case a by including local pressure changes at the inlet to each groove and ridge with the use of loss coefficients in a manner analogous to that used at the inlets to each region given by Equations (3-16) - (3-18). The treatment of these pressure changes as boundary pressure discontinuities assume that the length of the wake shown in Figure 9b is small compared with other relevant circumferential and transverse length dimensions. The relevant length for comparison with the wake length at the start of a region would be the transverse length of the region. In the case of spiral grooves within a region, the relevant lengths would be the widths of the grooves and ridges.

   The local pressures shown in Figure 11 are a generalization of those in Figure 10 to allow for local pressure jumps at the inlet to each groove and ridge. Unlike Case a, the upper and lower envelopes of the local pressure curves will not coalesce as the number of grooves becomes large since the magnitudes of the groove and ridge widths do not enter directly into the jump relationships given by Equations (3-16) - (3-18) and the magnitudes of the jumps will not approach 0 as long as Case b conditions prevail. The local pressure jumps for this case will be shown to give rise to a term of order $(\tilde{p}^* R^* N_g)$ which will be retained in the analysis. As with case 1, the other inertia terms will be neglected in the local analysis but maintained in the global analysis. These assumptions will thus give rise to asymptotic relationships as the number of grooves becomes very large in contrast to the limiting relationships corresponding to the assumptions used in Case a.

c. **Jet extends over entire groove.** As the number of grooves becomes very large a limiting flow should in fact occur as a jet forms that extends across the entire groove. The bulk flow theory which is based on the assumptions that the shear forces on the turbulent core arise directly from interactions between the core and the bounding surfaces break down at this point. A rigorous analysis would involve consideration of the jet, the wake, interactions between jet and wake, interactions between jet and wall etc. and would require three dimensional solutions to the momentum and continuity equations which is beyond the scope of the present effort. An alternative approach would involve the use of additional empirical relationships to characterize these interactions so that limiting behavior can be obtained. Examples of the use of such relationships are given in Reference 23 for labyrinth seals and in Reference 24 for straight through screw seals.

The narrow groove analysis contained in the rest of this section will refer to Case b unless otherwise specified. The theory requires the development of expressions for the local quantities in terms of continuous global quantities that become valid as the number of grooves becomes large. Local quantities will be denoted by the subscript g when referring to grooves and r when referring to ridges. Variables such as p,u,v appearing without r or g subscripts will henceforth denote global quantities. The subscript r denoting ridges has been used for consistency with existing literature and should not be confused with the radial position variable r which will not be used as a subscript.

Spiral groove patterns for a given region are characterized by three parameters which are defined in terms of quantities shown in Figure 11. These are the groove depth $\delta = h_g - h_r$, the groove to pitch ratio $\alpha = \Delta\theta_g/(\Delta\theta_g+\Delta\theta_r)$ and the groove angle β defined as the angle between the groove and the surface velocity direction, measured from the groove.

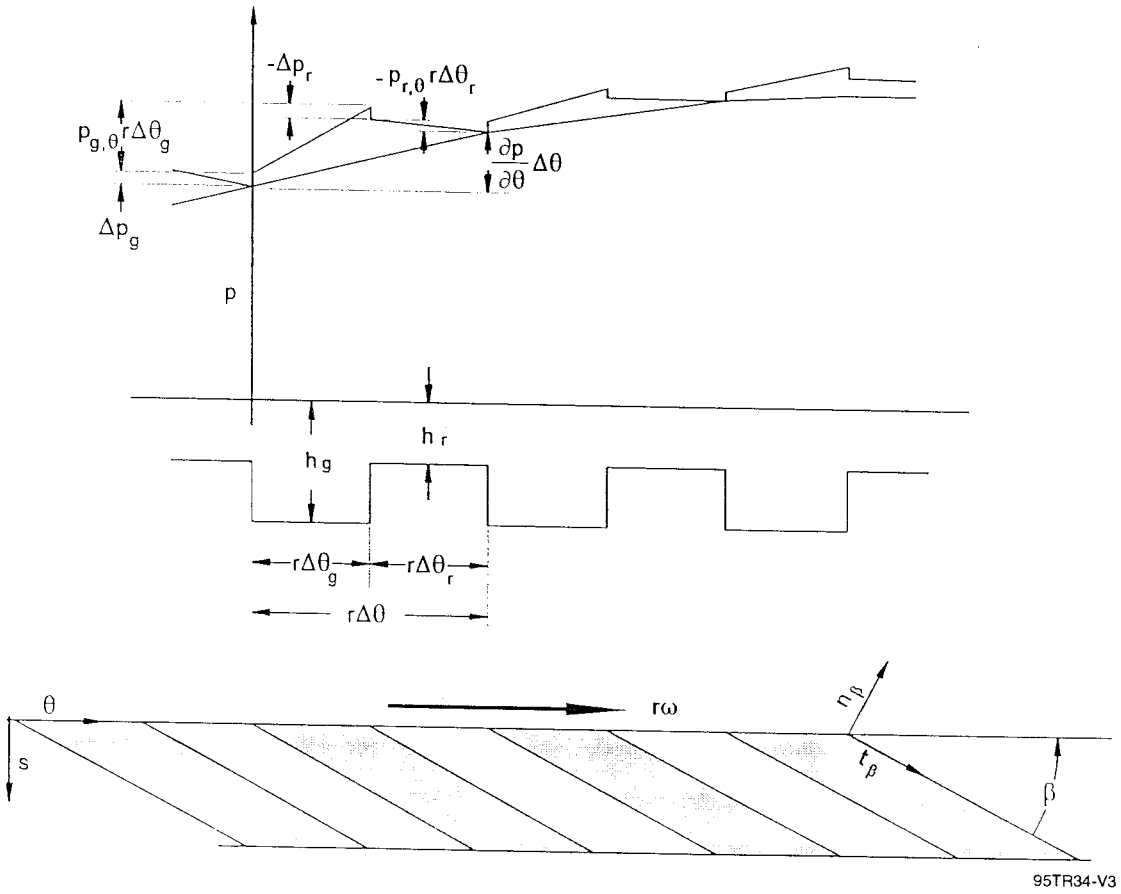

Figure 11. Schematic of Spiral Groove Parameters, Global and Local Pressures, Case b

One may now introduce the dimensionless groove and ridge flows in the θ and s directions

$$\tilde{q}_{g\theta} = \tilde{u}_g \tilde{h}_g \ , \quad \tilde{q}_{gs} = \tilde{v}_g \tilde{h}_g \ , \quad \tilde{q}_{r\theta} = \tilde{u}_r \tilde{h}_r \ , \quad \tilde{q}_{rs} = \tilde{v}_r \tilde{h}_r \ , \tag{3-21}$$

and express the turbulent shear functions Φ and Ψ defined by Equations (3-14) and (3-15) for the grooves as

$$\Phi_g = \Phi\left(\frac{\tilde{q}_{g\theta}}{\tilde{h}_g}, \frac{\tilde{q}_{gs}}{\tilde{h}_g}, \tilde{h}_g\right) \ , \quad \Psi_g = \Psi\left(\frac{\tilde{q}_{g\theta}}{\tilde{h}_g}, \frac{\tilde{q}_{gs}}{\tilde{h}_g}, \tilde{h}_g\right) \tag{3-22}$$

and for the ridges as

$$\Phi_r = \Phi\left(\frac{\tilde{q}_{r\theta}}{\tilde{h}_r}, \frac{\tilde{q}_{rs}}{\tilde{h}_r}, \tilde{h}_r\right) \ , \quad \Psi_r = \Psi\left(\frac{\tilde{q}_{r\theta}}{\tilde{h}_r}, \frac{\tilde{q}_{rs}}{\tilde{h}_r}, \tilde{h}_r\right) \ . \tag{3-23}$$

One may now write Equations (3-11) and (3-12) for the groove regions as

$$-\tilde{p}_{g,\theta} = -\frac{1}{\tilde{r}} \left.\frac{\partial \tilde{p}}{\partial \theta}\right|_g = \tilde{\rho}^* \Phi_g + \tilde{\rho}^* R^* \left(\frac{\partial \tilde{u}}{\partial \tilde{t}} + \tilde{v} \frac{\partial \tilde{u}}{\partial S} + \frac{\tilde{u}}{\tilde{r}} \frac{\partial \tilde{u}}{\partial \theta} + l_f \frac{\tilde{u}\tilde{v}}{\tilde{r}} \right) \ , \tag{3-24}$$

$$-\tilde{p}_{g,s} = -\left.\frac{\partial \tilde{p}}{\partial S}\right|_g = \tilde{\rho}^* \Psi_g + \tilde{\rho}^* R^* \left(\frac{\partial \tilde{v}}{\partial \tilde{t}} + \tilde{v} \frac{\partial \tilde{v}}{\partial S} + \frac{\tilde{u}}{\tilde{r}} \frac{\partial \tilde{v}}{\partial \theta} - l_f \frac{\tilde{u}^2}{\tilde{r}} \right) \tag{3-25}$$

and for the ridge regions as

$$-\tilde{p}_{r,\theta} = -\frac{1}{\tilde{r}} \left.\frac{\partial \tilde{p}}{\partial \theta}\right|_r = \tilde{\rho}^* \Phi_r + \tilde{\rho}^* R^* \left(\frac{\partial \tilde{u}}{\partial \tilde{t}} + \tilde{v} \frac{\partial \tilde{u}}{\partial S} + \frac{\tilde{u}}{\tilde{r}} \frac{\partial \tilde{u}}{\partial \theta} + l_f \frac{\tilde{u}\tilde{v}}{\tilde{r}} \right) \ , \tag{3-26}$$

$$-\tilde{p}_{r,s} = -\left.\frac{\partial \tilde{p}}{\partial S}\right|_r = \tilde{\rho}^* \Psi_r + \tilde{\rho}^* R^* \left(\frac{\partial \tilde{v}}{\partial \tilde{t}} + \tilde{v} \frac{\partial \tilde{v}}{\partial S} + \frac{\tilde{u}}{\tilde{r}} \frac{\partial \tilde{v}}{\partial \theta} - l_f \frac{\tilde{u}^2}{\tilde{r}} \right) \ . \tag{3-27}$$

The unit tangent and normal vectors for the logarithmic spiral as shown in Figure 11 are given by

$$\vec{t}_\beta = \cos\beta \vec{i} + \sin\beta \vec{j} \ , \quad \vec{n}_\beta = \sin\beta \vec{i} - \cos\beta \vec{j} \tag{3-28}$$

If local inertia effects were neglected, the pressure would be continuous at each groove-ridge interface and the derivative of the pressure in the direction tangential to the interface, $\vec{\nabla}p \bullet \vec{t}_\beta$, would also be continuous. In keeping with the assumption that the only *local* inertia effect to be considered is the pressure jump normal to the interface, continuity of the tangential pressure derivative will be maintained even when this effect is considered. Continuity of the tangential derivative of pressure at the interface may be expressed as

$$\cos\beta\, \tilde{p}_{g,\theta} + \sin\beta\, \tilde{p}_{g,s} = \cos\beta\, \tilde{p}_{r,\theta} + \sin\beta\, \tilde{p}_{r,s} \quad . \tag{3-29}$$

One may now substitute Equations (3-24) - (3-27) for the corresponding pressure derivatives in the above equation to obtain

$$\cos\beta\, \Phi_g + \sin\beta\, \Psi_g = \cos\beta\, \Phi_r + \sin\beta\, \Psi_r \quad . \tag{3-30}$$

The flow rate relative to a groove-ridge interface in the direction normal to that interface, $\tilde{q}_n$, must be continuous. For grooves on the stationary surface (b), that flow rate would be $h\vec{u} \bullet \vec{n}_\beta$ and for grooves on the moving surface (a), it would be $h(\vec{u} - r\omega\, \vec{i}) \bullet \vec{n}_\beta$. One may use the dimensionless groove and ridge flow rates defined by Equation (3-21) and perform the indicated dot products to express this continuity condition as

$$\tilde{q}_n = (\tilde{q}_{g\theta} - \tilde{r}\tilde{\omega}\tilde{h}_g I_\omega)\sin\beta - \tilde{q}_{gs}\cos\beta = (\tilde{q}_{r\theta} - \tilde{r}\tilde{\omega}\tilde{h}_r I_\omega)\sin\beta - \tilde{q}_{rs}\cos\beta \ , \tag{3-31}$$

where I_ω is equal to **1** if the grooves are on the moving surface and 0 if the grooves are on the stationary surface. The two equalities on the right may be rearranged to obtain the relationship

$$\sin\beta\, \tilde{q}_{g\theta} - \cos\beta\, \tilde{q}_{gs} - \sin\beta\, \tilde{q}_{r\theta} + \cos\beta\, \tilde{q}_{rs} = \tilde{r}\tilde{\omega}\tilde{\delta} I_\omega \sin\beta \quad . \tag{3-32}$$

One may now equate flow the across a groove-ridge pair in the θ direction to the global flow in that direction and express the result in dimensionless form as

$$\alpha\tilde{q}_{g\theta} + (1-\alpha)\tilde{q}_{r\theta} = \tilde{u}\tilde{h} \quad . \tag{3-33}$$

A similar balance in the **s** direction results in the relationship

$$\alpha\tilde{q}_{gs} + (1-\alpha)\tilde{q}_{rs} = \tilde{v}\tilde{h} \quad . \tag{3-34}$$

The global film thickness, h is the value which results in the same flow area as that produced by the local film thickness variation and may be expressed in dimensionless form as

$$\tilde{h} = \alpha\tilde{h}_g + (1-\alpha)\tilde{h}_r = \tilde{h}_r + \alpha\tilde{\delta} \tag{3-35}$$

Equations (3-30) and (3-32) - (3-34) represent four algebraic equations which may be solved for the four local flow rates $\tilde{q}_{g\theta}$, $\tilde{q}_{gs}$, $\tilde{q}_{r\theta}$ and $\tilde{q}_{rs}$. Iterative solutions are obtained numerically with the use of a Newton-Raphson procedure to linearize Equation (3-30).

The pressure changes (downstream - upstream) incurred at the entrance to a groove, Δp_g, and at the entrance to a ridge, Δp_r, may be expressed in dimensionless form with the aid of the jump function χ, defined by Equations (3-16) - (3-18), as follows:

$$\Delta\tilde{p}_g = \frac{1}{2}\tilde{p}^{*}R^{*}\chi\left(\frac{\tilde{q}_n}{\tilde{h}_g},\tilde{h}_g,\tilde{\delta}\right), \quad \Delta\tilde{p}_r = \frac{1}{2}\tilde{p}^{*}R^{*}\chi\left(\frac{\tilde{q}_n}{\tilde{h}_r},\tilde{h}_r,-\tilde{\delta}\right) . \tag{3-36}$$

The normal flow component, $\tilde{q}_n$, may be expressed in terms of the global velocities and film thickness with the use of Equations (3-31) and (3-33) - (3-35) as

$$\tilde{q}_n = (\tilde{u}\tilde{h} - \tilde{r}\tilde{\omega}\tilde{h}l_\omega)\sin\beta - \tilde{v}\tilde{h}\cos\beta . \tag{3-37}$$

By equating the change in pressure over a groove-ridge pair to the changes in the global pressure, first in the θ direction, as shown in Figure 11, and then in the s direction and expressing the result in dimensionless form, the following equations are obtained:

$$\frac{1}{\tilde{r}}\frac{\partial\tilde{p}}{\partial\theta} = \alpha\tilde{p}_{g,\theta} + (1-\alpha)\tilde{p}_{r,\theta} + \frac{\Delta\tilde{p}_g + \Delta\tilde{p}_r}{\tilde{r}\Delta\theta}\,\mathrm{sign}(\tilde{q}_n\vec{n}_\beta\cdot\vec{i}) , \tag{3-38}$$

$$\frac{\partial\tilde{p}}{\partial S} = \alpha\tilde{p}_{g,s} + (1-\alpha)\tilde{p}_{r,s} + \frac{\Delta\tilde{p}_g + \Delta\tilde{p}_r}{\tilde{r}\Delta\theta\,|\tan\beta|}\,\mathrm{sign}(\tilde{q}_n\vec{n}_\beta\cdot\vec{j}) , \tag{3-39}$$

where the sign functions appearing in the above equations are either 1 or -1 depending on the direction of the normal component of flow with respect to the corresponding coordinate direction.

Finally, noting that $\Delta\theta = 2\pi/N_g$ and the definition of $\vec{n}_\beta$ given by Equation (3-28), one may substitute Equations (3-24) - (3-27) for the corresponding local pressure gradients and Equation (3-34) for the pressure jumps in Equations (3-38) and (3-39), and write the resulting equations in the form

$$-\frac{1}{\tilde{r}}\frac{\partial\tilde{p}}{\partial\theta} = \tilde{p}^{*}\Phi(\tilde{u},\tilde{v},\tilde{h},l_f) + \tilde{p}^{*}R^{*}\left(\frac{\partial\tilde{u}}{\partial\tilde{t}} + \tilde{v}\frac{\partial\tilde{u}}{\partial S} + \frac{\tilde{u}}{\tilde{r}}\frac{\partial\tilde{u}}{\partial\theta}\right) , \tag{3-40}$$

$$-\frac{\partial\tilde{p}}{\partial S} = \tilde{p}^{*}\Psi(\tilde{u},\tilde{v},\tilde{h},l_f) + \tilde{p}^{*}R^{*}\left(\frac{\partial\tilde{v}}{\partial\tilde{t}} + \tilde{v}\frac{\partial\tilde{v}}{\partial S} + \frac{\tilde{u}}{\tilde{r}}\frac{\partial\tilde{v}}{\partial\theta}\right) , \tag{3-41}$$

where

$$\Phi = \alpha\Phi_g + (1-\alpha)\Phi_r + R^* \left\{ I_f \frac{\tilde{u}\tilde{v}}{\tilde{r}} - \frac{N_g}{4\pi\tilde{r}} \mathrm{sign}(\tilde{q}_n \sin\beta) \left[\chi\left(\frac{\tilde{q}_n}{\tilde{h}_g}, \tilde{h}_g, \tilde{\delta}\right) + \chi\left(\frac{\tilde{q}_n}{\tilde{h}_r}, \tilde{h}_r, -\tilde{\delta}\right) \right] \right\} \quad 3\text{-}42$$

and

$$\Psi = \alpha\Psi_g + (1-\alpha)\Psi_r + R^* \left\{ -I_f \frac{\tilde{u}^2}{\tilde{r}} + \frac{N_g}{4\pi\tilde{r}\,|\tan\beta|} \mathrm{sign}(\tilde{q}_n \cos\beta) \left[\chi\left(\frac{\tilde{q}_n}{\tilde{h}_g}, \tilde{h}_g, \tilde{\delta}\right) + \chi\left(\frac{\tilde{q}_n}{\tilde{h}_r}, \tilde{h}_r, -\tilde{\delta}\right) \right] \right\} \quad 3\text{-}43$$

The Coriolis and centrifugal inertia terms for face seals and the spiral groove local inertia term have been combined with the turbulent shear resistance terms in Equations (3-42) and (3-43). This has been done for convenience because of their algebraic nature and will simplify the development and solution of the first and second order flow equations to be discussed in the next section.

The actual number of grooves, N_g, does not usually appear in a narrow groove analysis. It enters here only to characterize the cumulative effects of losses due to sudden changes in cross section between ridges and grooves. Formally setting $N_g=0$ would therefore only eliminate the inclusion of these local inertia effects and would maintain all of the other spiral groove effects under consideration. Caution should be exercised when groove or ridge widths become the same order of magnitude as the clearance. This would invalidate one of the basic geometric assumptions of the bulk flow theory used throughout this analysis and could have a particularly pronounced affect on the validity of the above local inertia terms.

Equations (3-40) and (3-41) represent the generalization of Equations (3-11) and (3-12) to spiral groove seals and reduce to Equations (3-11) and (3-12) when both α and N_g are set equal to 0. The continuity equation [Equation (3-13)], and the continuity and boundary conditions given by Equations (3-16) - (3-20) remain unchanged subject to the interpretation of $\tilde{u}$, $\tilde{v}$, $\tilde{p}$ and $\tilde{h}$ as their global values when $\alpha > 0$.

Development of First- and Second-Order Equations for Small Displacements

The first-order variables will be the global film thickness, pressure and tangential and transverse velocities for an undisplaced shaft. They will depend only on s and their dimensionless forms will be denoted by $\tilde{H}(S)$, $\tilde{P}(S)$, $\tilde{U}(S)$ and $\tilde{V}(S)$ respectively. Substitution of the above variables for $\tilde{h}$, $\tilde{p}$, $\tilde{u}$, and $\tilde{v}$ respectively, in Equations (3-40), (3-41), and (3-13) yields the following set of ordinary differential equations:

$$\Phi(\tilde{U},\tilde{V},\tilde{H},I_f) + R^* \tilde{V} \frac{d\tilde{U}}{dS} = 0 \quad , \quad 3\text{-}44$$

$$-\frac{d\tilde{P}}{dS} = \tilde{p}^* \Psi(\tilde{U},\tilde{V},\tilde{H},I_f) + \tilde{p}^* R^* \tilde{V} \frac{d\tilde{V}}{dS} \quad , \quad 3\text{-}45$$

$$\frac{d(\tilde{r}\tilde{H}\tilde{V})}{dS} = 0 \quad . \quad 3\text{-}46$$

The boundary and jump conditions for the first-order variables are prescribed by Equations (3-16) - (3-20) with $\tilde{h}, \tilde{p}, \tilde{u}$, and $\tilde{v}$ replaced by the corresponding first-order variables. The boundary conditions are given by

$$\tilde{U} = \tilde{u}_{in} \ , \quad \tilde{P} = \tilde{p}_{in} + \tfrac{1}{2}\tilde{\rho}\tilde{R}\chi(\tilde{V},\tilde{H},-\infty) = \tilde{p}_{in} - \tfrac{1}{2}\tilde{\rho}\tilde{R}(1+\zeta)\tilde{V}^2 \quad @\ S = S_{in} \tag{3-47}$$

and

$$\tilde{P} = p_{ex} \quad @\ S = S_{ex} \ . \tag{3-48}$$

One may now add a small displacement, h′(s,θ,t) to H(s) and express the resulting film thickness, pressure and velocities in dimensionless form as

$$\begin{aligned} &\tilde{h} = \tilde{H}(S) + \tilde{h}'(S,\theta,\tilde{t}) \ , \quad \tilde{u} = \tilde{U}(S) + \tilde{u}'(S,\theta,\tilde{t}) \ , \\ &\tilde{v} = \tilde{V}(S) + \tilde{v}'(S,\theta,\tilde{t}) \ , \quad \tilde{p} = \tilde{P}(S) + \tilde{p}'(S,\theta,\tilde{t}) \ . \end{aligned} \tag{3-49}$$

When above relationships are substituted for the corresponding variables in Equations (3-40), (3-41) and (3-13) and quadratic terms in second-order (primed) quantities are neglected, the following second-order, linearized momentum and continuity equations are obtained:

$$-\frac{1}{\tilde{r}\tilde{\rho}}\frac{\partial\tilde{p}'}{\partial\theta} = \tilde{R}\left(\frac{\partial\tilde{u}'}{\partial\tilde{t}} + \tilde{V}\frac{\partial\tilde{u}'}{\partial S} + \frac{d\tilde{U}}{dS}\tilde{v}' + \frac{\tilde{U}}{\tilde{r}}\frac{\partial\tilde{u}'}{\partial\theta}\right) + \Phi_{\tilde{U}}\tilde{u}' + \Phi_{\tilde{V}}\tilde{v}' + \Phi_{\tilde{H}}\tilde{h}' \ , \tag{3-50}$$

$$-\frac{1}{\tilde{\rho}}\frac{\partial\tilde{p}'}{\partial S} = \tilde{R}\left(\frac{\partial\tilde{v}'}{\partial\tilde{t}} + \tilde{V}\frac{\partial\tilde{v}'}{\partial S} + \frac{d\tilde{V}}{dS}\tilde{v}' + \frac{\tilde{U}}{\tilde{r}}\frac{\partial\tilde{v}'}{\partial\theta}\right) + \Psi_{\tilde{U}}\tilde{u}' + \Psi_{\tilde{V}}\tilde{v}' + \Psi_{\tilde{H}}\tilde{h}' \ , \tag{3-51}$$

$$\tilde{V}\frac{\partial(\tilde{r}\tilde{h}')}{\partial S} + \frac{d\tilde{V}}{dS}\tilde{r}\tilde{h}' + \tilde{r}\tilde{H}\frac{\partial v'}{\partial S} + \frac{d(\tilde{r}\tilde{H})}{dS}\tilde{v}' + \tilde{U}\frac{\partial\tilde{h}'}{\partial\theta} + \tilde{H}\frac{\partial\tilde{u}'}{\partial\theta} + \tilde{r}\frac{\partial\tilde{h}'}{\partial\tilde{t}} = 0 \ . \tag{3-52}$$

The subscripts $\tilde{U}$, $\tilde{V}$ and $\tilde{H}$ are used to denote partial differentiation with respect to those variables.

The continuity requirements for $\tilde{p}'$ and $\tilde{v}'$ at values of s where h is discontinuous are obtained by performing a similar linearization on Equation (3-16) and are given below:

$$\tilde{v}' = \frac{\tilde{V}\Delta\tilde{h}}{\tilde{H}(\tilde{H}-\Delta\tilde{h})}\tilde{h}' + \frac{(\tilde{H}-\Delta\tilde{h})}{\tilde{H}}\tilde{v}_J' \ , \quad \Delta\tilde{p}' = \tfrac{1}{2}\tilde{\rho}\tilde{R}(\chi_{\tilde{V}}\tilde{v}' + \chi_{\tilde{H}}\tilde{h}') \quad @S = S_J \ . \tag{3-53}$$

The tangential velocity $\tilde{u}'$ will be continuous. The end conditions given below are obtained by linearizing Equations (3-19) and (3-20) and substituting the values of $\tilde{U}$, $\tilde{V}$ and $\tilde{P}$ prescribed by Equations (3-47) and (3-48):

$$\tilde{u}' = 0 \ , \quad \tilde{p}' = \frac{1}{2}\tilde{\rho}R^*(\chi_{\tilde{V}}\tilde{v}' + \chi_{\tilde{H}}\tilde{h}') \quad @S = S_{in} \tag{3-54}$$

and

$$\tilde{p}' = 0 \quad @ \ S = S_{ex} \ . \tag{3-55}$$

Solution to First-Order Flow Equations

The first-order flow equations are solved by a fairly straightforward numerical procedure. To begin with one may integrate Equation (3-46) and express the result in the form

$$\tilde{V} = \frac{\tilde{r}_{in}\tilde{H}_{in}\tilde{V}_{in}}{\tilde{r}\tilde{H}} \ ,$$

where the dimensionless transverse inlet velocity $\tilde{V}_{in}$, is unknown and must be initially assumed. One may compute $\tilde{V}(S)$, from the above equation, for the assumed value of $\tilde{V}_{in}$. The tangential velocity, $\tilde{U}(S)$, may now be determined by solving Equation (3-44) numerically subject the first boundary condition in Equation (3-47). Once $\tilde{U}(S)$ and $\tilde{V}(S)$ have been established, $\tilde{P}(S)$ may be determined by numerical integration of Equation (3-45) subject to the second boundary condition in Equation (3-47). The correct value of $\tilde{V}_{in}$ will be that which results in a pressure distribution that satisfies Equation (3-48) and is determined numerically by Newton's method. The transverse flow rate, Q, may then be calculated as $Q = 2\pi r_0 C V_0 \tilde{r}_{in}\tilde{H}_{in}\tilde{V}_{in}$.

A semi-implicit algorithm has been used for solving Equation (3-44). Examples of semi-implicit algorithms may be found in many texts on numerical methods such as Reference 25. Although they are slightly more complex than some of the widely used explicit methods such as Runge-Kutta, they provide increased stability for "stiff" systems such as that which may occur here at small values of R^*. Although Equation (3-44) is a single first-order differential equation, the algorithm is presented below for a system of N first-order ordinary differential equations, as will occur later in the development of the second-order solution.

The system of differential equations may be represented in the form

$$\frac{dY_i}{dS} = F_i(S, Y_1, Y_2, \ldots, Y_N) \ , \quad i = 1,2,\ldots,N \ , \tag{3-56}$$

where Y_i denotes the dependent variables. If the values of Y_i at the new position (S + ΔS) are denoted by the column vector $\{Y^{new}\}$, and the values at the old position by $\{Y\}$, the equation used for computing $\{Y^{new}\}$ may be written as

$$\{Y^{new}\} = \{Y\} + \Delta S\left([I] - \frac{\Delta S}{2}[k]\right)^{-1}\left\{F\left(S+\frac{\Delta S}{2}, Y_1, Y_2, \ldots, Y_N\right)\right\} \quad , \qquad 3\text{-}57$$

where [I] is the unit diagonal matrix of order N and [k] is a matrix of derivatives whose components are

$$k_{ij} = \frac{\partial}{\partial Y_j} F_i\left(S+\frac{\Delta S}{2}, Y_1, Y_2, \ldots, Y_j, \ldots, Y_N\right) \quad , \quad i,j = 1,2,\ldots,N \quad . \qquad 3\text{-}58$$

Solution to Second-Order Flow Equations

Although the global film thickness $\tilde{H}$, remains an arbitrary function of the transverse position S, the displacement of the center of the seal will be taken to have the form of a small oscillatory translation, e_x, in the x direction, for a cylindrical seal or e_z, in the z direction, for a face seal and a small oscillatory rotation about the y axis, ψ, for either type of seal. If the seal oscillates at speed Ω, the dimensionless film displacement, $-\tilde{h}'$, will take the form

$$-\tilde{h}' = \left[\tilde{\psi}_0 S\cos\theta + l_c \tilde{e}_{x0}\cos\theta + l_f \tilde{e}_{z0}\right]\cos\tilde{\Omega}\tilde{t} \quad , \qquad 3\text{-}59$$

where

$$l_c = 1 - l_f \quad , \quad \tilde{\Omega} = \frac{\Omega r_0}{V_0} \quad , \quad \psi = \frac{r_0}{C}\tilde{\psi}_0\cos\tilde{\Omega}\tilde{t} \quad , \quad e_x = \frac{\tilde{e}_{x0}}{C}\cos\tilde{\Omega}\tilde{t} \quad , \quad e_z = \frac{\tilde{e}_{z0}}{C}\cos\tilde{\Omega}\tilde{t} \quad . \qquad 3\text{-}60$$

Each of the three terms on the right hand side of Equation (3-59) may be defined as component film displacements, δ_k and the equation may be rewritten as

$$-\tilde{h}' = \sum_{k=1}^{3} \delta_k \quad . \qquad 3\text{-}61$$

The component film displacements may be expressed in complex form as

$$\delta_k = \frac{1}{2}\Re\left(\delta_k^{+} + \delta_k^{-}\right) \quad , \qquad 3\text{-}62$$

where

$$\delta_k^{\pm} = \epsilon_k \eta_k(S) e^{i(J_k\theta \pm \tilde{\Omega}\tilde{t})} \quad . \qquad 3\text{-}63$$

The functions $\Re(Z)$ in the above equation and $\Im(Z)$ to be used later denote the real and imaginary parts of the complex variable Z respectively. The values of ϵ_k, η_k and J_k are given below:

$$\begin{array}{llll} k = & 1, & 2, & 3 \\ \epsilon_k = & \tilde{\Psi}_0, & \tilde{e}_{x0}, & \tilde{e}_{z0} \\ \eta_k = & S, & I_c, & I_f \\ J_k = & 1, & 1, & 0 \end{array} \qquad 3\text{-}64$$

Since the second-order flow equations are linear one may superimpose component solutions obtained for $\tilde{h}'$ appearing in Equations (3-50) - (3-54) replaced by the various values of $-\delta_k^{\pm}$. If the component solutions for the dimensionless second-order pressure and velocities are denoted by $\hat{p}_k^{\pm}$, $\hat{u}_k^{\pm}$ and $\hat{v}_k^{\pm}$ respectively, then the values of $\tilde{p}'$, $\tilde{u}'$ and $\tilde{v}'$ may be expressed as

$$\tilde{p}' = \sum_{k=1}^{3} \hat{p}_k \ , \quad \tilde{u}' = \sum_{k=1}^{3} \hat{u}_k \ , \quad \tilde{v}' = \sum_{k=1}^{3} \hat{v}_k \ , \qquad 3\text{-}65$$

where

$$\hat{p}_k = \frac{1}{2}\Re(\hat{p}_k^{+} + \hat{p}_k^{-}) \ , \quad \hat{u}_k = \frac{1}{2}\Re(\hat{u}_k^{+} + \hat{u}_k^{-}) \ , \quad \hat{v}_k = \frac{1}{2}\Re(\hat{v}_k^{+} + \hat{v}_k^{-}) \ . \qquad 3\text{-}66$$

One may now attempt to separate variables by looking for component solutions in the form

$$\hat{p}_k^{\pm} = \bar{p}_k^{\pm}(S)\, e^{i(J_k\theta \pm \tilde{\Omega}\tilde{t})} \ , \quad \hat{u}_k^{\pm} = \bar{u}_k^{\pm}(S)\, e^{i(J_k\theta \pm \tilde{\Omega}\tilde{t})} \ , \quad \hat{v}_k^{\pm} = \bar{v}_k^{\pm}(S)\, e^{i(J_k\theta \pm \tilde{\Omega}\tilde{t})} \ . \qquad 3\text{-}67$$

When the above expressions for $\hat{p}_k^{\pm}$, $\hat{u}_k^{\pm}$ and $\hat{v}_k^{\pm}$ are substituted for $\tilde{p}'$, $\tilde{u}'$ and $\tilde{v}'$ in Equations (3-50) - (3-53) a set of ordinary differential equations is obtained which may be arranged in the form

$$R\tilde{V}\frac{d\bar{u}_k^{\pm}}{dS} + (\Phi_{\tilde{U}} + iR\tilde{\Omega}^{\pm})\bar{u}_k^{\pm} + \left(\Phi_{\tilde{V}} + R\frac{d\tilde{U}}{dS}\right)\bar{v}_k^{\pm} + \frac{iJ_k}{\tilde{\rho}\tilde{r}}\bar{p}_k^{\pm} = \epsilon_k\eta_k\Phi_H^{\pm} \ , \qquad 3\text{-}68$$

$$\frac{d\bar{v}_k^{\pm}}{ds} + i\frac{J_k}{\tilde{r}}\bar{u}_k^{\pm} + \frac{1}{\tilde{r}\tilde{H}}\frac{d(\tilde{r}\tilde{H})}{dS}\bar{v}_k^{\pm} = \frac{\epsilon_k}{\tilde{r}\tilde{H}}\left[\tilde{V}\frac{d(\tilde{r}\eta_k)}{dS} + \left(\frac{d\tilde{V}}{dS} + i\tilde{\Omega}^{\pm}\right)r\eta_k\right] \ , \qquad 3\text{-}69$$

$$\begin{aligned} &\frac{1}{\tilde{\rho}}\frac{d\bar{p}_k^{\pm}}{ds} + \left(\Psi_{\tilde{U}} - iR\frac{\tilde{V}}{\tilde{r}}\right)\bar{u}_k^{\pm} + \left[\Psi_{\tilde{V}} + R\left(\frac{d\tilde{V}}{dS} - \frac{\tilde{V}}{\tilde{r}\tilde{H}}\frac{d(\tilde{r}\tilde{H})}{dS} + i\tilde{\Omega}^{\pm}\right)\right]\bar{v}_k^{\pm} \\ &\quad = \epsilon_k\Psi_{\tilde{H}}\eta_k - \epsilon_k R\frac{\tilde{V}}{\tilde{r}\tilde{H}}\left[\tilde{V}\frac{d(\tilde{r}\eta_k)}{dS} + \left(\frac{d\tilde{V}}{dS} + i\tilde{\Omega}^{\pm}\right)r\eta_k\right] \ , \end{aligned} \qquad 3\text{-}70$$

where

$$\tilde{\Omega}^{\pm} = \pm\tilde{\Omega} + \frac{\tilde{U}}{\tilde{r}} \quad . \tag{3-71}$$

The transformations given in Equation (3-66) satisfy the periodicity requirements in θ. The remaining boundary and continuity conditions are obtained by substituting the variables defined in Equation (3-67) for the corresponding variables in Equations (3-53) - (3-55). The form of the equations remains unchanged and the results are given below:

$$\bar{v}_k^{\pm} = -\frac{\tilde{V}\Delta\tilde{h}}{\tilde{H}(\tilde{H}-\Delta\tilde{h})}\epsilon_k\eta_k + \frac{(\tilde{H}-\Delta\tilde{h})}{\tilde{H}}\bar{v}_{kJ}^{\pm}, \quad \Delta\bar{p}_k^{\pm} = \frac{1}{2}\tilde{p}^{*}R^{*}(X_{\tilde{V}}\bar{v}_k^{\pm} - X_{\tilde{H}}\epsilon_k\eta_k) \quad @S = S_J, \tag{3-72}$$

$$\bar{u}_k^{\pm} = 0, \quad \bar{p}_k^{\pm} = \frac{1}{2}\tilde{p}^{*}R^{*}(X_{\tilde{V}}\bar{v}_k^{\pm} - X_{\tilde{H}}\epsilon_k\eta_k) \quad @S = S_{in} \tag{3-73}$$

and

$$\bar{p}_k^{\pm} = 0 \quad @\ S = S_{ex} \quad . \tag{3-74}$$

Equations (3-68) - (3-70) are solved numerically using the algorithm defined by Equations (3-56) - (3-58). Complimentary and particular solutions are constructed and combined so that the boundary conditions given by Equations (3-72) - (3-74) can be satisfied without having to iterate.

The real component pressures $\hat{p}_k$, can be expressed in terms of the real and imaginary parts of $\bar{p}_k^{+}$ and $\bar{p}_k^{-}$ by expanding the complex pressures, $\hat{p}_k^{\pm}$, substituting the result for the complex pressures in Equation (3-66) and extracting the real part as indicated. The result may be written as

$$\hat{p}_k = \frac{1}{2}\left[\Re(\bar{p}_k^{+} + \bar{p}_k^{-})\cos J_k\theta - \Im(\bar{p}_k^{+} + \bar{p}_k^{-})\sin J_k\theta\right]\cos\tilde{\Omega}\tilde{t} - \frac{1}{2}\left[\Im(\bar{p}_k^{+} - \bar{p}_k^{-})\cos J_k\theta + \Re(\bar{p}_k^{+} - \bar{p}_k^{-})\sin J_k\theta\right]\sin\tilde{\Omega}\tilde{t} \quad . \tag{3-75}$$

The first term on the right in the above equation will be in phase with the displacement and related to the stiffness of the seal. The negative of the second term will be in phase with oscillatory velocity and related to the damping coefficient.

Forces, Moments and Dynamic Coefficients

The dimensionless applied loads and moments obtained by integrating the pressure over the seal area are

$$\tilde{w}_x = l_c\int_0^{2\pi}\int_{S_L}^{S_R}\tilde{p}\cos\theta\,\tilde{r}\,dS\,d\theta, \quad \tilde{w}_y = l_c\int_0^{2\pi}\int_{S_L}^{S_R}\tilde{p}\sin\theta\,\tilde{r}\,dS\,d\theta, \quad \tilde{w}_z = l_f\int_0^{2\pi}\int_{S_L}^{S_R}\tilde{p}\,\tilde{r}\,dS\,d\theta,$$

$$\tilde{M}_x = -\int_0^{2\pi}\int_{S_L}^{S_R}\tilde{p}\sin\theta\,\tilde{r}S\,dS\,d\theta, \quad \tilde{M}_y = \int_0^{2\pi}\int_{S_L}^{S_R}\tilde{p}\cos\theta\,\tilde{r}S\,dS\,d\theta \quad . \tag{3-76}$$

All first-order applied loads and moments will be zero with the exception of the first-order axial load acting on a face seal, W_z, which is given in dimensionless form by

$$\tilde{W}_z = 2\pi l_f \int_{S_L}^{S_R} \tilde{P}\tilde{r}\,dS \quad . \tag{3-77}$$

The various stiffnesses can be obtained by substituting the first term on the right hand side of Equation (3-75) for the pressure, $\tilde{p}$, appearing in the force and moment integrals in Equation (3-76) and dividing the result by the associated displacement of the center of the seal. The dimensionless translations and rotations that have been included in Equation (3-59) are a rotation about the y axis of magnitude $\tilde{\psi}_0\cos\tilde{\Omega}\tilde{t}$ (corresponding to k=1), a translation in the x direction of magnitude $\tilde{e}_{x0}\cos\tilde{\Omega}\tilde{t}$ (corresponding to k=2) for a cylindrical seal and a translation in the axial direction of magnitude $\tilde{e}_{z0}\cos\tilde{\Omega}\tilde{t}$ (corresponding to k=3) for a face seal. The damping coefficients may be obtained in a similar manner by substituting the second term on the right hand side of Equation (3-75) for the pressure in Equation (3-76) and dividing the result by the velocity $-\tilde{\Omega}\tilde{t}\ \tilde{\psi}_0\sin\tilde{\Omega}\tilde{t}$ for k=1, $-\tilde{\Omega}\tilde{e}_{x0}\sin\tilde{\Omega}\tilde{t}$ for k=2 and $-\tilde{\Omega}\tilde{e}_{z0}\sin\tilde{\Omega}\tilde{t}$ for k=3.

For small displacements about the centered position, stiffness and damping values associated with translations in the y direction or rotations about the x axis may be obtained from symmetry considerations. For example, a displacement in the y direction will produce a force in that direction of the same magnitude as that which would be produced in the x direction for an equivalent displacement in that direction ($K_{yy}=K_{xx}$). Similarly, a displacement in the y direction will produce a force at 90° from that direction (which would be the negative x direction) as would be produced in the positive y direction for an equivalent displacement in the x direction ($K_{xy}=-K_{yx}$).

The symbols ϕ and ψ, when appearing as second subscripts on the dynamic coefficients, will denote rotations about the x and y axes respectively. When appearing as first subscripts they will denote moments about the x and y axes. The dimensionless stiffness and damping coefficients relating moments about the x and y axes to a rotation about the y axis (k=1) for both face and cylindrical seals are

$$\tilde{K}_{\phi\psi} = \frac{\pi}{2\epsilon_1}\int_{S_L}^{S_R} \Im(\bar{p}_1^{+} + \bar{p}_1^{-})S\,dS \ , \quad \tilde{K}_{\psi\psi} = \frac{\pi}{2\epsilon_1}\int_{S_L}^{S_R} \Re(\bar{p}_1^{+} + \bar{p}_1^{-})S\,dS \ ,$$

$$\tilde{B}_{\phi\psi} = -\frac{\pi}{2\tilde{\Omega}\epsilon_1}\int_{S_L}^{S_R} \Re(\bar{p}_1^{+} - \bar{p}_1^{-})S\,dS \ , \quad \tilde{B}_{\psi\psi} = \frac{\pi}{2\tilde{\Omega}\epsilon_1}\int_{S_L}^{S_R} \Im(\bar{p}_1^{+} - \bar{p}_1^{-})S\,dS \ . \tag{3-78}$$

The corresponding coefficients for a rotation about the x axis obtained from symmetry considerations are

$$\tilde{K}_{\phi\phi} = \tilde{K}_{\psi\psi} \ , \quad \tilde{K}_{\psi\phi} = -\tilde{K}_{\phi\psi} \ , \quad \tilde{B}_{\phi\phi} = \tilde{B}_{\psi\psi} \ , \quad \tilde{B}_{\psi\phi} = -\tilde{B}_{\phi\psi} \ . \tag{3-79}$$

The dimensionless dynamic coefficients relating the x and y force components to a rotation about the y axis (k=1) for a cylindrical seal are

$$\tilde{K}_{x\psi} = \frac{\pi l_c}{2\epsilon_1}\int_{S_L}^{S_R} \Re(\bar{p}_1^+ + \bar{p}_1^-)\,dS\ ,\quad \tilde{K}_{y\psi} = -\frac{\pi l_c}{2\epsilon_1}\int_{S_L}^{S_R} \Im(\bar{p}_1^+ + \bar{p}_1^-)\,dS\ ,$$

$$\tilde{B}_{x\psi} = \frac{\pi l_c}{2\tilde{\Omega}\epsilon_1}\int_{S_L}^{S_R} \Im(\bar{p}_1^+ - \bar{p}_1^-)\,dS\ ,\quad \tilde{B}_{y\psi} = -\frac{\pi l_c}{2\tilde{\Omega}\epsilon_1}\int_{S_L}^{S_R} \Re(\bar{p}_1^+ - \bar{p}_1^-)\,dS \qquad 3\text{-}80$$

and the corresponding coefficients for a rotation about the x axis are

$$\tilde{K}_{x\phi} = \tilde{K}_{y\psi}\ ,\quad \tilde{K}_{y\phi} = -\tilde{K}_{x\psi}\ ,\quad \tilde{B}_{x\phi} = \tilde{B}_{y\psi}\ ,\quad \tilde{B}_{y\phi} = -\tilde{B}_{x\psi}\ . \qquad 3\text{-}81$$

The dimensionless stiffness and damping coefficients relating moments about the x and y axes to a translation in the x direction (k=2) for a cylindrical seal are

$$\tilde{K}_{\phi x} = \frac{\pi}{2\epsilon_2}\int_{S_L}^{S_R} \Im(\bar{p}_2^+ + \bar{p}_2^-)\,S\,dS\ ,\quad \tilde{K}_{\psi x} = \frac{\pi}{2\epsilon_2}\int_{S_L}^{S_R} \Re(\bar{p}_2^+ + \bar{p}_2^-)\,S\,dS\ ,$$

$$\tilde{B}_{\phi x} = -\frac{\pi}{2\tilde{\Omega}\epsilon_2}\int_{S_L}^{S_R} \Re(\bar{p}_2^+ - \bar{p}_2^-)\,S\,dS\ ,\quad \tilde{B}_{\psi x} = \frac{\pi}{2\tilde{\Omega}\epsilon_2}\int_{S_L}^{S_R} \Im(\bar{p}_2^+ - \bar{p}_2^-)\,S\,dS \qquad 3\text{-}82$$

and the corresponding coefficients for a translation in the y direction are

$$\tilde{K}_{\phi y} = -\tilde{K}_{\psi x}\ ,\quad \tilde{K}_{\psi y} = \tilde{K}_{\phi x}\ ,\quad \tilde{B}_{\phi y} = -\tilde{B}_{\psi x}\ ,\quad \tilde{B}_{\psi y} = \tilde{B}_{\phi x}\ . \qquad 3\text{-}83$$

The dimensionless dynamic coefficients relating the x and y force components to a translation in the x direction (k=2) for a cylindrical seal are

$$\tilde{K}_{xx} = \frac{\pi l_c}{2\epsilon_2}\int_{S_L}^{S_R} \Re(\bar{p}_2^+ + \bar{p}_2^-)\,dS\ ,\quad \tilde{K}_{yx} = -\frac{\pi l_c}{2\epsilon_2}\int_{S_L}^{S_R} \Im(\bar{p}_2^+ + \bar{p}_2^-)\,dS\ ,$$

$$\tilde{B}_{xx} = \frac{\pi l_c}{2\tilde{\Omega}\epsilon_2}\int_{S_L}^{S_R} \Im(\bar{p}_2^+ - \bar{p}_2^-)\,dS\ ,\quad \tilde{B}_{yx} = -\frac{\pi l_c}{2\tilde{\Omega}\epsilon_2}\int_{S_L}^{S_R} \Re(\bar{p}_2^+ - \bar{p}_2^-)\,dS \qquad 3\text{-}84$$

and the corresponding coefficients for a translation in the y direction are

$$\tilde{K}_{xy} = -\tilde{K}_{yx}\ ,\quad \tilde{K}_{yy} = \tilde{K}_{xx}\ ,\quad \tilde{B}_{xy} = -\tilde{B}_{yx}\ ,\quad \tilde{B}_{yy} = \tilde{B}_{xx}\ . \qquad 3\text{-}85$$

Finally, the stiffness and damping coefficients relating the axial force to an axial translation (k=3) for a face seal are

$$\tilde{K}_{zz} = \frac{\pi l_f}{\epsilon_3} \int_{S_L}^{S_R} \Re(\bar{p}_3^+ + \bar{p}_3^-) dS \ , \quad \tilde{B}_{zz} = \frac{\pi l_f}{\tilde{\Omega}\epsilon_3} \int_{S_L}^{S_R} \Im(\bar{p}_3^+ - \bar{p}_3^-) dS \ . \tag{3-86}$$

As a result of the assumption of small displacements about the centered position used in this analysis, the remaining dynamic coefficients for a face seal will all be zero:

$$\tilde{K}_{z\phi} = \tilde{K}_{\phi z} = \tilde{K}_{z\psi} = \tilde{K}_{\psi z} = \tilde{B}_{z\phi} = \tilde{B}_{\phi z} = \tilde{B}_{z\psi} = \tilde{B}_{\psi z} = 0 \ . \tag{3-87}$$

Relationships of the following type may be used to calculate the physical stiffness and damping coefficients from the dimensionless ones

$$K_{xx} = \frac{p_0 r_0^2}{C} \tilde{K}_{xx} \ , \quad K_{\phi\phi} = \frac{p_0 r_0^4}{C} \tilde{K}_{\phi\phi} \ , \quad K_{x\phi} = \frac{p_0 r_0^3}{C} \tilde{K}_{x\phi} \tag{3-88}$$

and

$$B_{xx} = \frac{p_0 r_0^3}{C V_0} \tilde{B}_{xx} \ , \quad B_{\phi\phi} = \frac{p_0 r_0^5}{C V_0} \tilde{B}_{\phi\phi} \ , \quad B_{x\phi} = \frac{p_0 r_0^4}{C V_0} \tilde{B}_{x\phi} \ . \tag{3-89}$$

The stiffness coefficients, which relate to forces in phase with the displacements and the damping coefficients, which relate to forces 90° out of phase with the displacements, are both, in general, functions of $\tilde{\Omega}$. For the case of incompressible flow under consideration, the damping coefficients and the cross coupled stiffness coefficients ($\tilde{K}_{xy}$, $\tilde{K}_{\phi\psi}$, $\tilde{K}_{yx}$, $\tilde{K}_{\psi\phi}$) are nearly independent of $\tilde{\Omega}$. Under these circumstances, it has been found that the frequency dependence may be described adequately with the introduction of an apparent mass matrix [A] such that $[K] = [K^0] - \Omega^2[A]$, where $[K^0]$ is the stiffness matrix evaluated at $\Omega=0$. The components of [A] may be evaluated by computing [K] at a characteristic speed such as $\Omega=V_0/r_0$ corresponding to $\tilde{\Omega}=1$ or synchronous speed ($\Omega=\omega$) and using the formula

$$A_{ij} = \frac{K_{ij} - K_{ij}^0}{\Omega^2} \tag{3-90}$$

The cross coupled components of [A] which have been included for completeness are not significant and the direct components are indeed found to be nearly independent of Ω.

Although the linearizations that have been used in obtaining the second-order flow equations are only valid for small values of ϵ_k, once they have been performed the resulting equations for the dynamic coefficients may be shown, by rescaling variables, to be independent of the value ϵ_k actually used. Any convenient value such as $\epsilon_k=1$ may be used in computations.

Determination of Power Loss and Flow

When the rotating surface (a) is ungrooved, the power loss will be proportional to the integral of $r\vec{\tau}_a \cdot \vec{i}$ over the surface of the seal. When the rotating surface is grooved, an additional term will be needed to correct for the pressures acting edges of the grooves. Although the solution to the equations based on bulk flow theory used here does provide for the prediction the shear stress on each surface, the validity of power loss predictions is somewhat doubtful. This is due to the difference in characterizing the bulk flow behavior for velocity distributions associated with Couette and Poiseuille flow.

One may write $\vec{\tau}_a$ as $\vec{\tau}_a = \vec{\tau}_c + \vec{\tau}_p$ where $\vec{\tau}_c$ denotes the Couette part of the shear stress defined as $\vec{\tau}_c = (\vec{\tau}_a + \vec{\tau}_b)/2$ and $\vec{\tau}_p$ denotes the Poiseuille portion of the shear stress defined as $\vec{\tau}_p = (\vec{\tau}_a - \vec{\tau}_b)/2$. It can be seen from Equations (3-1) and (3-2) that only $\vec{\tau}_p$ appears in the primary and secondary flow equations used to predict load, flow and dynamic coefficients. Comparisons between theory and experiments based on measurements of flow and dynamic coefficients alone may be used to validate or determine values of $\vec{\tau}_p$, but will not necessarily result in a bulk flow model that accurately predicts power loss. This weakness in the bulk flow model was recognized by Hirs (Reference 14) who suggested the use of different friction factor representations based on measurements obtained from experiments based on Couette and Poiseuille flow. The method for predicting power loss used here will be a highly approximate one based on generalizations of an approach used by Hirs for cases where both surfaces were smooth and the flow was predominantly in the tangential direction.

If the scaler shear stress, τ, is used to represent the tangential shear stress, ($\tau = \vec{\tau} \cdot \vec{i}$), then the dimensionless forms of the tangential shear stresses τ_a and τ_b, can be obtained from Equations (3-4), (3-5), (3-8), and (3-10) as

$$\tilde{f}_a = \tilde{p}' R_a f_a(R_a) \frac{\tilde{u} - \tilde{r}\tilde{\omega}}{\tilde{h}} \quad , \quad \tilde{f}_b = -\tilde{p}' R_b f_b(R_b) \frac{\tilde{u}}{\tilde{h}} \quad . \tag{3-91}$$

One may attempt to compensate for the influence of the Couette portion of the shear stress by replacing $\tilde{\tau}_a$ with the effective shear stress, $\tilde{\tau}^*$, defined as

$$\tilde{f}^* = \frac{\tilde{f}_a + \tilde{f}_b}{2\lambda} + \frac{\tilde{f}_a - \tilde{f}_b}{2} = \frac{\tilde{f}_c}{\lambda} + \tilde{f}_p \tag{3-92}$$

in the integral used for determining power loss. The correct value of the "Couette reduction factor", λ, may be shown to be $\lambda=3$ for laminar flow. A value of $\lambda=1.2$ will be used for turbulent flow. This value was suggested by Hirs based on one dimensional Couette flow measurements and provides power predictions that are in good agreement with those obtained with Ng and Pan theory (Reference 26) over its range of validity.

The dimensionless power loss, $\tilde{\mathcal{P}} = \mathcal{P}/(Cp_0 r_0^2 \omega)$, obtained from the solution to the first-order flow equations is given by

$$\tilde{\mathcal{P}} = -2\pi \int_{S_L}^{S_R} \left[\alpha \tilde{f}_g^* + (1-\alpha)\tilde{f}_r^* + I_\omega \tilde{\delta} \left(\alpha \tilde{P}_{g,\theta} + \frac{N_g \tilde{p}' R^*}{4\pi \tilde{r}} \chi\left(\frac{\tilde{q}_n}{\tilde{h}_g}, \tilde{h}_g, \tilde{\delta}\right) \mathrm{sign}(\tilde{q}_n \sin\beta) \right) \right] \tilde{r}^2 \, dS \quad . \tag{3-93}$$

The quantities $\tilde{\tau}_g^*$ and $\tilde{\tau}_r^*$ appearing in the above equation denote the values of the effective shear stress, $\tilde{\tau}^*$, based on the first-order velocities and film thicknesses for the grooves and ridges respectively. The effective shear stress is defined by Equations (3-91) and (3-92) and the local velocities are obtained from the solution to Equations (3-30) and (3-32) - (3-34) and the definitions provided by Equation (3-21). The sum of the first two terms appearing inside the brackets of the integrand in Equation (3-93) represent the global value of $\tilde{\tau}^*$. The third term has been added to include the forces acting on the edges of the grooves when the grooves are on the rotor. The quantity $\tilde{P}_{g,\theta}$ is obtained by substituting first-order variables for the corresponding quantities in Equation (3-24) and is given below:

$$\tilde{P}_{g,\theta} = -\tilde{p}^* \Phi_g - \tilde{p}^* R^* \left(\tilde{V} \frac{d\tilde{U}}{dS} + I_f \frac{\tilde{U}\tilde{V}}{\tilde{r}} \right) \quad . \qquad 3\text{-}94$$

3.2 Overview of Computer Code SPIRALI

SPIRALI has been written to implement the analysis that is contained in the preceding section. Full input and output descriptions along with a number of sample runs are given in Reference 28. A brief discussion of a few items not covered in Section 2.1 is given below.

Although SPIRALI is designed to run over a full range of conditions of laminar or turbulent flow, certain precautions need to be taken when the transverse flow rate is small. It can be seen, for example, that Equation (3-44) becomes singular as $R^*\tilde{V}$ approaches 0. Numerical problems can be avoided here by setting $R^*\tilde{V}=0$ and numerically solving Equation (3-44) as an algebraic equation rather than as a differential equation. SPIRALI provides an option for the user to exclude the transverse inertia effects arising from the terms $\tilde{v}\partial\tilde{u}/\partial S$ and $I_f\tilde{u}\tilde{v}/\tilde{r}$ in Equation (3-11) and $\tilde{v}\partial\tilde{v}/\partial S$ in Equation (3-12) and the associated discontinuities in pressure that occur at the inlet and at jump discontinuities in film thickness. This option, which is controlled by the input parameter NOI (see input description) is particularly useful for situations where the rotation speed is high but the seal pressure difference is low.

If transverse inertia is included, the location of the upstream or inlet boundary must be specified. When the seal pressure difference is sufficiently high, the upstream boundary will be at the high pressure side of the seal. At lower pressure differences the upstream boundary may depend on the rotor speed and the spiral groove parameters. The input parameter IFLOW is used to select the upstream boundary. If one is not sure of the flow direction, he may first run the program with transverse inertia excluded. One may then include transverse inertia by adjusting IFLOW in accordance with the sign of the transverse flow rate given in the preceding output and rerunning the program with transverse inertia included.

The analytical procedure contained in Section 2 has been oriented toward determining pressure distribution, load, flow, power loss, stiffness and damping for a given centered film thickness distribution. Face seals will, in general, have a non-zero first-order axial load component and it is often desirable to determine the equilibrium film thickness from a prescribed load used to balance the seal. SPIRALI provides an iterative homing option for this purpose that is controlled by the input parameter IHOME. The homing option should be used with caution since convergence is sensitive to the starting film thickness which is determined from the input

parameter C. It is recommended that the program be run for various values of C without the homing option so that a good starting value of C (one that produces an output value of the load to balance the face seal that is reasonably close to the prescribed load) can be obtained for the homing process.

Although the analysis provides for an arbitrary transverse film thickness variation, SPIRALI is limited to a quadratic film variation with coefficients determined from the parameters H_{TAP}, H_{BRL} and C as shown in Figure 12. These parameters may be positive, as shown or negative and should be able to characterize a fairly general film variation without the complexity of required inputs at every grid point.

The logic used in SPIRALI for solving the first and second-order flow equations, computing load, flow, power loss, stiffness, damping, apparent mass coefficients, etc. for a given case is shown in Figure 13.

3.3 Verification

An available MTI computer code, PN471, has been used to obtain a partial check on the results of SPIRALI. This code implements a two dimensional finite difference solution to the spiral groove equations that is quite different from the perturbation methods used in SPIRALI. It does not treat inertia effects and uses the Ng and Pan (Ref. 25) linearized turbulence theory which limits its validity to cases where turbulence is dominated by circumferential component of the flow. The assumptions used in the MTI code will be identical to those used in SPIRALI when the flow is laminar and inertia effects are neglected. The bulk flow model used in SPIRALI should also produce similar (although not identical) results to those obtained with the MTI code under turbulent conditions when inertia effects are neglected, there is no significant seal pressure difference, the circumferential Reynolds numbers are between 10^4 and 10^5 and the transverse Reynolds numbers are small compared with the circumferential ones.

Four test cases* obtained with SPIRALI are presented for comparison with the MTI code. Cases 1 and 3 correspond to laminar flow in a spiral grooved cylindrical and face seal respectively. It can be seen that the results of both cases agree extremely well with the results of the MTI code. The small discrepancies can easily be explained by truncation error associated with the finite difference solution used in the MTI code. Cases 2 and 4 provide comparisons similar to cases 1 and 3 under conditions of turbulent flow. It can be seen that the Reynolds numbers are in the general range of validity of the MTI code and all results agree to within 10% for both cases which is acceptable considering the differences in the turbulent flow models.

While the above cases provide a partial check on turbulent, spiral groove seals, they do not provide any validation on the treatment of inertia effects or seal behavior under high imposed pressure gradients. In order to obtain verification of the treatment of these effects, comparisons are presented between the results published by Childs in Reference 17 and those obtained with SPIRALI for a plain ungrooved cylindrical seal. The output from SPIRALI is given as cases 5 - 8 and comparisons of flow rates and rotordynamic coefficients with those published by Childs are given in Table 1. Although agreement is fairly good, discrepancies in results of up to 10%, such as that which occurs in the direct stiffness for case 6 where $u_{in}=r_0\omega/2$ and L/D=1, are somewhat surprising since the assumptions for that case are identical with those used by Childs. In order to

*SPIRALI test cases and output are presented as cases 1-8 beginning on page 78.

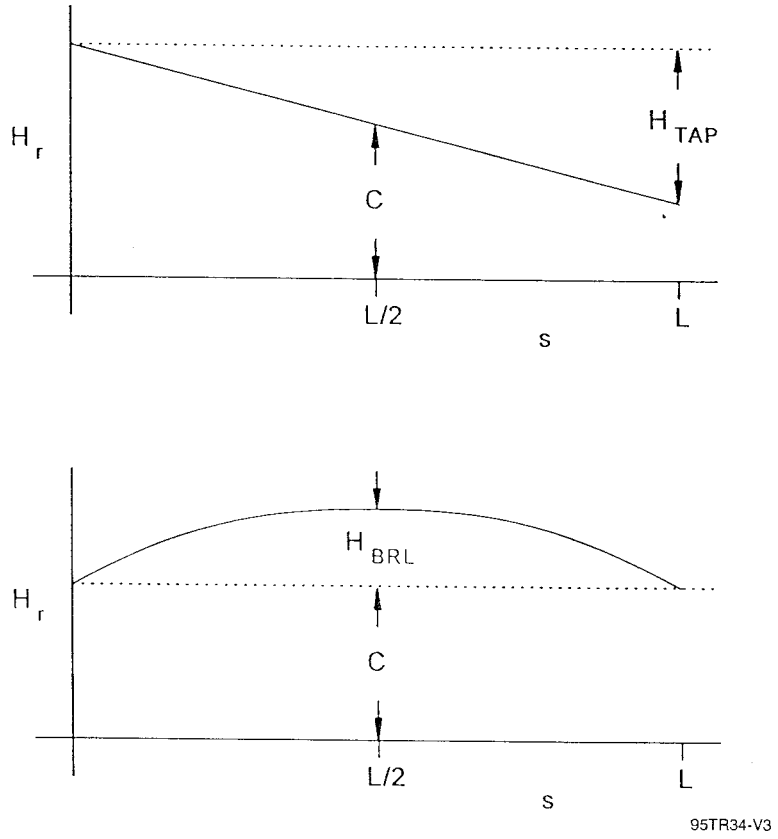

Figure 12. Parameters for Characterizing Quadratic Film Variation

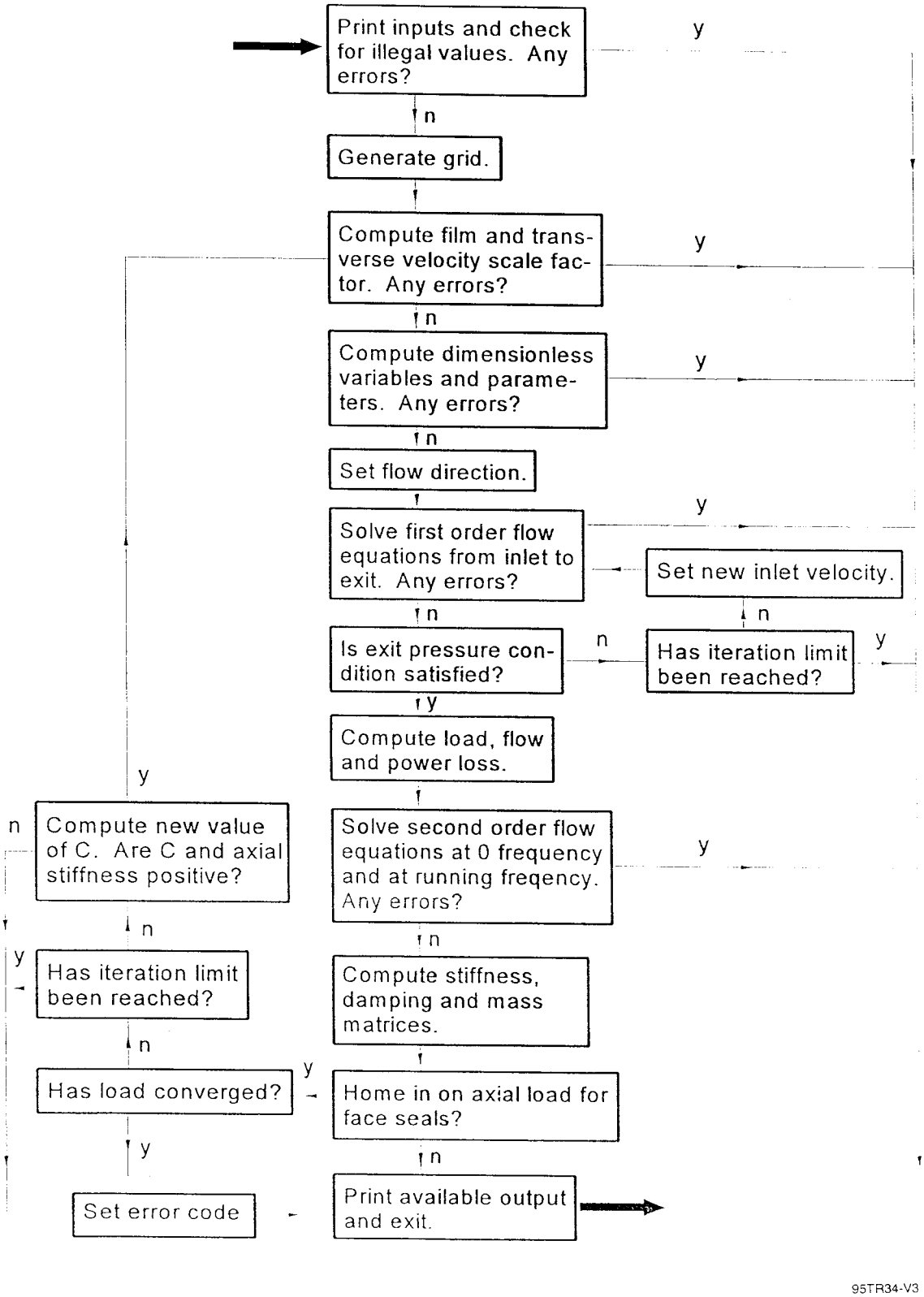

Figure 13. Flow Diagram for Overall Logic Used in Computations

Table 1. Comparison of Test Cases 5 -8 with Data Published by D.W. Childs (Ref. 17)

	$u_{in}=r_0\omega/2$, L/D=.2		$u_{in}=r_0\omega/2$, L/D=1		$u_{in}=0$, L/D=.2		$u_{in}=0$, L/D=1	
	SPIRALI	Childs	SPIRALI	Childs	SPIRALI	Childs	SPIRALI	Childs
Q (cm^3/s)	4006.	4019.	1771.	1779.	3989.	4019.	1767.	1779.
K_{xx} (MN/m)	18.90	18.65	10.79	9.756	18.58	18.52	13.25	12.48
K_{xy} (MN/m)	4.127	4.213	91.78	94.05	-.3027	-.3000	75.18	77.61
B_{xx} (KN-s/m)	21.89	22.35	487.2	500.6	21.89	22.47	489.5	502.2
B_{xy} (KN-s/m)	1.140	1.206	102.9	107.5	.8518	.8932	89.26	93.39
A_{xx} (kg)	3.020	3.200	272.6	285.3	3.003	3.189	272.1	285.3

95TR34-V3

obtain a further independent check on the results, a reduced form of the differential equations published by Childs for predicting the direct and cross stiffness coefficients when $u_{in}=r_0\omega/2$, were programmed and solved by the Runge-Kutta method. The program produced values of K_{xx}, K_{yy} and Q that agree to four places with the case 6 results produced by SPIRALI. It is thus likely that the small discrepancies between results obtained from SPIRALI and those published in Reference 17 are due to truncation errors in the latter solution.

Parallel groove geometrics can be analyzed by using the separated region option of SPIRALI. Analysis was conducted of the parallel groove and stator 1 of Reference 27 by treating each groove and ridge as a separate region. The clearance and groove geometry are shown in Figure 14.

A total of 19 regions were used consisting of nine grooves, eight lands between grooves, an inlet land and an exit land. (The parameter statements in SPIRALI governing the maximum number of regions were enlarged appropriately). The inlet and exit land lengths were enlarged slightly to make the sum of the lengths of the individual regions equal to the total seal length (50.8 mm). The seal radius is 50.8 mm. The viscosity and density are 1.54 x 104 Pa-s and 1570 kg/m^3, respectively. The program default values for flow parameters of m = -0.25, n = 0.0791 (Hirs coefficients for smooth surfaces as given by Blasius theory), and loss coefficient of $\zeta = 0$ were used. Although it was stated in Reference 27 that no intentional swirl was provided, a swirl speed of 25% of the rotor speed was used in all computations to characterize the swirl that might naturally be present.

Comparison of Flow Rates and Force Coefficients

Experimental flow rates are presented in terms of a discharge coefficient, C_D, defined by Equation (3) of Reference 27. The value of $C_D^{-1/2}$ for stator 1 is shown in Figure 6 of Reference 27 to have a constant value of approximately 0.5 for all measured pressures. A comparison between that value and those predicted by SPIRALI is shown in Figure 15. The agreement is good and the results are predicted to be relatively insensitive to the rotating speed over the range of conditions covered, as indicated in Reference 27.

The dynamic coefficients presented in Table 1 of Reference 27 are computed from measured force coefficients based on the assumption that the coefficients are independent of speed. For purposes of comparison, the measured force coefficients, f_θ and f_r, were retrieved with the use of Equation 6 in Reference 27. The seal pressure drops, ΔP, were calculated from the axial Reynolds number, R_a, using Equation (3) of Reference 27 with $C_D^{-1/2} = 0.5$. Values of f_θ versus ΔP obtained in this manner and those predicted by SPIRALI appear to be in good agreement, as shown in Figure 16. The predicted variation in f_r with rotating speed (Figure 17) is somewhat weaker than that obtained by experiment. Discrepancies in f_r can, in part, be due to sensitivity to the input values to SPIRALI provided for the friction factor and loss coefficients. Also, the effective mass, M_{ef}, in Table 1 of Reference 27 shows a significant jump at a Reynolds number of 200,000 that may be suspect.

Effective stiffness values are compared in Figure 18. The experimental stiffnesses are based on extrapolations to zero speed. Stiffness is assumed to be caused principally by the pressure gradient and inlet Bernoulli effect which causes a circumferential pressure gradient and positive stiffness if the rotor goes eccentric. As Figure 18 indicates, the predicted values approach the experimental values as the speed is reduced. The predicted decrease in K with increasing rotating speed is to be expected due to the Bernoulli effect associated with fluid rotation. A corresponding comparison of C_{ef} with $C - k/\omega$ is given in Figure 19. In both cases, the agreement improves as the rotational speed is decreased and the physical interpretation of the data becomes valid.

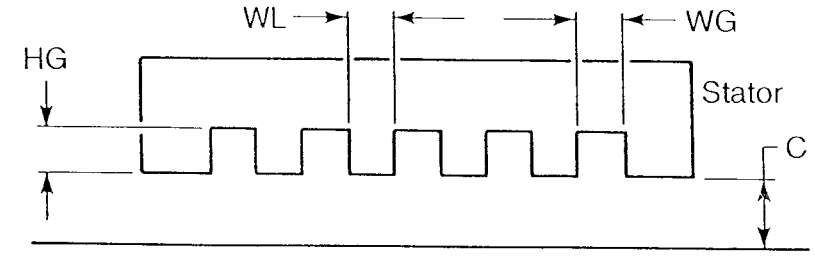

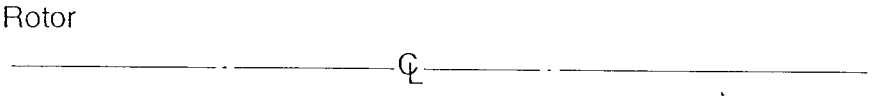

N.G	WL	WG	HG	C
9 Grooves	2.38 mm	2.38 mm	0.38 mm	0.356 mm

94144

Figure 14. Parallel-Groove Pressure Breakdown Seal

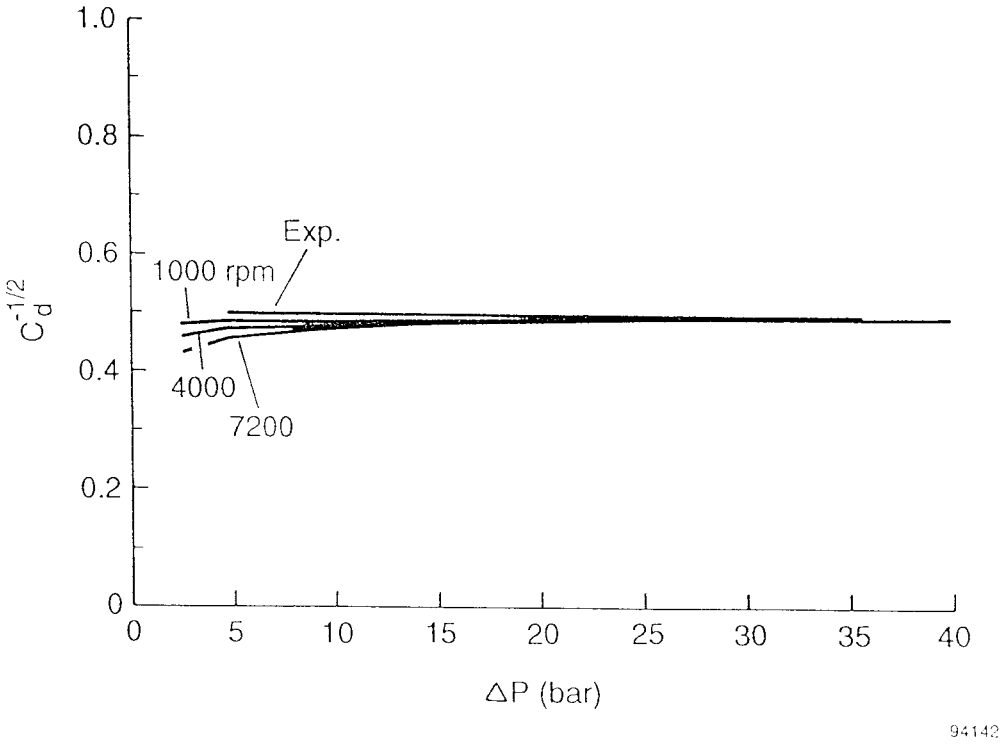

94142

Figure 15. Parallel-Groove Seal Flow Coefficient

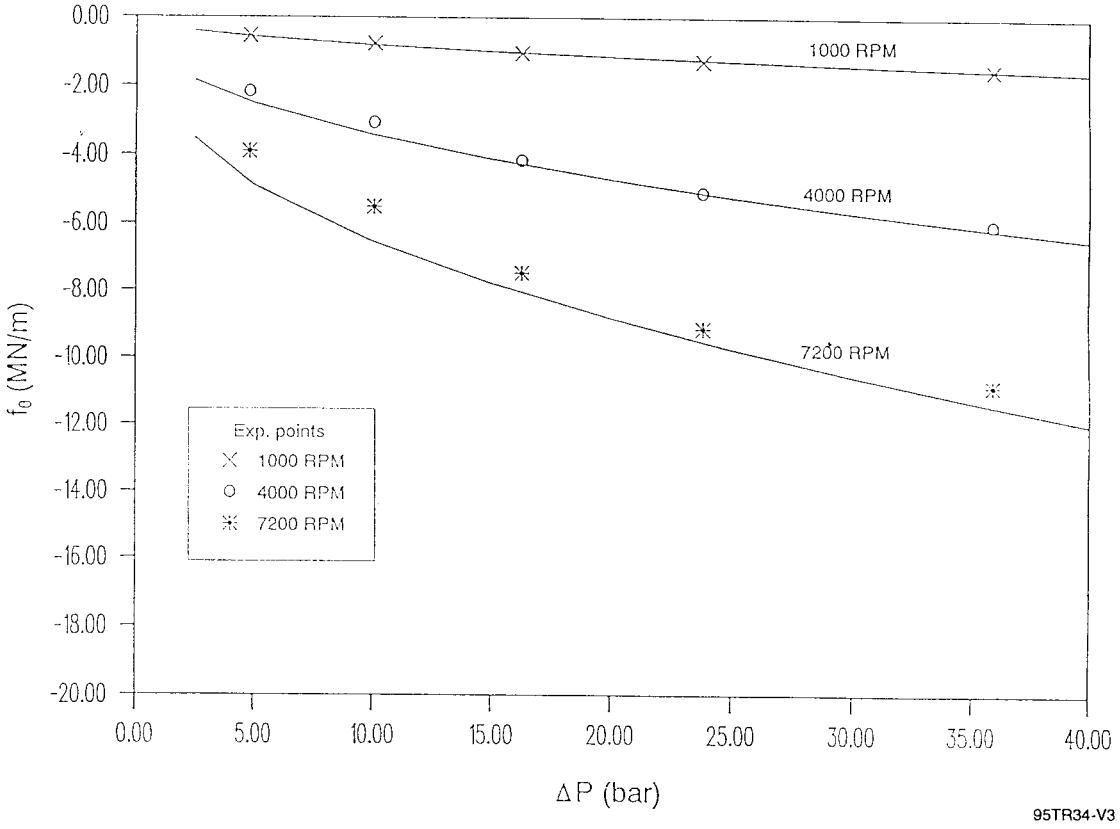

Figure 16. Tangential Force Coefficients

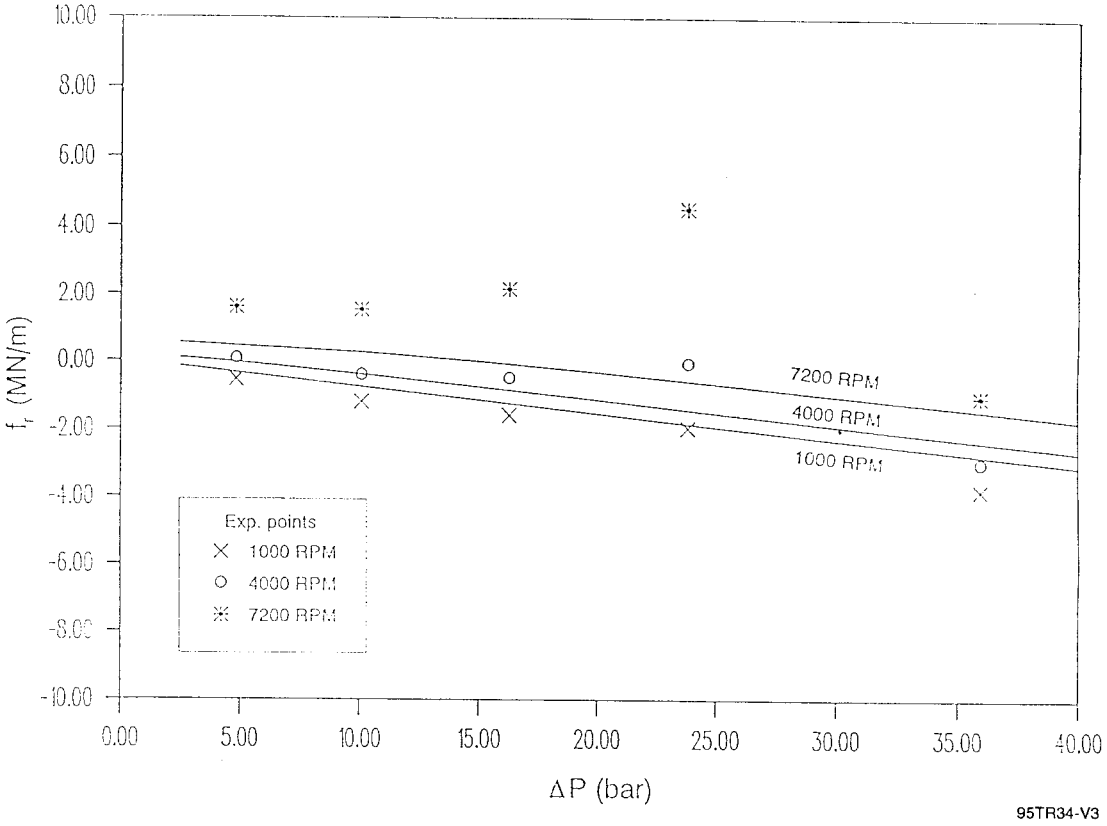

Figure 17. Normal Force Coefficients

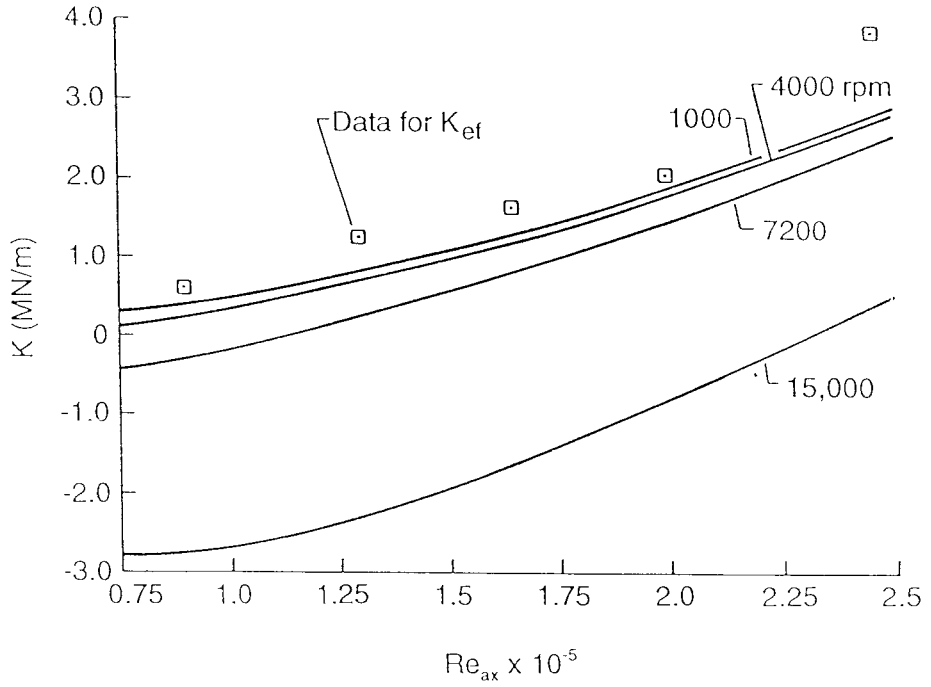

Figure 18. Parallel-Groove Seal Effective Stiffness

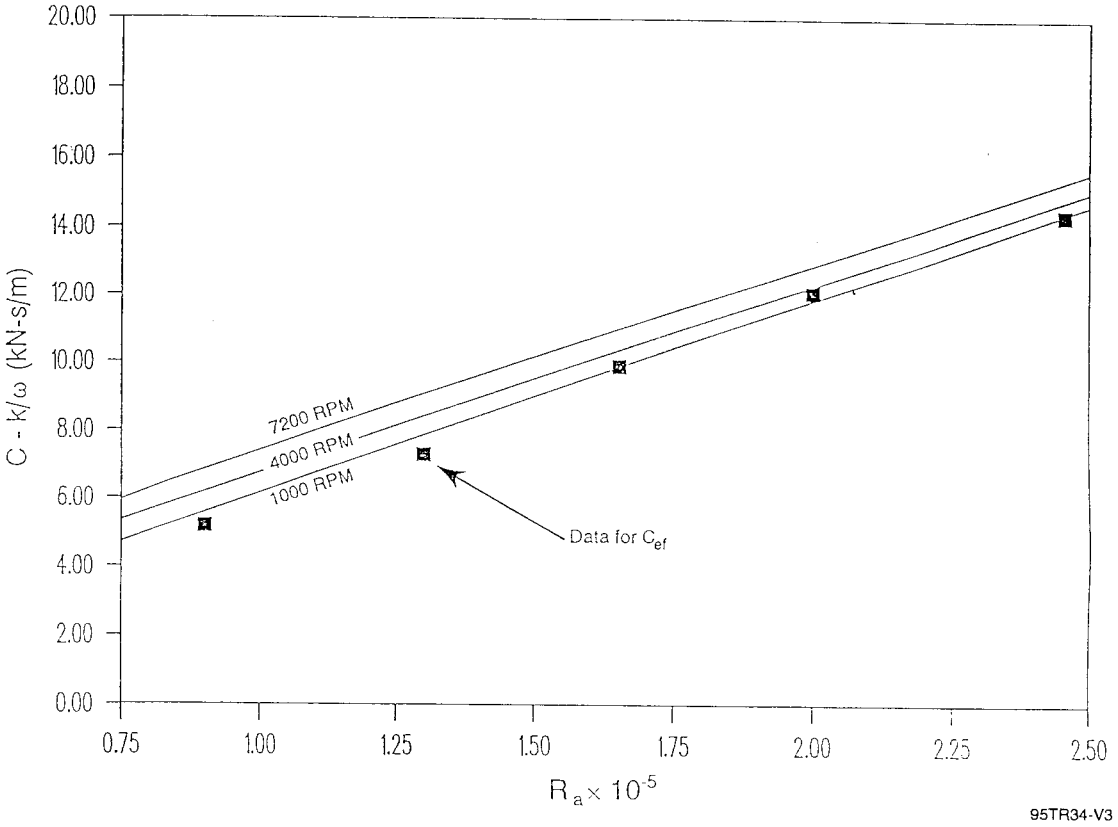

Figure 19. Comparison Between C - k/ω and C_{ef} at Various Rotating Speeds

Effect of Local Pressure Discontinuities on Predicted Flow

As described above, the effects of pressure jumps at the grooves are accounted for by SPIRALI in the prediction of flow and force coefficients. An estimate of these terms can be obtained by comparing the flow rate for circular grooves with that which would be predicted to occur if the effects of pressure jumps at the groove interfaces were neglected. This comparison is made at 1000 rpm in Figure 20. The large discrepancies between the two curves indicate a significant effect of local inertia that must be accounted for.

Check cases were also run against the helical groove results of Reference 27. Figure 21 shows comparisons of the flow coefficient for varying groove angles at a loss coefficient equal to 1, and the theory predicts results accurately. Cross-coupled force comparisons are shown on Figure 22. Cross-coupled effects are important because they are a measure of the stability of the seal, and in some cases, cross-coupled forces cause subsynchronous whirling of the rotor. The comparative results are very good. It is noted that cross-coupled forces were compared rather than the stiffnesses indicated in Reference 27. The experimental procedure measures forces and computes stiffness and damping based on the assumption that the cross-coupled coefficients vary directly with speed. The assumption of zero cross coupling at zero speed is suspect for helical grooves because the grooves apply a pressure-driven tangential flow at zero speed opposite the direction of rotation. As shown in Figure 23, the comparisons of direct stiffness, K_{ef}, were not as good as the parameters presented above. This may be due to the experimental assumptions or code assumptions.

The net results of these studies is that SPIRALI is an effective tool for analyzing many parallel and helical groove seals. The principal limitation is the bulk flow model that does not treat flow variations across gaps. If large gaps are used, then more sophisticated CFD analysis is required.

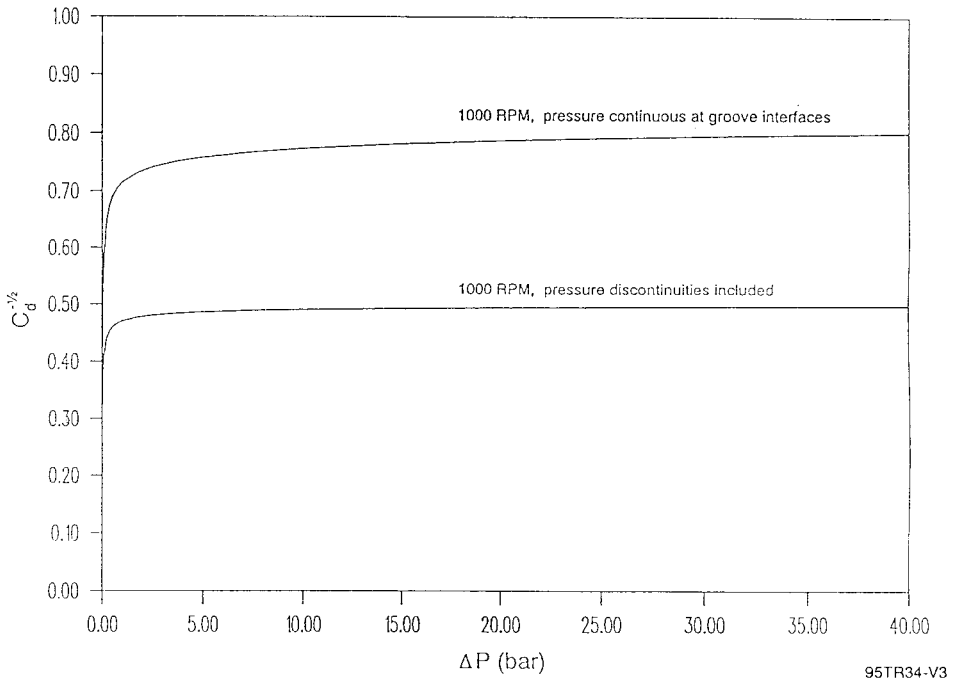

Figure 20. Effect of Local Pressure Discontinuities on Predicted Axial Flow Rates

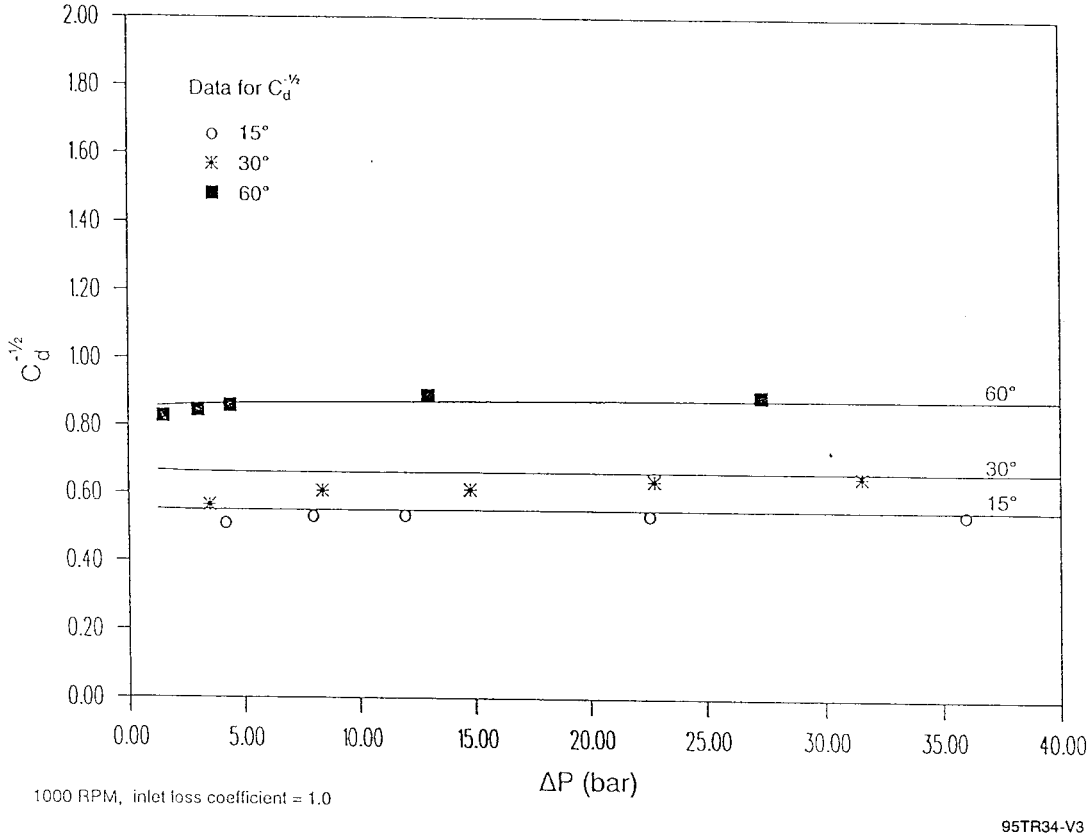

Figure 21. Flow Coefficient: SPIRALI Compared to Reference 27

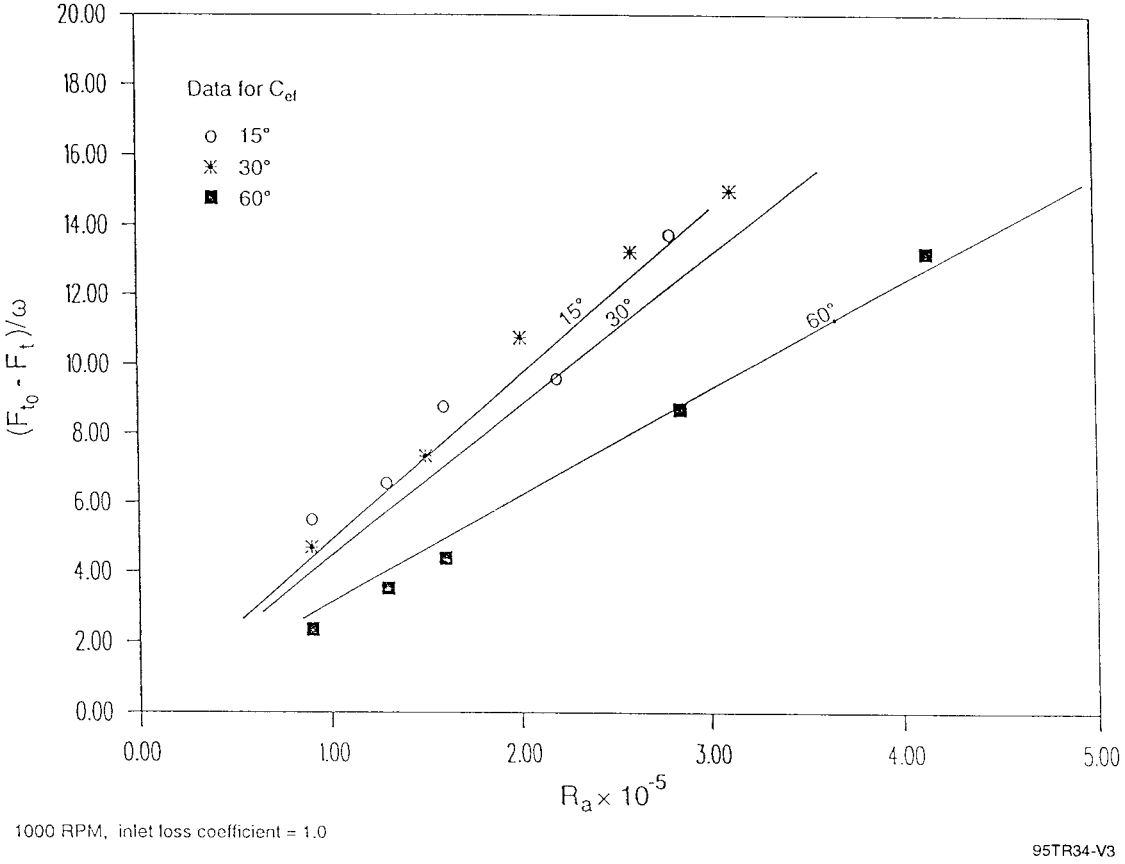

Figure 22. Effective Damping: SPIRALI Compared to Reference 27

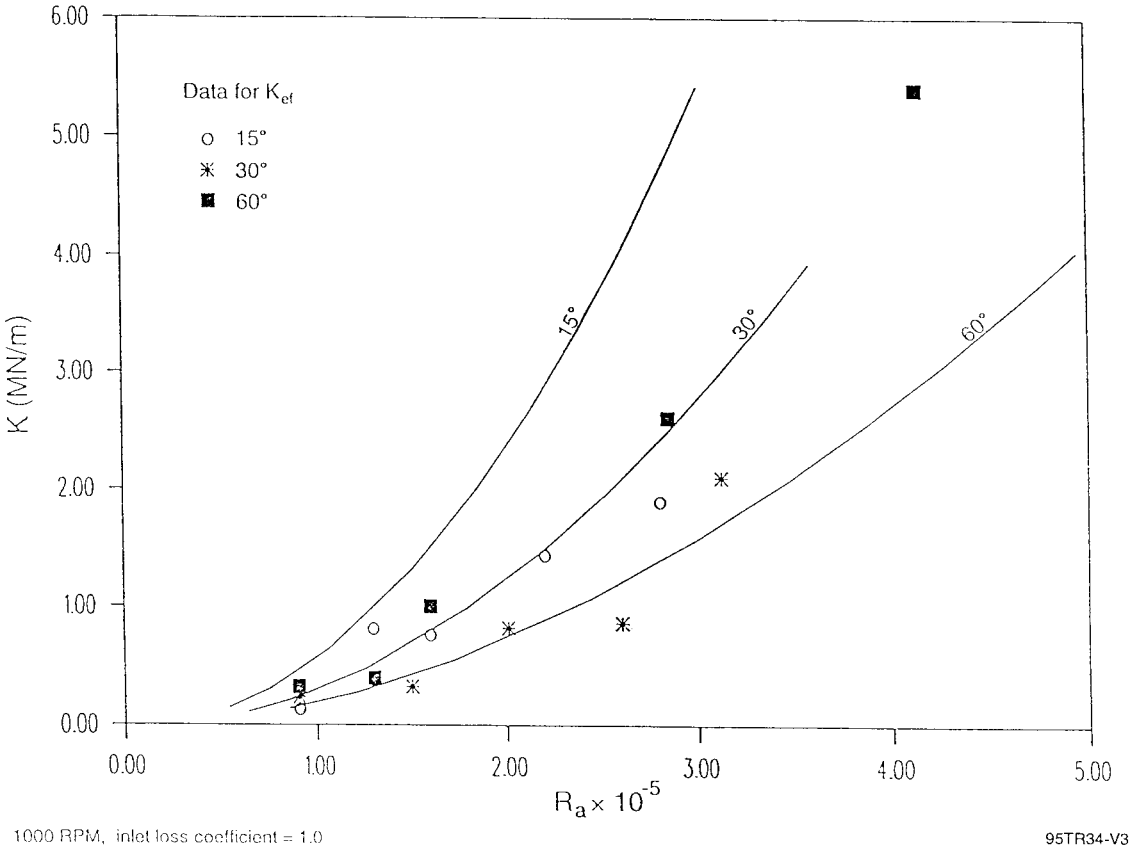

Figure 23. Direct Stiffness: SPIRALI Compared to Reference 27

(CASE 1) Cylindrical seal with grooves, laminar, no press. grad.

CYLINDRICAL SEAL, INERTIA NEGLECTED

LENGTH, DIAMETER, CLEARANCE = 5.0000E-01, 2.0000E+00, 1.0000E-03 (IN)

ROTOR, SWIRL AND DIST. SPEEDS = 5.0000E+04, 2.5000E+04, 0.0000E+00 (RPM)

PRESSURE AT START, END AXIAL BOUNDARIES = 0.0000E+00, 0.0000E+00 (PSI)

VISCOSITY = 3.0000E-08 (PSI-SEC), DENSITY = 0.0000E+00 ($LB\text{-}SEC^2/IN^4$)

FLOW = 1.1506E+00 (IN^3/SEC)

TORQUE = 4.3909E-01 (IN-LB), FILM POWER LOSS = 3.4835E-01 (HP)

AXIAL REYNOLDS NUMBER = 0.0000E+00
CIRC. REYNOLDS NUMBERS FOR ROTOR AT SEAL ENDS = 0.0000E+00, 0.0000E+00

DYNAMIC COEFFICIENTS (FORCE UNIT / DISP. UNIT)

DISP.	x (IN)	y (IN)	ϕ (RAD)	ψ (RAD)	FORCE UNIT
Kx	2.7021E+04	1.3511E+04	-6.3081E+02	-1.2959E+03	LB
Ky	-1.3511E+04	2.7021E+04	1.2959E+03	-6.3081E+02	LB
Kϕ	2.3387E+02	-6.5242E+01	1.6699E+02	8.6419E+01	IN-LB
Kψ	6.5242E+01	2.3387E+02	-8.6419E+01	1.6699E+02	IN-LB
Bx	5.1297E+00	7.8477E-11	-2.0242E-02	1.3973E-01	LB-SEC
By	-7.8477E-11	5.1297E+00	-1.3973E-01	-2.0242E-02	LB-SEC
Bϕ	-2.0242E-02	-1.3973E-01	3.0437E-02	3.8319E-13	IN-LB-SEC
Bψ	1.3973E-01	-2.0242E-02	-3.8319E-13	3.0437E-02	IN-LB-SEC
Ax	4.7708E-19	4.0552E-18	7.4544E-20	-1.7891E-19	$LB\text{-}SEC^2$
Ay	-4.0552E-18	4.7708E-19	1.7891E-19	7.4544E-20	$LB\text{-}SEC^2$
Aϕ	1.1927E-19	5.4045E-20	-1.8636E-20	3.3545E-20	$IN\text{-}LB\text{-}SEC^2$
Aψ	-5.4045E-20	1.1927E-19	-3.3545E-20	-1.8636E-20	$IN\text{-}LB\text{-}SEC^2$

RESULTS OF MTI SPIRAL GROOVE CODE FOR COMPARISON WITH CASE 1

FLOW = 1.1506E+00 (IN^3/SEC)

TORQUE = 4.3909E-01 (IN-LB), FILM POWER LOSS = 3.4835E-01 (HP)

DYNAMIC COEFFICIENTS (FORCE UNIT / DISP. UNIT)

DISP.	x (IN)	y (IN)	ϕ (RAD)	ψ (RAD)	FORCE UNIT
Kx	2.6996E+04	1.3497E+04	-6.2966E+02	-1.2947E+03	LB
Ky	-1.3497E+04	2.6996E+04	1.2947E+03	-6.2966E+02	LB
Kϕ	2.3429E+02	-6.4947E+01	1.6666E+02	8.6250E+01	IN-LB
Kψ	6.4947E+01	2.3429E+02	-8.6250E+01	1.6666E+02	IN-LB
Bx	5.1280E+00	2.4507E-07	-2.0178E-02	1.3967E-01	LB-SEC
By	9.3415E-09	5.1280E+00	-1.3967E-01	-2.0178E-02	LB-SEC
Bϕ	-2.0178E-02	-1.3967E-01	3.0411E-02	3.0462E-09	IN-LB-SEC
Bψ	1.3967E-01	-2.0178E-02	4.9311E-09	3.0411E-02	IN-LB-SEC

(CASE 2) Cylindrical seal with grooves, turbulent, no press. grad.

CYLINDRICAL SEAL, INERTIA NEGLECTED

LENGTH, DIAMETER, CLEARANCE = 5.0000E-01, 2.0000E+00, 1.0000E-03 (IN)

ROTOR, SWIRL AND DIST. SPEEDS = 5.0000E+04, 2.5000E+04, 0.0000E+00 (RPM)

PRESSURE AT START, END AXIAL BOUNDARIES = 0.0000E+00, 0.0000E+00 (PSI)

VISCOSITY = 3.0000E-08 (PSI-SEC), DENSITY = 1.0000E-04 ($LB\text{-}SEC^2/IN^4$)

FLOW = 1.7348E+00 (IN^3/SEC)

TORQUE = 6.1300E+00 (IN-LB), FILM POWER LOSS = 4.8631E+00 (HP)

AXIAL REYNOLDS NUMBER = 1.8407E+03
CIRC. REYNOLDS NUMBERS FOR ROTOR AT SEAL ENDS = 3.8561E+04, 1.7453E+04

DYNAMIC COEFFICIENTS (FORCE UNIT / DISP. UNIT)

DISP.	x (IN)	y (IN)	ϕ (RAD)	ψ (RAD)	FORCE UNIT
Kx	2.0689E+05	1.0073E+05	-1.9681E+03	-9.2019E+03	LB
Ky	-1.0073E+05	2.0689E+05	9.2019E+03	-1.9681E+03	LB
Kϕ	8.8445E+02	-2.4291E+02	1.1123E+03	4.9214E+02	IN-LB
Kψ	2.4291E+02	8.8445E+02	-4.9214E+02	1.1123E+03	IN-LB
Bx	3.7161E+01	3.3996E-07	-6.9734E-02	5.2914E-01	LB-SEC
By	-3.3996E-07	3.7161E+01	-5.2914E-01	-6.9734E-02	LB-SEC
Bϕ	-6.9734E-02	-5.2914E-01	1.7825E-01	2.1459E-12	IN-LB-SEC
Bψ	5.2914E-01	-6.9734E-02	-2.1459E-12	1.7825E-01	IN-LB-SEC
Ax	3.8167E-18	7.6333E-18	2.3854E-18	-1.6698E-18	$LB\text{-}SEC^2$
Ay	-7.6333E-18	3.8167E-18	1.6698E-18	2.3854E-18	$LB\text{-}SEC^2$
Aϕ	1.2076E-18	-3.5781E-19	1.4909E-19	-4.4727E-20	$IN\text{-}LB\text{-}SEC^2$
Aψ	3.5781E-19	1.2076E-18	4.4727E-20	1.4909E-19	$IN\text{-}LB\text{-}SEC^2$

RESULTS OF MTI SPIRAL GROOVE CODE FOR COMPARISON WITH CASE 2

FLOW = 1.7076E+00 (IN^3/SEC)

TORQUE = 5.8953E+00 (IN-LB), FILM POWER LOSS = 4.6770E+00 (HP)

DYNAMIC COEFFICIENTS (FORCE UNIT / DISP. UNIT)

DISP.	x (IN)	y (IN)	ϕ (RAD)	ψ (RAD)	FORCE UNIT
Kx	2.1565E+05	1.0203E+05	-2.0751E+03	-9.8637E+03	LB
Ky	-1.0203E+05	2.1565E+05	9.8637E+03	-2.0751E+03	LB
Kϕ	9.7231E+02	-2.4006E+02	1.1627E+03	5.0513E+02	IN-LB
Kψ	2.4006E+02	9.7231E+02	-5.0513E+02	1.1627E+03	IN-LB
Bx	3.7602E+01	2.8881E-06	-6.8925E-02	5.6836E-01	LB-SEC
By	3.6843E-07	3.7602E+01	-5.6836E-01	-6.8930E-02	LB-SEC
Bϕ	-6.8929E-02	-5.6836E-01	1.8265E-01	6.4583E-08	IN-LB-SEC
Bψ	5.6836E-01	-6.8929E-02	-3.9709E-09	1.8265E-01	IN-LB-SEC

(CASE 3) Face seal with grooves, laminar, no press. grad.

FACE SEAL, INERTIA NEGLECTED

ID, OD, NOMINAL FILM THICKNESS = 1.0000E+00, 2.0000E+00, 1.0000E-03 (IN)

ROTOR, SWIRL AND DIST. SPEEDS = 5.0000E+04, 2.5000E+04, 0.0000E+00 (RPM)

INSIDE, OUTSIDE PRESSURE = 0.0000E+00, 0.0000E+00 (PSI)

VISCOSITY = 3.0000E-08 (PSI-SEC), DENSITY = 0.0000E+00 ($LB\text{-}SEC^2/IN^4$)

AXIAL LOAD TO BALANCE FACE SEAL = 1.0391E+01 (LB)

FLOW = 5.7837E-01 (IN^3/SEC)

TORQUE = 2.1724E-01 (IN-LB), FILM POWER LOSS = 1.7234E-01 (HP)

RADIAL REYNOLDS NUMBER AT ID, OD = 0.0000E+00, 0.0000E+00
CIRC. REYNOLDS NUMBERS FOR ROTOR AT ID, OD = 0.0000E+00, 0.0000E+00

DYNAMIC COEFFICIENTS (FORCE UNIT / DISP. UNIT)

DISP.	z (IN)	ϕ (RAD)	ψ (RAD)	FORCE UNIT
Kz	2.3640E+04	0.0000E+00	0.0000E+00	LB
Kϕ	0.0000E+00	6.2646E+03	7.0922E+03	IN-LB
Kψ	0.0000E+00	-7.0922E+03	6.2646E+03	IN-LB
Bz	8.9011E+00	0.0000E+00	0.0000E+00	LB-SEC
Bϕ	0.0000E+00	2.5921E+00	2.6323E-05	IN-LB-SEC
Bψ	0.0000E+00	-2.6323E-05	2.5921E+00	IN-LB-SEC
Az	0.0000E+00	0.0000E+00	0.0000E+00	$LB\text{-}SEC^2$
Aϕ	0.0000E+00	-1.1927E-19	1.1927E-19	$IN\text{-}LB\text{-}SEC^2$
Aψ	0.0000E+00	-1.1927E-19	-1.1927E-19	$IN\text{-}LB\text{-}SEC^2$

RESULTS OF MTI SPIRAL GROOVE CODE FOR COMPARISON WITH CASE 3

AXIAL LOAD TO BALANCE FACE SEAL = 1.0391E+01 (LB)

FLOW = 5.7837E-01 (IN^3/SEC)

TORQUE = 2.1724E-01 (IN-LB), FILM POWER LOSS = 1.7234E-01 (HP)

DYNAMIC COEFFICIENTS (FORCE UNIT / DISP. UNIT)

DISP.	z (IN)	ϕ (RAD)	ψ (RAD)	FORCE UNIT
Kz	2.3639E+04	7.1718E-03	7.1755E-03	LB
Kϕ	5.8063E-06	6.2581E+03	7.0834E+03	IN-LB
Kψ	1.1824E-05	-7.0834E+03	6.2581E+03	IN-LB
Bz	8.9022E+00	-2.7999E-07	-3.9768E-07	LB-SEC
Bϕ	-6.6333E-08	2.5909E+00	2.9199E-06	IN-LB-SEC
Bψ	-1.9181E-08	-2.9131E-06	2.5909E+00	IN-LB-SEC

(CASE 4) Face seal with grooves, turbulent, no press. grad.

FACE SEAL, INERTIA NEGLECTED

ID, OD, NOMINAL FILM THICKNESS = 1.0000E+00, 2.0000E+00, 1.0000E-03 (IN)

ROTOR, SWIRL AND DIST. SPEEDS = 5.0000E+04, 2.5000E+04, 0.0000E+00 (RPM)

INSIDE, OUTSIDE PRESSURE = 0.0000E+00, 0.0000E+00 (PSI)

VISCOSITY = 3.0000E-08 (PSI-SEC), DENSITY = 1.0000E-04 ($LB\text{-}SEC^2/IN^4$)

AXIAL LOAD TO BALANCE FACE SEAL = 5.8223E+01 (LB)

FLOW = 7.2459E-01 (IN^3/SEC)

TORQUE = 2.4948E+00 (IN-LB), FILM POWER LOSS = 1.9792E+00 (HP)

RADIAL REYNOLDS NUMBER AT ID, OD = 1.5376E+03, 7.6881E+02
CIRC. REYNOLDS NUMBERS FOR ROTOR AT ID, OD = 1.8985E+04, 1.7453E+04

DYNAMIC COEFFICIENTS (FORCE UNIT / DISP. UNIT)

DISP.	z (IN)	ϕ (RAD)	ψ (RAD)	FORCE UNIT
Kz	1.2740E+05	0.0000E+00	0.0000E+00	LB
Kϕ	0.0000E+00	3.4989E+04	3.8692E+04	IN-LB
Kψ	0.0000E+00	-3.8692E+04	3.4989E+04	IN-LB
Bz	4.8105E+01	0.0000E+00	0.0000E+00	LB-SEC
Bϕ	0.0000E+00	1.4225E+01	6.4594E-05	IN-LB-SEC
Bψ	0.0000E+00	-6.4594E-05	1.4225E+01	IN-LB-SEC
Az	0.0000E+00	0.0000E+00	0.0000E+00	$LB\text{-}SEC^2$
Aϕ	0.0000E+00	1.9083E-18	-9.5417E-19	$IN\text{-}LB\text{-}SEC^2$
Aψ	0.0000E+00	9.5417E-19	1.9083E-18	$IN\text{-}LB\text{-}SEC^2$

RESULTS OF MTI SPIRAL GROOVE CODE FOR COMPARISON WITH CASE 4

AXIAL LOAD TO BALANCE FACE SEAL = 5.8223E+01 (LB)

FLOW = 7.2032E-01 (IN^3/SEC)

TORQUE = 2.4013E+00 (IN-LB), FILM POWER LOSS = 1.9050E+00 (HP)

DYNAMIC COEFFICIENTS (FORCE UNIT / DISP. UNIT)

DISP.	z (IN)	ϕ (RAD)	ψ (RAD)	FORCE UNIT
Kz	1.3685E+05	5.1323E-02	5.1174E-02	LB
Kϕ	8.1427E-06	3.7351E+04	4.0251E+04	IN-LB
Kψ	3.8131E-05	-4.0251E+04	3.7351E+04	IN-LB
Bz	4.9999E+01	-3.3078E-06	-3.4927E-06	LB-SEC
Bϕ	9.6839E-07	1.4768E+01	7.7653E-06	IN-LB-SEC
Bψ	2.8875E-07	-6.9217E-06	1.4768E+01	IN-LB-SEC

(CASE 5) Childs finite length solution, RPM0=RPM/2, L/D=.2

CYLINDRICAL SEAL

LENGTH, DIAMETER, CLEARANCE = 3.0480E-02, 1.5240E-01, 1.9050E-04 (m)

ROTOR, SWIRL AND DIST. SPEEDS = 3.6000E+03, 1.8000E+03, 0.0000E+00 (RPM)

PRESSURE AT START, END AXIAL BOUNDARIES = 3.4400E+06, 0.0000E+00 (Pa)

VISCOSITY = 1.2950E-03 (Pa-SEC), DENSITY = 1.0000E+03 (Kg/m3)

FLOW = 4.0061E-03 (m^3/SEC)

TORQUE = 2.2528E+00 (N-m), FILM POWER LOSS = 8.4929E+02 (WATT)

DYNAMIC COEFFICIENTS (FORCE UNIT / DISP. UNIT)

DISP.	x (m)	y (m)	ϕ (RAD)	ψ (RAD)	FORCE UNIT
Kx	1.8896E+07	4.1269E+06	-3.3389E+04	1.4185E+06	N
Ky	-4.1269E+06	1.8896E+07	-1.4185E+06	-3.3389E+04	N
Kϕ	-1.2847E+04	9.8025E+04	-3.8943E+03	1.0298E+02	N-m
Kψ	-9.8025E+04	-1.2847E+04	-1.0298E+02	-3.8943E+03	N-m
Bx	2.1895E+04	1.1396E+03	-7.0298E-01	1.7716E+02	N-SEC
By	-1.1396E+03	2.1895E+04	-1.7716E+02	-7.0298E-01	N-SEC
Bϕ	-1.9373E-01	6.8162E+01	5.4617E-01	1.3431E-02	N-m-SEC
Bψ	-6.8162E+01	-1.9373E-01	-1.3431E-02	5.4617E-01	N-m-SEC
Ax	3.0199E+00	-1.1981E-02	2.1688E-04	1.8092E-03	N-SEC^2
Ay	1.1981E-02	3.0199E+00	-1.8092E-03	2.1688E-04	N-SEC^2
Aϕ	6.0437E-05	4.9833E-04	3.5919E-05	1.1575E-06	N-m-SEC^2
Aψ	-4.9833E-04	6.0437E-05	-1.1575E-06	3.5919E-05	N-m-SEC^2

(CASE 6) Childs finite length solution, RPM0=RPM/2, L/D=1

CYLINDRICAL SEAL

LENGTH, DIAMETER, CLEARANCE = 1.5240E-01, 1.5240E-01, 1.9050E-04 (m)

ROTOR, SWIRL AND DIST. SPEEDS = 3.6000E+03, 1.8000E+03, 0.0000E+00 (RPM)

PRESSURE AT START, END AXIAL BOUNDARIES = 3.4400E+06, 0.0000E+00 (Pa)

VISCOSITY = 1.2950E-03 (Pa-SEC), DENSITY = 1.0000E+03 (Kg/m3)

FLOW = 1.7711E-03 (m^3/SEC)

TORQUE = 6.9241E+00 (N-m), FILM POWER LOSS = 2.6103E+03 (WATT)

DYNAMIC COEFFICIENTS (FORCE UNIT / DISP. UNIT)

DISP.	x (m)	y (m)	ϕ (RAD)	ψ (RAD)	FORCE UNIT
Kx	1.0794E+07	9.1778E+07	-1.5134E+06	1.5966E+07	N
Ky	-9.1778E+07	1.0794E+07	-1.5966E+07	-1.5134E+06	N
Kϕ	-4.6942E+05	6.5852E+05	-4.7345E+04	5.3912E+04	N-m
Kψ	-6.5852E+05	-4.6942E+05	-5.3912E+04	-4.7345E+04	N-m
Bx	4.8718E+05	1.0293E+05	1.1505E+02	8.0173E+03	N-SEC
By	-1.0293E+05	4.8718E+05	-8.0173E+03	1.1505E+02	N-SEC
Bϕ	-6.5590E+01	2.4967E+03	2.8624E+02	5.1787E+01	N-m-SEC
Bψ	-2.4967E+03	-6.5590E+01	-5.1787E+01	2.8624E+02	N-m-SEC
Ax	2.7261E+02	-2.1579E+00	-8.7333E-02	-2.8743E-01	N-SEC^2
Ay	2.1579E+00	2.7261E+02	2.8743E-01	-8.7333E-02	N-SEC^2
Aϕ	4.7908E-02	1.6434E-01	1.3703E-01	-1.7189E-03	N-m-SEC^2
Aψ	-1.6434E-01	4.7908E-02	1.7189E-03	1.3703E-01	N-m-SEC^2

(CASE 7) Childs finite length solution, RPM0=0, L/D=.2

CYLINDRICAL SEAL

LENGTH, DIAMETER, CLEARANCE = 3.0480E-02, 1.5240E-01, 1.9050E-04 (m)

ROTOR, SWIRL AND DIST. SPEEDS = 3.6000E+03, 0.0000E+00, 0.0000E+00 (RPM)

PRESSURE AT START, END AXIAL BOUNDARIES = 3.4400E+06, 0.0000E+00 (Pa)

VISCOSITY = 1.2950E-03 (Pa-SEC), DENSITY = 1.0000E+03 (Kg/m3)

FLOW = 3.9890E-03 (m^3/SEC)

TORQUE = 3.6677E+00 (N-m), FILM POWER LOSS = 1.3827E+03 (WATT)

DYNAMIC COEFFICIENTS (FORCE UNIT / DISP. UNIT)

DISP.	x (m)	y (m)	ϕ (RAD)	ψ (RAD)	FORCE UNIT
Kx	1.8583E+07	-3.0274E+05	-3.0756E+04	1.4106E+06	N
Ky	3.0274E+05	1.8583E+07	-1.4106E+06	-3.0756E+04	N
Kϕ	2.1014E+03	9.6616E+04	-3.8676E+03	-1.6999E+01	N-m
Kψ	-9.6616E+04	2.1014E+03	1.6999E+01	-3.8676E+03	N-m
Bx	2.1892E+04	8.5184E+02	1.6580E+00	1.7615E+02	N-SEC
By	-8.5184E+02	2.1892E+04	-1.7615E+02	1.6580E+00	N-SEC
Bϕ	-1.0540E+00	6.8066E+01	5.4479E-01	1.9870E-02	N-m-SEC
Bψ	-6.8066E+01	-1.0540E+00	-1.9870E-02	5.4479E-01	N-m-SEC
Ax	3.0025E+00	-8.3743E-02	-5.4944E-04	1.8925E-03	$N-SEC^2$
Ay	8.3743E-02	3.0025E+00	-1.8925E-03	-5.4944E-04	$N-SEC^2$
Aϕ	3.7677E-04	4.5070E-04	3.5698E-05	-2.5857E-06	$N-m-SEC^2$
Aψ	-4.5070E-04	3.7677E-04	2.5857E-06	3.5698E-05	$N-m-SEC^2$

(CASE 8) Childs finite length solution, RPM0=0, L/D=1

CYLINDRICAL SEAL

LENGTH, DIAMETER, CLEARANCE = 1.5240E-01, 1.5240E-01, 1.9050E-04 (m)

ROTOR, SWIRL AND DIST. SPEEDS = 3.6000E+03, 0.0000E+00, 0.0000E+00 (RPM)

PRESSURE AT START, END AXIAL BOUNDARIES = 3.4400E+06, 0.0000E+00 (Pa)

VISCOSITY = 1.2950E-03 (Pa-SEC), DENSITY = 1.0000E+03 (Kg/m3)

FLOW = 1.7673E-03 (m^3/SEC)

TORQUE = 7.8249E+00 (N-m), FILM POWER LOSS = 2.9499E+03 (WATT)

DYNAMIC COEFFICIENTS (FORCE UNIT / DISP. UNIT)

DISP.	x (m)	y (m)	ϕ (RAD)	ψ (RAD)	FORCE UNIT
Kx	1.3250E+07	7.5182E+07	-1.8882E+06	1.5946E+07	N
Ky	-7.5182E+07	1.3250E+07	-1.5946E+07	-1.8882E+06	N
Kϕ	-3.3283E+04	7.0821E+05	-4.8210E+04	4.1331E+04	N-m
Kψ	-7.0821E+05	-3.3283E+04	-4.1331E+04	-4.8210E+04	N-m
Bx	4.8952E+05	8.9262E+04	-1.4507E+02	7.9030E+03	N-SEC
By	-8.9262E+04	4.8952E+05	-7.9030E+03	-1.4507E+02	N-SEC
Bϕ	2.5693E+02	2.5639E+03	2.8825E+02	4.4699E+01	N-m-SEC
Bψ	-2.5639E+03	2.5693E+02	-4.4699E+01	2.8825E+02	N-m-SEC
Ax	2.7214E+02	-3.2538E+00	-1.5739E-01	-2.5660E-01	$N-SEC^2$
Ay	3.2538E+00	2.7214E+02	2.5660E-01	-1.5739E-01	$N-SEC^2$
Aϕ	6.4178E-02	1.5751E-01	1.3636E-01	-3.2263E-03	$N-m-SEC^2$
Aψ	-1.5751E-01	6.4178E-02	3.2263E-03	1.3636E-01	$N-m-SEC^2$

4.0 REFERENCES

1. Munson, J. and Steinetz, B., *"Specific Fuel Consumption and Increased Thrust Performance Benefits Possible with Advanced Seal Technology,"* Preprint AIAA-94-2700, presented at 1994 Joint Propulsion Conference, Indianapolis, IN, (June 27, 1994).
2. Walowit, J., *"Users Manual for Computer Code SPIRALG: Gas Lubricated Spiral Groove Cylindrical and Face Seals,"* MTI Technical Manual 91TM11.
3. Walowit, J. and Shapiro, W., *"Users Manual for Computer Code SPIRALI: Incompressible, Turbulent Spiral Grooved Cylindrical and Face Seals,"* MTI Technical Manual 95TM5.
4. Vohr, J.H. and Pan, C.H.T., *"On the Spiral Grooved Self Acting Gas Bearing,"* MTI-63TR52, Mechanical Technology Incorporated, Latham, NY, (1962).
5. Vohr, J.H. and Pan, C.H.T., *"Design Data: Gas Lubricated Spin-Axis Bearings for Gyroscopes,"* MTI-68TR29, Mechanical Technology Incorporated, Latham, NY, (1968).
6. Smalley, A.J., *"The Narrow Groove Theory of Spiral Grooved Gas Bearings: Development and Application of a Generalized Formulation for Numerical Solution"*, ASME J. Lub. Tech., V 94, 1, (1972), pp. 86-92.
7. Castelli, V. and Pirvics, J., *"Review of Methods in Gas Bearing Film Analysis,"* Trans. ASME, (1968), pp. 777-792.
8. Press, W.H., Flannery, B.P., Teukolsky, S.A. and Vetterling, W.T., *"Numerical Recipes,"* Cambridge University Press, (1986).
9. Artiles, A.,A., Walowit, J.A. and Shapiro, W., *"Analysis of Hybrid Fluid Film Journal Bearings with Turbulence and Inertia Effects,"* Proc. ASME Symposium in Advances in Computer-Aided Design, (1982), pp. 25-52.
10. Castelli, V., *"Design of Gas Bearings - Volume 1, Part 4: Numerical Methods,"* Gas Bearing Course Notes, Mechanical Technology Incorporated, Latham, NY, (1971).
11. Shapiro, W., *"Computer Code SPIRALP for Gas-Lubricated Spiral-Groove Bearings and Seals,"* MTI 88TM2, Prepared for NASA under Contract No. NAS3-24645, (1988).
12. Sato, Y., Ono, K. and Iwama, A., *"The Optimum Groove Geometry for Spiral Groove Viscous Pumps,"* ASME J. Tribology, V 112, 2, (1990), pp. 409-112.
13. Walowit, J. *"Users Manual for Computer Code SPRIALG Gas Lubricated Spiral Grooved Cylindrical and Face Seals,"* MTI report 91TM11, September 1991.
14. Hirs, G.G., *"A Bulk Flow Theory for Turbulence in Lubricant Films,"* ASME J. Lub. Tech., V 95, 2, (1973), pp. 137-146.
15. Schlichting, H., *"Boundary-Layer Theory,"* Seventh Ed., McGraw-Hill, New York, (1987).

16. Childs, D.W., *"Dynamic Analysis of Turbulent Annular Seals Based on Hirs Lubrication Equation,"* ASME J. Lub. Tech., V 105, 3, (1983), pp. 429-436.

17. Childs, D.W., *"Finite Length Solutions for Rotordynamic Coefficients of Turbulent Annular Seals,"* ASME J. Lub. Tech., V 105, 3, (1983), pp. 437-445.

18. Childs, D.W. and Kim, C.H., *"Analysis and Testing for Rotordynamic Coefficients of Turbulent Annular Seals With Different, Directionally Homogeneous Surface Roughness Treatment for Rotor and Stator Elements,"* ASME J. Tribology, V 107, 3, (1985), pp. 296-306.

19. San Andrés, L.A., *"Turbulent Hybrid Bearings With Fluid Inertia Effects,"* ASME J. Tribology, V 112, 4, (1990), pp. 699-707.

20. Shames, I.H., *"Mechanics of Fluids,"* McGraw-Hill, New York, (1963).

21. Shapiro, W. et. al., *"Numerical, Analytical, Experimental Study of Fluid Dynamic Forces in Seals - Interim Report No. 1,"* MTI-92TR6, Mechanical Technology Incorporated, Latham, NY, (1991).

22. Vohr, J.H. and Pan, C.H.T., *"Design Data: Gas Lubricated Spin-Axis Bearings for Gyroscopes,"* MTI-68TR29, Mechanical Technology Incorporated, Latham, NY, (1968).

23. Tipton, D.L., Scott, T.E. and Vogel, R.E., *"Labyrinth Seals Analysis: Volume III -- Analytical and Experimental Development of a Design Model for Labyrinth Seals,"* AFWAL-TR-85-2103, (1986).

24. Iwatsubo,T., Yang, B. and Ibaraki, R., *"Theoretical Approach to Obtaining Dynamic Characteristics of Noncontacting Spiral-Grooved Seals,"* NASA Conf. Pub. 2443, Rotordynamic Instability Problems in High-Performance Turbomachinery, (1986), pp 155-188.

25. Press, W.H., Flannery, B.P., Teukolsky, S.A. and Vetterling, W.T., *"Numerical Recipes,"* Cambridge University Press, (1986).

26. Ng, C.W. and Pan, C.H.T., *"A Linearized Turbulent Lubrication Theory,"* ASME J. Bas. Eng., V 87, 3, (1965), pp. 675-688.

27. Childs, D.W., Nolan, S.A. and Kilgore, J.J., *"Test Results for Turbulent Annular Seals, Using Smooth Rotors and Helically Grooved Stators,"* ASME J. Tribology, V 112, 2, (1990), pp. 254-258.

28. Walowit, J.A. and Shapiro, W. *"Users Manual for Computer Code SPIRALI,"* MTI 95TM5, (March 1995).

REPORT DOCUMENTATION PAGE

Form Approved
OMB No. 0704-0188

1. AGENCY USE ONLY (*Leave blank*)	2. REPORT DATE	3. REPORT TYPE AND DATES COVERED
	October 2004	Final Contractor Report

4. TITLE AND SUBTITLE

Numerical, Analytical, Experimental Study of Fluid Dynamic Forces in Seals
Volume 3—Description of Spiral-Groove Codes SPIRALG and SPIRALI

5. FUNDING NUMBERS

WBS–22–5000–0013
NAS3–25644

6. AUTHOR(S)

Jed Walowit and Wilbur Shapiro

7. PERFORMING ORGANIZATION NAME(S) AND ADDRESS(ES)

Mechanical Technology, Inc. (MTI)
968 Albany-Shaker Road
Latham, New York 12110

8. PERFORMING ORGANIZATION REPORT NUMBER

E–14708–3

9. SPONSORING/MONITORING AGENCY NAME(S) AND ADDRESS(ES)

National Aeronautics and Space Administration
Washington, DC 20546–0001

10. SPONSORING/MONITORING AGENCY REPORT NUMBER

NASA CR—2004-213199-VOL3

11. SUPPLEMENTARY NOTES

Project Manager, Anita D. Liang, Aeronautics Directorate, NASA Glenn Research Center, organization code 2200, 216–977–7439. Responsible person, Robert C. Hendricks, Research and Technology Directorate, NASA Glenn Research Center, organization code 5000, 216–977–7507.

12a. DISTRIBUTION/AVAILABILITY STATEMENT

Unclassified - Unlimited
Subject Categories: 07, 20, and 34 Distribution: Nonstandard

Available electronically at http://gltrs.grc.nasa.gov

This publication is available from the NASA Center for AeroSpace Information, 301–621–0390.

12b. DISTRIBUTION CODE

13. ABSTRACT ***(Maximum 200 words)***

The objectives of the program were to develop computational fluid dynamics (CFD) codes and simpler industrial codes for analyzing and designing advanced seals for air-breathing and space propulsion engines. The CFD code SCISEAL is capable of producing full three-dimensional flow field information for a variety of cylindrical configurations. An implicit multidomain capability allow the division of complex flow domains to allow optimum use of computational cells. SCISEAL also has the unique capability to produce cross-coupled stiffness and damping coefficients for rotordynamic computations. The industrial codes consist of a series of separate stand-alone modules designed for expeditious parametric analyses and optimization of a wide variety of cylindrical and face seals. Coupled through a Knowledge-Based System (KBS) that provides a user-friendly Graphical User Interface (GUI), the industrial codes are PC based using an OS/2 operating system. These codes were designed to treat film seals where a clearance exists between the rotating and stationary components. Leakage is inhibited by surface roughness, small but stiff clearance films, and viscous pumping devices. The codes have demonstrated to be a valuable resource for seal development of future air-breathing and space propulsion engines.

14. SUBJECT TERMS

CFD seal code; Industrial seal codes; User-friendly seal codes; Fluid-film seal codes; Clearance seal codes; Seals; Dynamics; Design; Computational analysis; Fluid forces

15. NUMBER OF PAGES
109

16. PRICE CODE

17. SECURITY CLASSIFICATION OF REPORT	18. SECURITY CLASSIFICATION OF THIS PAGE	19. SECURITY CLASSIFICATION OF ABSTRACT	20. LIMITATION OF ABSTRACT
Unclassified	Unclassified	Unclassified	